

NOAA Technical Memorandum
NWS ER-90



**NUMERICAL SIMULATION STUDIES OF THE MESOSCALE
ENVIRONMENT CONDUCTIVE TO THE RALEIGH TORNADO**

MICHAEL L. KAPLAN
ROBERT A. ROZUMALSKI
RONALD P. WEGLARZ
YUH-LANG LIN
STEVEN BUSINGER

Department of Marine, Earth, and Atmospheric Sciences
North Carolina State University
Raleigh, North Carolina

RODNEY F. GONSKI

National Weather Service Forecast Office
Raleigh, North Carolina

Scientific Services Division
Eastern Region Headquarters
Bohemia, New York
November 1995

TO: W/CR3

FROM: W/ER3

**U.S. DEPARTMENT OF
COMMERCE**

**National Oceanic and
Atmospheric Administration**

**National Weather
Service**

NOAA TECHNICAL MEMORANDA
National Weather Service, Eastern Region Subseries

The National Weather Service Eastern Region (ER) Subseries provides an informal medium for the documentation and quick dissemination of results not appropriate, or not yet ready for formal publications. The series is used to report on work in progress, to describe technical procedures and practices, or to relate progress to a limited audience. These Technical Memoranda will report on investigations devoted primarily to regional and local problems of interest mainly to ER personnel, and usually will not be widely distributed.

Papers 1 to 22 are in the former series, ESSA Technical Memoranda, Eastern Region Technical Memoranda (ERTM); papers 23 to 37 are in the former series, ESSA Technical Memoranda, Weather Bureau Technical Memoranda (WBTM). Beginning with 38, the papers are now part of the series, NOAA Technical Memoranda NWS.

Papers 1 to 22 are available from the National Weather Service Eastern Region, Scientific Services Division, 630 Johnson Avenue, Bohemia, NY 11716. Beginning with 23, the papers are available from the National Technical Information Service, U.S. Department of Commerce, Sills Bldg., 5285 Port Royal Road, Springfield, VA 22161. Prices vary for paper copy and for microfiche. Order by accession number shown in parentheses at end of each entry.

ESSA Technical Memoranda

- | | | |
|---------|----|--|
| ERTM | 1 | Local Uses of Vorticity Prognoses in Weather Prediction. Carlos R. Dunn. April 1965. |
| ERTM | 2 | Application of the Barotropic Vorticity Prognostic Field to the Surface Forecast Problem. Silvio G. Simplicio. July 1965. |
| ERTM | 3 | A Technique for Deriving an Objective Precipitation Forecast Scheme for Columbus, Ohio. Robert Kuessner. September 1965. |
| ERTM | 4 | Stepwise Procedures for Developing Objective Aids for Forecasting the Probability of Precipitation. Carlos R. Dunn. November 1965. |
| ERTM | 5 | A Comparative Verification of 300 mb. Winds and Temperatures Based on NMC Computer Products Before and After Manual Processing. Silvio G. Simplicio. March 1966. |
| ERTM | 6 | Evaluation of OFDEV Technical Note No. 17. Richard M. DeAngelis. March 1966. |
| ERTM | 7 | Verification of Probability of Forecasts at Hartford, Connecticut, for the Period 1963-1965. Robert B. Wassall. March 1966. |
| ERTM | 8 | Forest-Fire Pollution Episode in West Virginia, November 8-12, 1964. Robert O. Weedfall. April 1966. |
| ERTM | 9 | The Utilization of Radar in Meso-Scale Synoptic Analysis and Forecasting. Jerry D. Hill. March 1966. |
| ERTM | 10 | Preliminary Evaluation of Probability of Precipitation Experiment. Carlos R. Dunn. May 1966. |
| ERTM | 11 | Final Report. A Comparative Verification of 300 mb. Winds and Temperatures Based on NMC Computer Products Before and After Manual Processing. Silvio G. Simplicio. May 1966. |
| ERTM | 12 | Summary of Scientific Services Division Development Work in Sub-Synoptic Scale Analysis and Prediction - Fiscal Year 1966. Fred L. Zuckerberg. |
| ERTM | 13 | A Survey of the Role of Non-Adiabatic Heating and Cooling in Relation of the Development of Mid-Latitude Synoptic Systems. Constantine Zois. July 1966. |
| ERTM | 14 | The Forecasting of Extratropical Onshore Gales at the Virginia Capes. Glen V. Sachse. August 1966. |
| ERTM | 15 | Solar Radiation and Clover Temperatures. Alex J. Kish. September 1966. |
| ERTM | 16 | The Effects of Dams, Reservoirs and Levers on River Forecasting. Richard M. Greening. September 1966. |
| ERTM | 17 | Use of Reflectivity Measurements and Reflectivity Profiles for Determining Severe Storms. Robert E. Hamilton. October 1966. |
| ERTM | 18 | Procedure for Developing a Nomograph for Use in Forecasting Phenological Events from Growing Degree Days. John C. Purvis and Milton Brown. December 1966. |
| ERTM | 19 | Snowfall Statistics for Williamsport, Pa. Jack Hummel. January 1967 |
| ERTM | 20 | Forecasting Maturity Date of Snap Beans in South Carolina. Alex J. Kish. March 1967. |
| ERTM | 21 | New England Coastal Fog. Richard Fay. April 1967. |
| ERTM | 22 | Rainfall Probability at Five Stations Near Pickens, South Carolina, 1957-1963. John C. Purvis. April 1967. |
| WBTM ER | 23 | A Study of the Effect of Sea Surface Temperature on the Areal Distribution of Radar Detected Precipitation Over the South Carolina Coastal Waters. Edward Paquet. June 1967. (PB-180-612). |
| WBTM ER | 24 | An Example of Radar as a Tool in Forecasting Tidal Flooding. Edward P. Johnson. August 1967 (PB-180-613). |
| WBTM ER | 25 | Average Mixing Depths and Transport Wind Speeds over Eastern United States in 1965. Marvin E. Miller. August 1967. (PB-180-614). |
| WBTM ER | 26 | The Sleet Bright Band. Donald Marier. October 1967. (PB-180-615). |
| WBTM ER | 27 | A Study of Areas of Maximum Echo Tops in the Washington, D.C. Area During the Spring and Fall Months. Marie D. Fellechner. April 1968. (PB-179-339). |
| WBTM ER | 28 | Washington Metropolitan Area Precipitation and Temperature Patterns. C.A. Woollum and N.L. Canfield. June 1968. (PB-179-340). |
| WBTM ER | 29 | Climatological Regime of Rainfall Associated with Hurricanes after Landfall. Robert W. Schoner. June 1968. (PB-179-341). |
| WBTM ER | 30 | Monthly Precipitation - Amount Probabilities for Selected Stations in Virginia. M.H. Bailey. June 1968. (PB-179-342). |
| WBTM ER | 31 | A Study of the Areal Distribution of Radar Detected Precipitation at Charleston, S.C. S.K. Parrish and M.A. Lopez. October 1968. (PB-180-480). |
| WBTM ER | 32 | The Meteorological and Hydrological Aspects of the May 1968 New Jersey Floods. Albert S. Kachic and William Long. February 1969. (Revised July 1970). (PB-194-222). |
| WBTM ER | 33 | A Climatology of Weather that Affects Prescribed Burning Operations at Columbia, South Carolina. S.E. Wasserman and J.D. Kanupp. December 1968. (COM-71-00194). |
| WBTM ER | 34 | A Review of Use of Radar in Detection of Tornadoes and Hail. R.E. Hamilton. December 1969. (PB-188-315). |
| WBTM ER | 35 | Objective Forecasts of Precipitation Using PE Model Output. Stanley E. Wasserman. July 1970. (PB-193-378). |
| WBTM ER | 36 | Summary of Radar Echoes in 1967 Near Buffalo, N.Y. Richard K. Sheffield. September 1970. (COM-71-00310). |
| WBTM ER | 37 | Objective Mesoscale Temperature Forecasts. Joseph P. Sobel. September 1970. (COM-71-0074). |

NOAA Technical Memoranda NWS

- | | | |
|--------|----|---|
| NWS ER | 38 | Use of Primitive Equation Model Output to Forecast Winter Precipitation in the Northeast Coastal Sections of the United States. Stanley E. Wasserman and Harvey Rosenblum. December 1970. (COM-71-00138). |
| NWS ER | 39 | A Preliminary Climatology of Air Quality in Ohio. Marvin E. Miller. January 1971. (COM-71-00204). |
| NWS ER | 40 | Use of Detailed Radar Intensity Data in Mesoscale Surface Analysis. Robert E. Hamilton. March 1971. (COM-71-00573). |
| NWS ER | 41 | A Relationship Between Snow Accumulation and Snow Intensity as Determined from Visibility. Stanley E. Wasserman and Daniel J. Monte. (COM-71-00763). |
| NWS ER | 42 | A Case Study of Radar Determined Rainfall as Compared to Rain Gage Measurements. Martin Ross. July 1971. (COM-71-00897). |
| NWS ER | 43 | Snow Squalls in the Lee of Lake Erie and Lake Ontario. Jerry D. Hill. August 1971. (COM-72-00959). |
| NWS ER | 44 | Forecasting Precipitation Type at Greer, South Carolina. John C. Purvis. December 1971. (COM-72-10332). |
| NWS ER | 45 | Forecasting Type of Precipitation. Stanley E. Wasserman. January 1972. (COM-72-10316). |

(CONTINUED ON INSIDE REAR COVER)

NOAA Technical Memorandum NWS ER-90

**NUMERICAL SIMULATION STUDIES OF THE MESOSCALE
ENVIRONMENT CONDUCIVE TO THE RALEIGH TORNADO**

**MICHAEL L. KAPLAN
ROBERT A. ROZUMALSKI
RONALD P. WEGLARZ
YUH-LANG LIN
STEVEN BUSINGER**

**Department of Marine, Earth, and Atmospheric Sciences
North Carolina State University
Raleigh, North Carolina**

RODNEY F. GONSKI

**National Weather Service Forecast Office
Raleigh, North Carolina**

**Scientific Services Division
Eastern Region Headquarters
Bohemia, New York
November 1995**

**United States
Department of Commerce
Ronald H. Brown
Secretary**

**National Oceanic and
Atmospheric Administration
D. James Baker
Under Secretary**

**National Weather Service
Elbert W. Friday, Jr.
Assistant Administrator**



Table of Contents

Section	Page
List of Figures	iii
List of Tables	viii
Executive Summary	ix
1. Introduction	1
2. Numerical Experiments	3
3. Synoptic Scale Structure	5
<i>3.1 Rawinsonde/Surface Data Analyses</i>	5
<i>3.2 Simulated Duct Structure</i>	14
<i>3.3 Summary of Synoptic Scale Structure</i>	20
4. Hydrostatic Mesoscale Dynamics	22
<i>4.1 Stage A - Observations</i>	22
<i>4.2 Stage A - Simulation Results</i>	24
<i>4.3 Summary of Stage A</i>	30
<i>4.4 Stage B - Observations</i>	30
<i>4.5 Stage B - Simulation Results</i>	43
<i>4.6 Summary of Stage B</i>	55
<i>4.7 Stage C - Observations</i>	55
<i>4.8 Stage C - Simulation Results</i>	65
<i>4.9 Summary of Stage C</i>	68
<i>4.10 Stage D - Observations</i>	71
<i>4.11 Stage D - Simulation Results</i>	72

<i>4.12 Summary of Stage D</i>	<i>78</i>
5. Overall Summary of the Raleigh Tornado Outbreak	80
6. Exit Versus Entrance Region in Southern Tornado Outbreaks	83
7. Operational Aspects and Considerations	88
8. Acknowledgements	97
9. References	98

List of Figures

Figure	Page(s)
1. Tornado paths and F-scale intensity from November 27 - 28 1988	2
2. Coarse and fine mesh domains for model simulations	4
3. NWS 200 mb analyses for 25 - 28 November 1988	6
4. NWS 850 mb analyses for 25 - 28 November 1988	7
5. NWS 700 and 500 mb analyses for 27 - 28 November 1988	8
6. Flux convergence of mixing ratio for 1200 and 0000 UTC 27 - 28 November.....	9
7. Observed relative vorticity at 300, 500, 700, and 850mb from 0000 UTC 28 November.....	10
8. Objectively analyzed cross sections of potential temperature, isotachs, and relative humidity from 1200 UTC 27 November 1988	11-12
9. Observed vertical cross section of potential temperature and wind barbs from 0000 UTC 28 November 1988	13
10. Objectively analyzed Vertical lapse rate between 400 and 250mb from 1200 and 0000 UTC 27 - 28 November.....	14
11. Vertical cross sections of relative humidity analyzed from the 00 hour forecast from MOB to GSO and TUP to VLD	15
12. Objectively analyzed soundings of initial state model initial data for CLT, GSO, CAE, and CKL.....	16
13. Observed position of surface pressure rises and 18 hour pmsl falls between 1200 and 0600 UTC 27 - 28 November	17

14. Time line of observed convection derived from three-hourly NWS surface observations valid for the periods 1200-1500, 1500-1800, 1800-2100, 2100-0000, and 0000-0300 UTC 27 - 28 November 1988.....	18
15. Simulated cross sections of potential temperature, Richardson number, and critical level between MGM and RIC from 0000 UTC to 0600 UTC 28 November	19
16. NWS surface three-hourly mean sea level pressure analysis valid for 1200, 1500, and 1800 UTC November.....	23
17. NWS MDR summary valid at 1735 UTC 27 November 1988.....	24
18. Objective streamline analysis valid for 1600 - 2000 UTC 27 November	25
19. High resolution mean sea level pressure analyses from 1900 - 2000 UTC.....	26
20. Simulated pmsl and 850 mb winds for 1600 - 2000 UTC 27 November	27
21. Simulated cross sections of potential temperature, omega, and isotachs from JAN to DAB for 1600, 1800, and 2000 UTC November	28-29
22. High resolution mean sea level pressure analyses for 2100 - 0200 27-28 November.....	31
23. Objective streamline analysis valid for 2100-0400 UTC 27 - 28 November	32-33
24. Unfiltered microbarograph traces for GSP, AVL, HKY, CLT, GSO, and RDU from 27 - 28 November	34-35
25. GOES infrared and water vapor satellite imagery from 2100 - 0000 UTC 27 - 28 November.....	37-40
26. NWS MDR summary valid for 1935 - 0135 UTC 27-28 November.....	41
27. High resolution mean sea level pressure change for 1800 - 0300 UTC 27 - 28 November.....	42

28. Simulated 500 mb heights, winds, and omega for 1600 - 2200 UTC 27 November.....	44-45
29. Simulated 500 mb heights, winds, and temperature for 2000 - 0100 UTC 27-28 November.....	46
30. Simulated 300 mb heights, winds, and temperature for 2000 - 0100 UTC 27-28 November.....	48
31. Simulated relative vorticity for 300, 500, 700, and 850mb level at 0000 UTC 28 November	49
32. Simulated vertical cross section of relative humidity from BNA to CHS and TUP to SAV for 0000 UTC 28 November	50
33. Simulated vertical soundings for MCN, AHN, CLT, and RDU valid at 0000 UTC 28 November	51
34. Simulated PMSL and surface temperature for 2100 - 0200 UTC 27-28 November.....	52
35. Simulated 850mb vorticity and isotachs for 2100 - 0200 UTC 27-28 November	53
36. Location of simulated mid-tropospheric wind surges and LLJ's from 2200 - 0800 UTC 27 - 28 November.....	54
37. High resolution mean sea level pressure analyses for 0300 - 0600 28 November.....	56
38. Objective streamline analysis valid for 0300 - 0600 UTC 28 November	57
39. GOES infrared and water vapor imagery for 0100-0600 UTC 28 November	58-63
40. NWS MDR summary for 0335-0735 UTC 28 November	64
41. Simulated PMSL and surface temperature from 0300 to 0900 UTC 28 November.....	65-66

42. Simulated 850mb vorticity and isotachs from 0300 to 0900 UTC 28 November.....	67-68
43. Simulated 850mb wind vector and isotachs valid at 0800 UTC 28 November	69
44. Simulated vertical cross sections of potential temperature, omega, and isotachs from CSG to RDU valid between 0000 and 0600 UTC 28 November.....	70-71
45. Simulated vertical cross sections equivalent potential temperature and relative humidity from CSG to RDU valid between 0000 and 0600 UTC 28 November	72-73
46. Simulated 500mb height, wind vectors, and temperature for 0300 - 0600 UTC 28 November	74
47. Observed surface pressure, wind speed, and direction from Carolina Power and Light.....	75
48. Simulated fine mesh 500mb height, wind vectors, and temperature for 0300 - 0700 UTC 28 November	76-77
49. Simulated fine mesh cross section of equivalent potential temperature and relative humidity from FLO to ORF at 0640 UTC 28 November	78
50. Schematic depicting the coupled polar jet and subtropical jet streak transverse circulations	82
51. NWS 200 mb analyses from 24 - 25 January 1990	85
52. NWS 850 mb analyses from 24 - 25 January 1990	86
53. Goes water vapor channel satellite imagery valid at 1800 UTC 27 November 1988	92
54. Goes water vapor channel satellite imagery valid at 1200 UTC 25 January 1990	93

55. Goes water vapor channel satellite imagery valid at 1200 UTC 27	
November 1988	94
56. Goes water vapor channel satellite imagery valid at 2000 UTC 27	
November 1988	95
57. Skew-T diagram of a proximity sounding for RDU at 0000	
UTC 28 November 1988	96

List of Tables

Table	Page
1. Unfiltered gravity wave characteristics observed from barographs.....	36
2. Dual paradigms for southern tornado outbreaks	83
3. Similarities between exit and entrance region in southern tornado outbreaks	84
4. Checklist for tornadic outbreaks in the Southeast	89

Executive Summary

Numerical simulations and the analysis of observational data were employed to define the sequence of events which resulted in the development of an environment conducive for the tornadic convection that produced extensive damage and injury in Raleigh, North Carolina on 28 November 1988. This particular event was quite unusual in that a deadly F4 tornado occurred at ~1 AM local time during the late fall. Furthermore, the storm developed within an environment that was not considered dynamic enough to warrant a severe weather watch by the National Weather Service. Additionally, this environment occurred within the subgeostrophic *entrance* region of a polar jet streak. This opposes conventional synoptic wisdom in that severe weather is more frequently observed in the polar jet exit region. Positioned above the polar jet streak entrance region, a highly ageostrophic circulation associated with a subtropical *jet exit region* was present. The numerical model results as well as conventional asynoptic data analysis indicated that key features within the precursor environment could be traced back in time to at least 1200 UTC 27 November along the Gulf Coast. In-depth analysis of numerical model results and observational data show that the precursor processes which play a significant role in the development of the Raleigh tornado could be organized into four distinct "stages".

During the first stage, four different mesoscale pressure perturbations phase to produce a distinct cyclonic mesoscale circulation over southwestern Georgia. This mesoscale circulation will be referred to as the "the Georgia mesocyclone". These pressure perturbations, which are all coupled to preexisting convection, include: 1) a strong cold frontal trough/squall line propagating through the Mississippi and Tennessee River Valleys, 2) a surface mesolow propagating along a weak quasi-stationary cold front/trough over the western Appalachian Piedmont within

which convection is occurring, 3) an outflow boundary lying just north of the Florida Panhandle, and 4) a mesoscale high pressure region, which is wedged along the central and eastern Appalachian Piedmont.

The second stage involves the development of a mesoscale jet streak aloft over the Tennessee River Valley which rapidly propagates over the Appalachian Piedmont. The subsequent adjustment processes result in the destruction of the shallow, hydrostatic surface ridge which prevents the northeastward propagation of the Georgia mesocyclone prior to 2000 UTC. This mesoscale "jetlet" is the result of diabatically-forced geostrophic adjustment processes wherein convective latent heating accompanying the strong cold front modifies the northwestward-directed pressure gradient force within the subgeostrophic polar jet entrance region and subtropical jet exit region. The inertial-advective response to this pressure perturbation accelerates the mid-upper tropospheric winds at right angles away from the region of mass perturbation resulting from convective heating. Subsequently, this produces an independently propagating region of mass flux divergence which itself induces propagating gravity waves and significant pressure falls over western North Carolina and Virginia. Furthermore, the ageostrophic circulation associated with the new mesoscale jetlet results in the descent of dry air over the Western Piedmont. This mesoscale region of mass flux divergence propagates northeastward above the shallow dome of rain cooled air along the Carolina Piedmont.

The third stage represents an intensification of the Georgia mesocyclone through wave-CISK and its northeastward propagation along the Appalachian Piedmont. As the convectively-induced upper-level mass flux divergence amplifies the mesocyclone, the surface inflow increases, thus intensifying the low-level jet and low-level vorticity through vortex tube stretching. Part of the amplification also involves the development of upstream confluent flow aloft behind the CISK mode(s) resulting in downward momentum fluxes and the injection of dry air behind the propagating mesocyclone(s). Two well-developed gravity

waves, organized by the intersecting pressure perturbations along the Gulf coast, sustain the Georgia mesocyclone as well as a precursor mesolow which propagate in tandem northeastward along the Piedmont frontal boundary. Each mesocyclone is accompanied by a mesoscale jetlet aloft contributing to mass flux divergence (convergence) ahead of (behind) the propagating mesoscale jetlet.

Finally, during stage four, the Georgia mesocyclone and its accompanying low-level southeasterly jet intensify due to diabatically-induced vortex tube stretching. Coincidentally, the descent of westerly momentum in the rear of the mesocyclone increases the vertical wind shear and θ_e gradients above the system. The enhanced vertical wind shear in proximity to vortex tube stretching intensifies the tilting of horizontal vorticity into the vertical. This results in a simulated region of increased buoyancy and vertical vorticity approaching Raleigh from the southwest very close to the time of the actual tornadic event.

1. Introduction

The Raleigh, North Carolina tornado of 28 November 1988 was an extraordinary event which has stimulated a great deal of interest from the weather forecasting and research communities as evident by the remarkable number of papers written (Browning *et al.* 1989; Gonski *et al.* 1989; Mogil and Ellrod 1989; Przybylinski 1989; Korotky 1990; Funk 1991; Zack *et al.* 1993; and Kaplan *et al.* 1993, 1994a,b,c). This tornado violated climatology as it occurred at night in late November, with a raging F4 intensity. Furthermore, it occurred in the vicinity of the polar jet streak *entrance* region, not the exit region, wherein most severe weather events typically happen (Uccellini and Johnson 1979; Uccellini and Koch 1987; Zack and Kaplan 1987). The combination of a climatologically rare event and its development within the entrance region of a polar jet streak may have proved sufficient to deter the National Weather Service from issuing any severe thunderstorm or tornado watches prior to the initiation of the severe weather in Raleigh. This violent episode of severe weather was part of a devastating outbreak which produced several tornadoes including those at Alberta and Walters, Virginia, as well as Galatia, Raleigh, Bayboro, Fairfield, and Manteo, North Carolina as shown in Figure 1 (NOAA, 1988).

In section 2 of this monograph we will detail the numerical simulation experiments performed in an effort to outline the sequence of events leading up to the Raleigh tornado. Section 3 will involve a discussion of the synoptic scale state of the atmosphere over the central and eastern U. S. prior to the development of the severe weather in North Carolina and Virginia. In section 4, we will partition the asynoptic observations and mesoscale numerical model results chronologically. Each successive step in the sequence describes the hydrostatic mesoscale processes which evolve into an environment conducive to tornadogenesis over Virginia and North Carolina. During each stage

we will first introduce the observational data which include hourly surface, satellite, and radar reports as well barograph records. This will be followed by the simulation results and then a summary of the processes synthesized from both the observations and the model output. Section 5 will contain an overall summary of the conditions leading up to the severe weather outbreak as demonstrated by the material presented in section 4. Finally, section 6 will compare the analysis results for this case study with the widespread jet exit region outbreak of 28-29 March 1984 in an effort to focus on both similarities and differences between jet streak entrance and exit region tornado outbreaks over the southeastern U. S. In addition, we will compare the atmospheric environment preceding the RDU case study to the 25 January 1990 "non-tornadic" event in order to emphasize the interactions between polar and subtropical jet streaks that give rise to a favorable environment for severe weather. This research is aimed at defining the unique atmospheric conditions which are conducive to the development and evolution of severe weather over the southeastern U. S. as part of the research undertaken for NOAA by the Southeast Consortium on Severe Thunderstorms and Tornadoes.

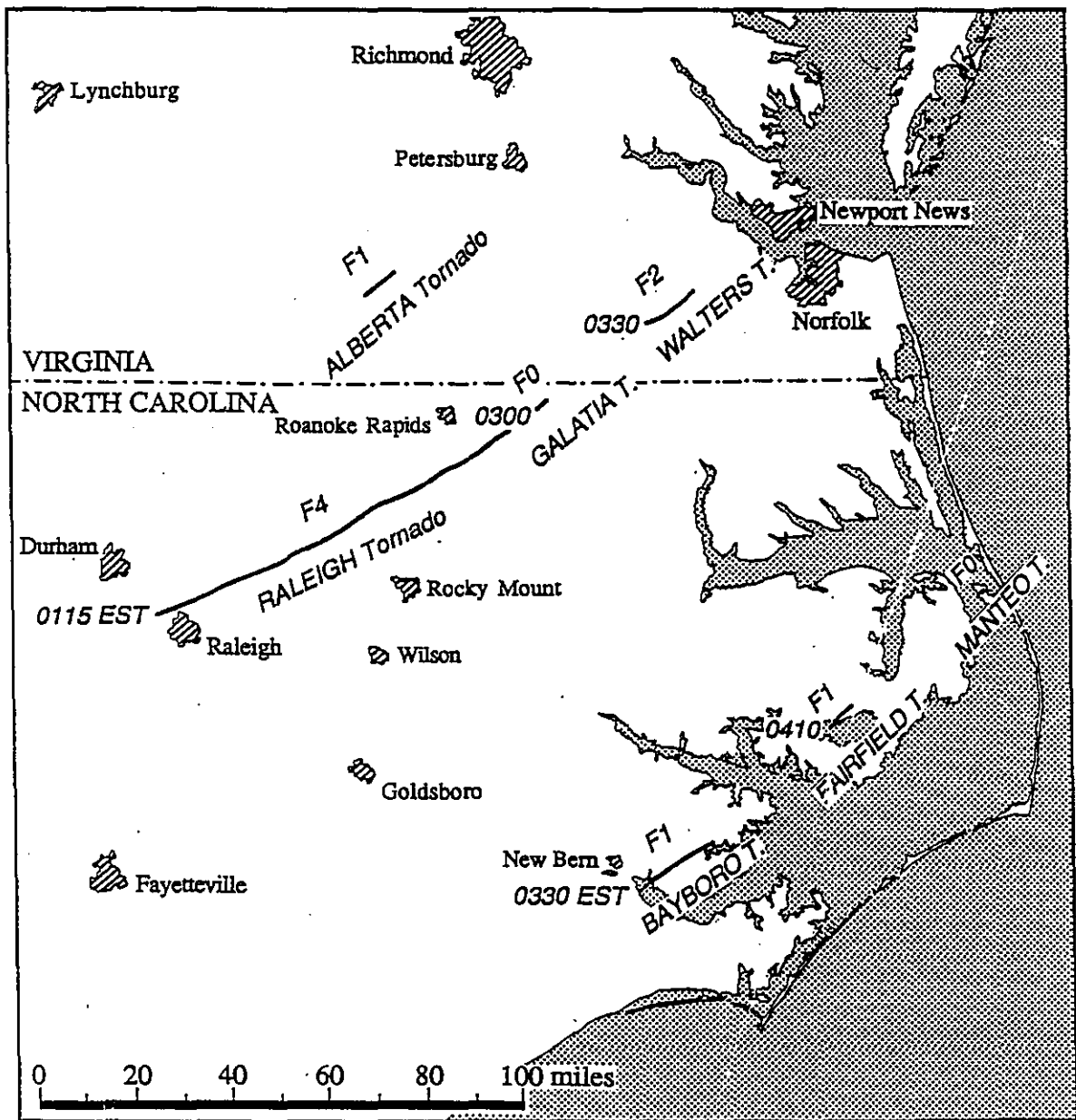


Figure 1. Tornado paths and estimated F-scale intensity observed on 28 November 1988 (Adapted from STORM DATA, 1988).

2. Numerical Experiments

The numerical model employed for these experiments was the GMASS model (Whitaker *et al.* 1988; Manobianco *et al.* 1992) which is a modified version of the MASS model developed by Kaplan *et al.* (1982a,b). This model has been used extensively for a variety of hydrostatic simulations of the meso- β scale environment accompanying severe convection (Koch *et al.* 1985; Cram and Kaplan 1985; Kaplan *et al.* 1985; Kocin *et al.* 1985a,b; Zack and Kaplan 1987; Cram *et al.* 1991; Kaplan and Karyampudi 1992a,b; Kaplan *et al.*, 1994a-c; Kaplan and Businger 1994, and Kaplan *et al.* 1995). The experiments performed for this case study consisted of both coarse (24km) and nested-grid (12km) simulations employing a 178x108x38 matrix of grid points. The horizontal resolution of both the nested and coarse mesh grids were true at 60° N for a stereographic map image plane projected onto a Cartesian grid. Therefore, the horizontal resolution of each grid was even finer (19km coarse, 9.5km nested) over the area of interest south of 37° N latitude between the Gulf Coast, Tennessee River Valley, and the North Carolina coast. The geographical region of coverage for the two numerical simulations is depicted in Figure 2a and the locations of NWS observing stations referenced in this paper are depicted in figure 2b.

The initial conditions for the coarse mesh grid is derived from the National Center for Atmospheric Research (NCAR) Global Optimum Interpolation (GOI) analyses valid at 1200 UTC 27 November 1988. This initial state data is then fortified with reanalyzed rawinsonde, aviation surface data, and climatological sea surface temperature (SST) data. The terrain employed was a slightly smoothed version of a high resolution terrain data set designed to approximate smooth 24 km gradients and a maximum Appalachian terrain height of ~900 m. The fine scale terrain was linearly interpolated from the coarse mesh terrain.

The coarse mesh simulation was run for 21 hours of real time to 0900 UTC 28 November 1988 with lateral boundary conditions derived from the GOI analyses which were temporally interpolated between analysis times. The 12 km nested-grid simulation was initialized at 0200 UTC 28 November with initial conditions derived from linearly interpolated simulated coarse mesh fields. This simulation was performed through 0700 UTC 28 November 1988 employing lateral one-way boundary conditions from the coarse mesh simulation.

Additionally, the model employs a fourth-order spatial differencing scheme, a split-explicit time marching scheme, and the Blackadar (1979) planetary boundary layer (PBL) scheme. The model assumes a uniform distribution of soil moisture, solves a prognostic equation for the surface energy budget, and is based on a σ - p vertical coordinate system with 38 σ -layers between the lower part of the PBL and the model rigid lid at 100 mb. The model's convective parameterization scheme is based on the one formulated by Molinari (1985), which incorporates moist downdrafts resulting from evaporative cooling. For these experiments both grid scale and convective latent heating were allowed because of the importance of convection in the physical processes at work in this case study. Extra diffusion is added in the stratosphere below the rigid lid to enhance the damping of vertically-propagating gravity waves.

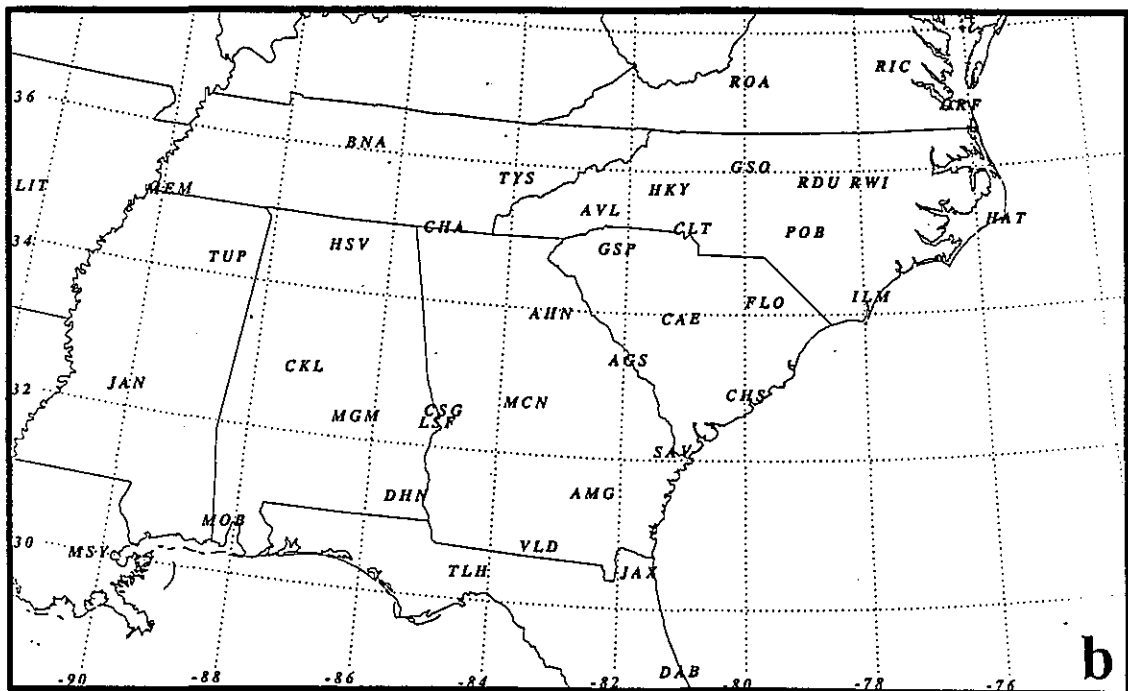
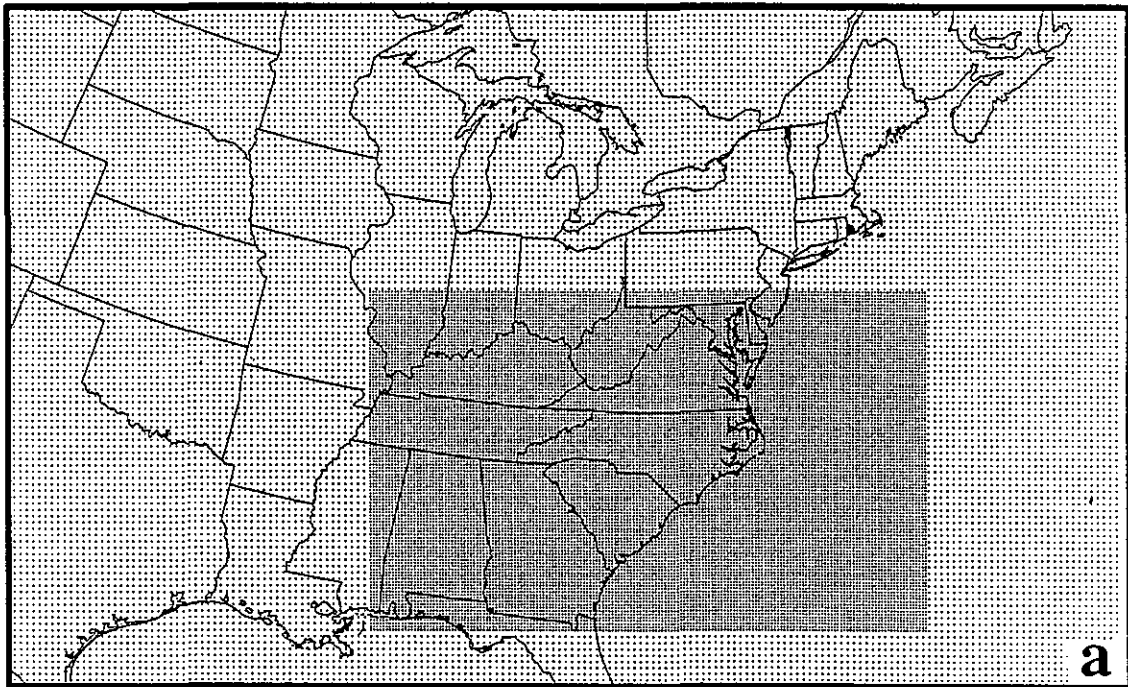


Figure 2. a) Region of coarse (24 km) mesh and fine mesh (12 km) model domains used in the numerical simulations. b) location of observing stations referenced in this paper.

3. Synoptic Scale Structure

3.1 Rawinsonde/Surface Data Analyses

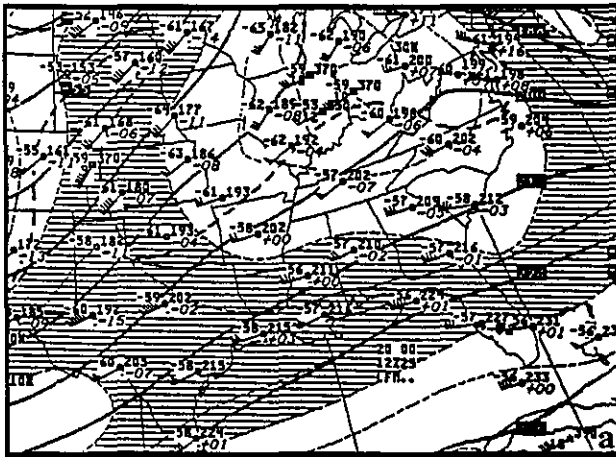
To appreciate this case study it is necessary to understand the time history of two distinct ageostrophic jet streak circulations which eventually come into direct contact and phase over the southeastern U. S. prior to the tornado outbreak. Figure 3 depicts the time evolution of the subtropical and polar jet streaks starting approximately 66 hours prior to the Raleigh tornado. Evident at 200 mb is a split in the jet stream structure with a subtropical jet (STJ) maximum that propagates out of Mexico towards the southeastern U. S.. Coincident with this, the polar jet (PJ) becomes better organized and drives southeastwards while undergoing baroclinic amplification within the trough located over the Great Plains. By 1200 UTC 27 November, the exit region of the STJ lies over the eastern Gulf Coast. The flow is decidedly supergeostrophic within the right exit region while it is clearly subgeostrophic within the left exit region. By 0000 UTC 28 November, the right exit region of the STJ has propagated northeastwards toward the Carolina coastal plain. Flow within the STJ continues to be decidedly supergeostrophic, while the PJ presses southeastward resulting in a near merger of the PJ's right entrance region with the STJ's left exit region. Thus, two deep transverse ageostrophic jet streak circulations containing intense regions of ascent one of which is thermally direct and one of which is thermally indirect, are phasing over the eastern Gulf of Mexico and the Tennessee River Valley approximately 6 hours prior to the observed tornado outbreak.

Corresponding to the sequence of events unfolding in the mid-upper troposphere, a merger of the two lower branches of these circulations is illustrated through the time series of 850 mb analysis in Fig. 4. As the STJ advances eastwards and the PJ intensifies, the subtropical high pressure ridge amplifies and builds southwestwards into the

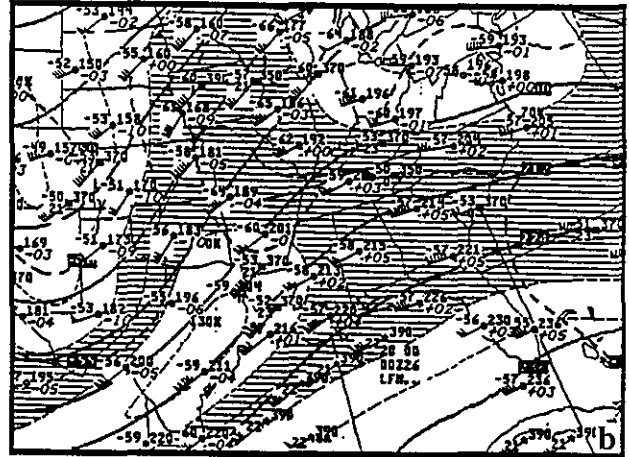
Gulf of Mexico. This gives rise to low-level confluence and a strong cross-stream ageostrophic circulation associated with a developing low-level jet (LLJ) over the Gulf states by 0000 UTC 27 November. This LLJ is a direct consequence of the increasing height gradient between the subtropical ridge building into the Gulf of Mexico and the amplifying trough over the Central Great Plains. Over the subsequent 24 hours, this LLJ intensifies and propagates northeastwards. The growing northwestward directed pressure gradient force over the southeastern U. S. supports and maintains a region of subgeostrophic flow along the Georgia and Carolina Piedmont wherein the strongest branch of the ageostrophic return circulation develops immediately prior to the development of the Raleigh tornado. This coupled subtropical/polar jet streak circulation is analogous to that diagnosed during east coast cyclogenesis by Uccellini and Kocin (1987) *wherein a thermally indirect circulation accompanying the subtropical jet exit region is in phase with the thermally direct circulation accompanying the PJ entrance region.*

Figure 5 depicts the 300, 500, and 700 mb NWS synoptic analyses valid at 1200 UTC 27 and 0000 UTC 28 November 1988. The mid-upper tropospheric fields indicate a well-developed PJ extending from northeastern Texas to the eastern Great Lakes at 0000 UTC which propagates slowly east-northeastward. This places the right *entrance* region of the PJ over the Gulf Coast and southern Appalachian states by 0000 UTC, while the right *exit* region is in southern Ontario and Quebec at the same time (not shown). The very strong cold front associated with the polar jet extends from the surface to above 500 mb and slopes upstream with height from the eastern Tennessee River Valley to the Mississippi River Valley at this time. The jet core stretches from Buffalo, New York (BUF) to Little Rock, Arkansas (LIT) at 0000 UTC.

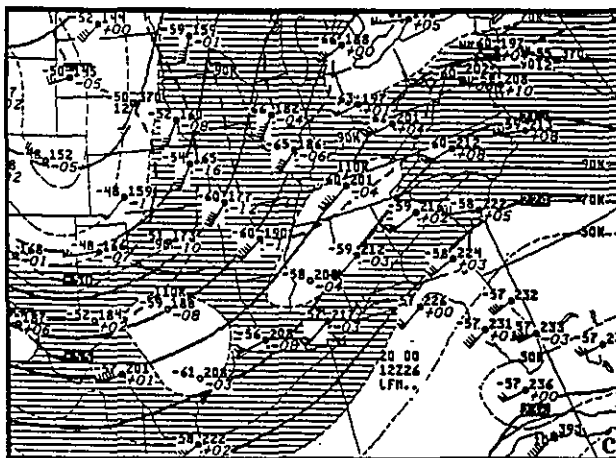
Of particular interest is the vertical variation of potential temperature, wind, and relative humidity over the southern Appalachians at 0000 UTC. The 0000 UTC mid-upper



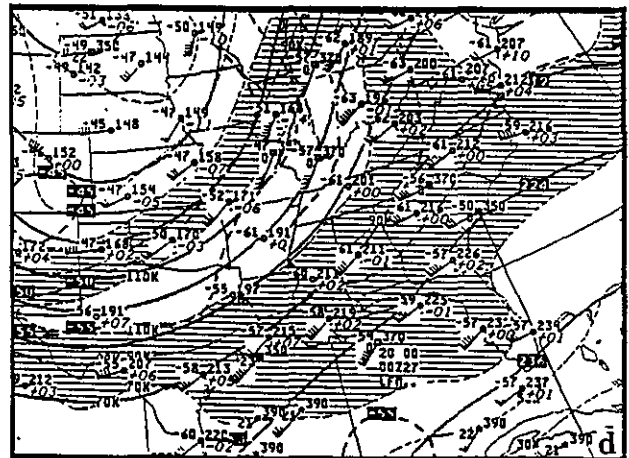
1200 UTC 25 NOV 1988 200 MB ANALYSIS



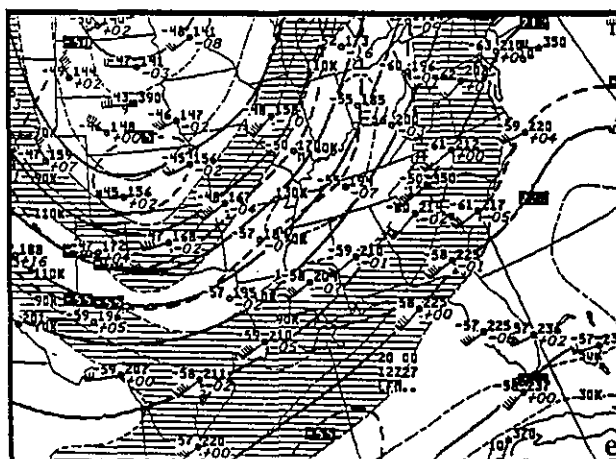
0000 UTC 26 NOV 1988 200 MB ANALYSIS



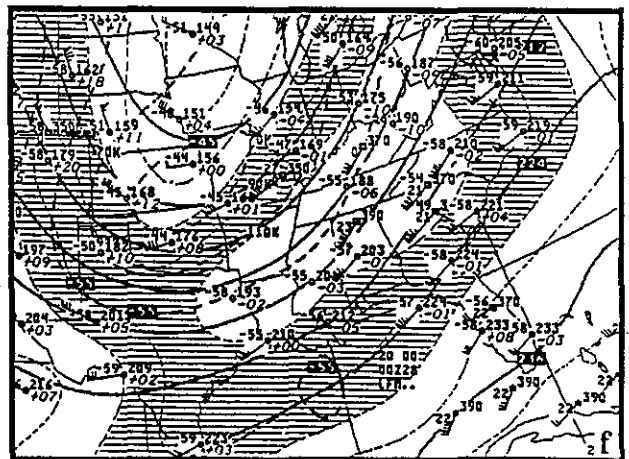
1200 UTC 26 NOV 1988 200 MB ANALYSIS



0000 UTC 27 NOV 1988 200 MB ANALYSIS

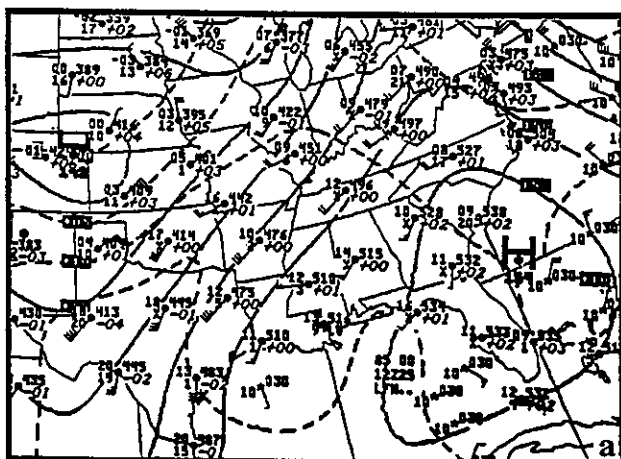


1200 UTC 27 NOV 1988 200 MB ANALYSIS

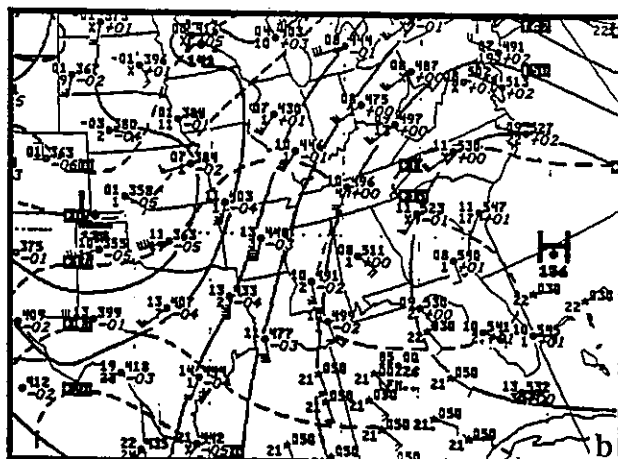


0000 UTC 28 NOV 1988 200 MB ANALYSIS

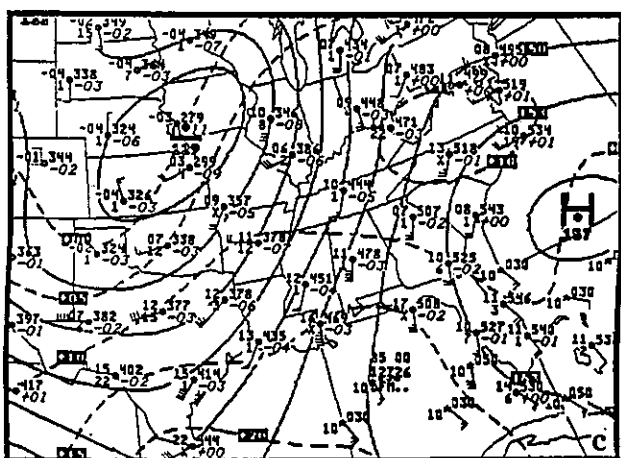
Figure 3. NWS 200 mb analyses charts valid at (a) 1200 UTC 25 November, (b) 0000 UTC 26 November, (c) 1200 UTC 26 November, (d) 0000 UTC 27 November, (e) 1200 UTC 27 November, and (f) 0000 UTC 28 November 1988.



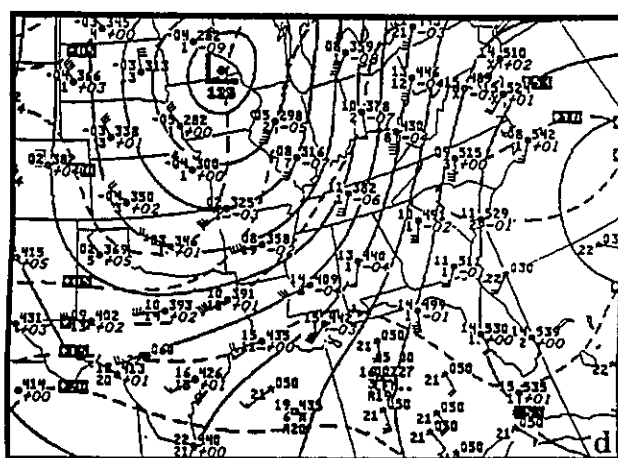
1200 UTC 25 NOV 1988 850 MB ANALYSIS



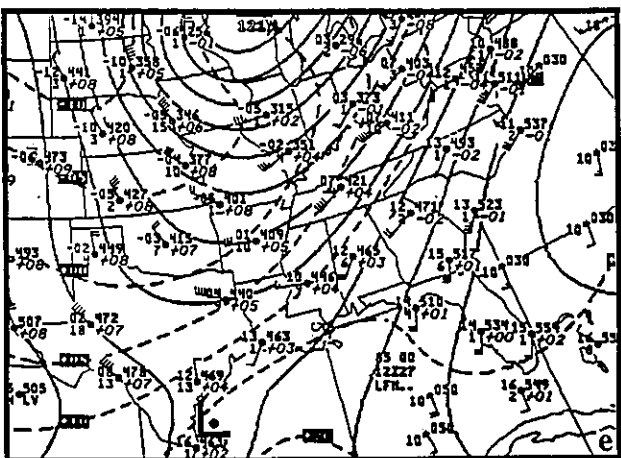
0000 UTC 26 NOV 1988 850 MB ANALYSIS



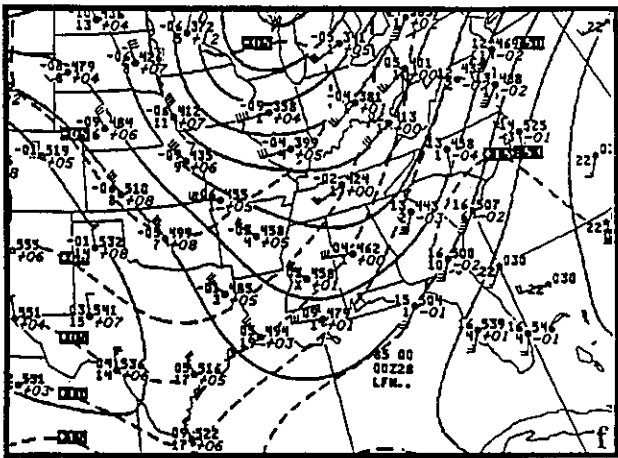
1200 UTC 26 NOV 1988 850 MB ANALYSIS



0000 UTC 27 NOV 1988 850 MB ANALYSIS

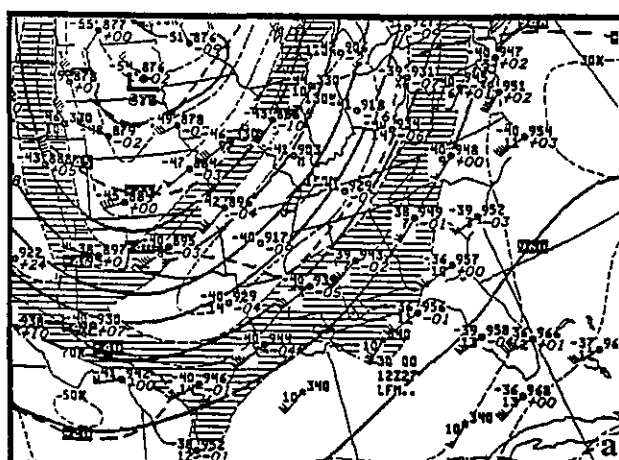


1200 UTC 27 NOV 1988 850 MB ANALYSIS

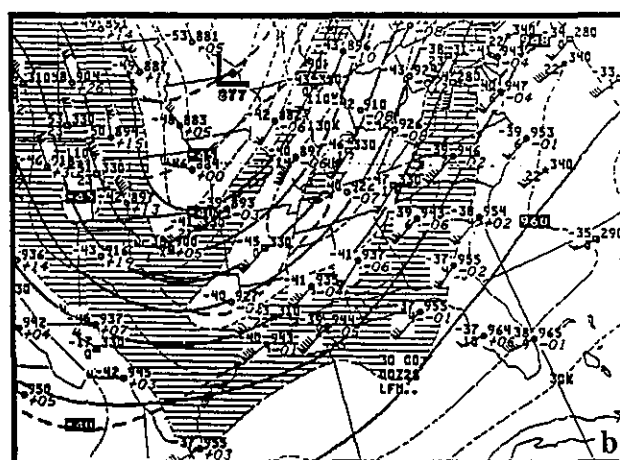


0000 UTC 28 NOV 1988 850 MB ANALYSIS

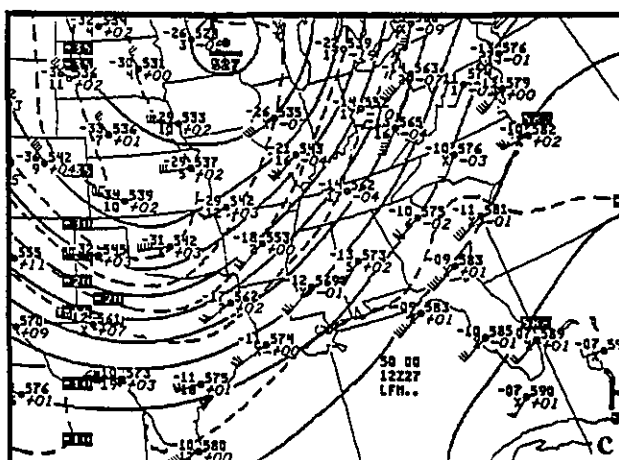
Figure 4. NWS 850 mb analyses charts valid at (a) 1200 UTC 25 November, (b) 0000 UTC 26 November, (c) 1200 UTC 26 November, (d) 0000 UTC 27 November, (e) 1200 UTC 27 November, and (f) 0000 UTC 28 November 1988.



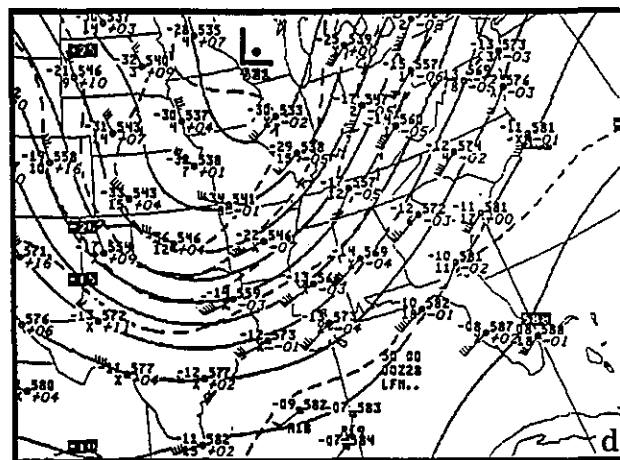
1200 UTC 27 NOV 1988 300 MB ANALYSIS



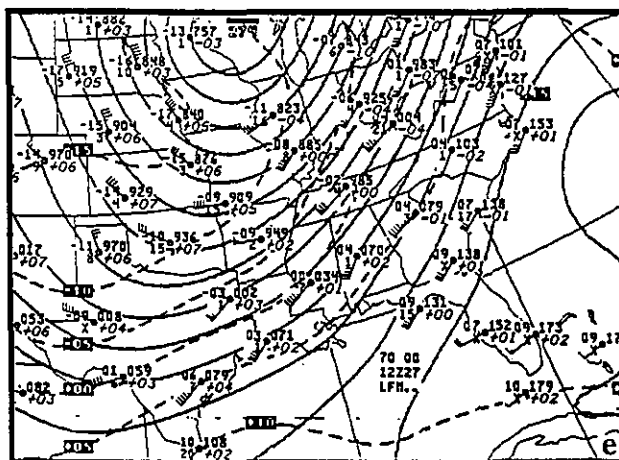
0000 UTC 28 NOV 1988 300 MB ANALYSIS



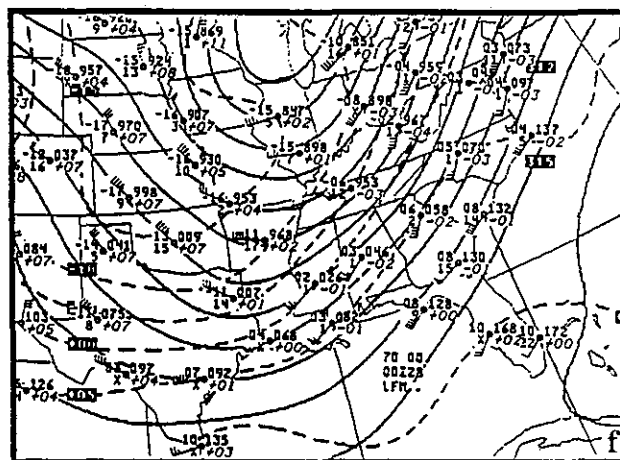
1200 UTC 27 NOV 1988 500 MB ANALYSIS



0000 UTC 28 NOV 1988 500 MB ANALYSIS



1200 UTC 27 NOV 1988 700 MB ANALYSIS



0000 UTC 28 NOV 1988 700 MB ANALYSIS

Figure 5. NWS 300, 500, and 700 mb analyses charts valid at (a,c,e) 1200 UTC 27 November 1988 and (b,d,f) 0000 UTC 28 November 1988.

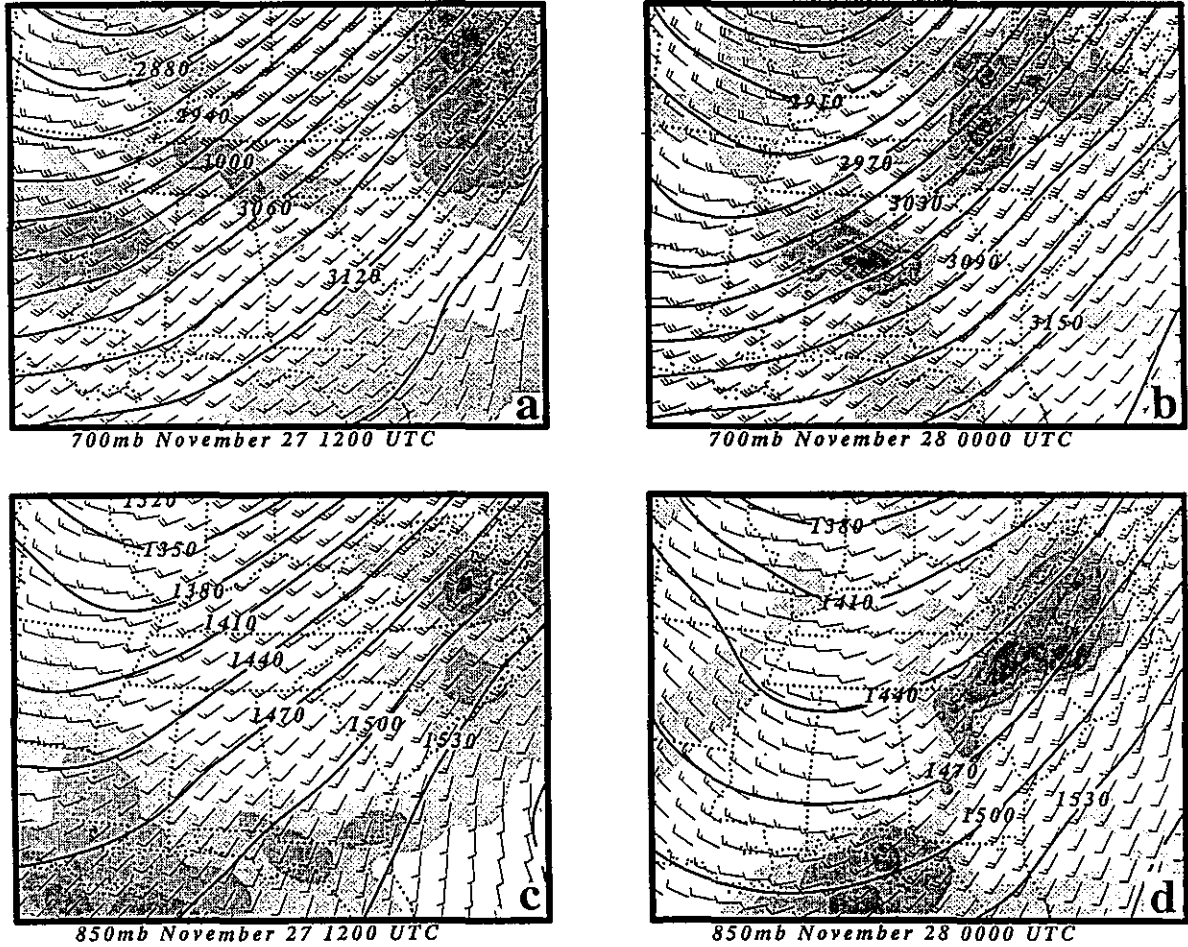


Figure 6. Flux convergence of mixing ratio (positive values shaded every 10^{-5} g/kg/s), heights (m), and wind barbs (long barb represents 10 ms^{-1} , short barbs, 5 ms^{-1}), objectively analyzed from rawinsonde data for (a) 700 mb field for 1200 UTC 27 November 1988, (b) 700 mb field for 0000 UTC 28 November 1988 (c) 850 mb field for 1200 UTC 27 November 1988, (d) 850 mb field for 0000 UTC 28 November 1988.

tropospheric wind vectors at Greensboro, North Carolina (GSO) and Athens, Georgia (AHN) indicate slightly *supergeostrophic* flow directed to the right across the geostrophic stream, while the vectors at Nashville, Tennessee (BNA) and Centerville, Alabama (CKL) indicate slightly *subgeostrophic* flow directed to the left of the geostrophic stream. This divergence of the mid-upper tropospheric flow increases to the level of the STJ circulation, and is superimposed on a highly confluent ageostrophic flow at the 700 and 850 mb levels, wherein there is significant horizontal warm and moist air advection (Fig. 6). Incidentally, the

850 mb confluent flow at 0000 UTC over the southern Appalachians is synonymous with a region of low-level cyclonic vorticity originally located over southeastern Texas and southern Louisiana at 1200 UTC which propagated into Georgia and Alabama by 0000 UTC.

Arguably the most important element from a forecasting perspective at 0000 UTC is the *absence of observed cyclonic maximum relative vorticity at 500 mb between the two jet streaks*, i. e., between BNA and AHN in Fig. 7. The cyclonic vorticity does increase however, between the two jet streaks

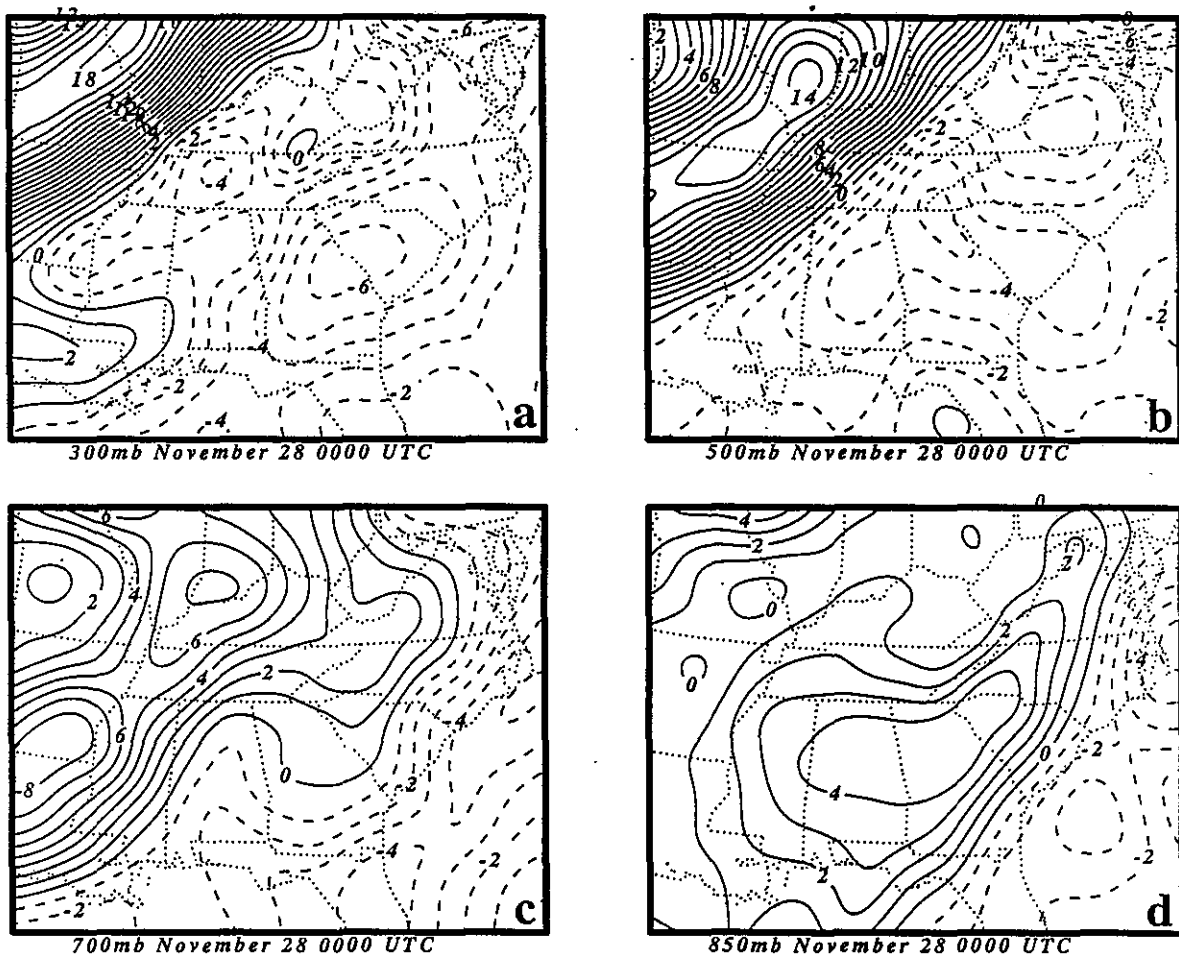


Figure 7. Observed relative vorticity (10^{-5}s^{-1}) valid at 0000 UTC 28 November 1988 for (a) 300 mb, (b) 500 mb, (c) 700 mb, and (d) 850 mb.

at higher levels. At 850 mb more of a cyclonic trough structure in the mass field has resulted in some cyclonic vorticity production between AHN and Centerville, Alabama (CKL), just west of the developing subgeostrophic region over the Appalachian Piedmont.

The low-level confluent and upper-level diffluent flow at 0000 UTC is situated in a region wherein very strong mid-level vertical wind shear is capped by a dramatic change in the vertical lapse rate. Vertical cross sections orthogonal and parallel to the PJ at 0000 UTC are depicted in Fig. 8. The southern cross sections orthogonal to the jet

(Peoria, Illinois (PIA) to Charleston, South Carolina (CHS) and Evansville, Indiana (EVV) to Jacksonville, Florida (JAX)) are most revealing. Note the extraordinary southeastward shift in the vertical wind shear zone between BNA and AHN and between Chattanooga, Tennessee (CHA) and Asheville, North Carolina (AVL). In each of the cross sections, the vertical slope of the jet and its associated baroclinic zone do not reflect a coupled mass/momentum system but one which is vertically *decoupled*, as indicated by the phase shift between the ageostrophic polar and subtropical jet streak circulations. Note that the mid-level vertical

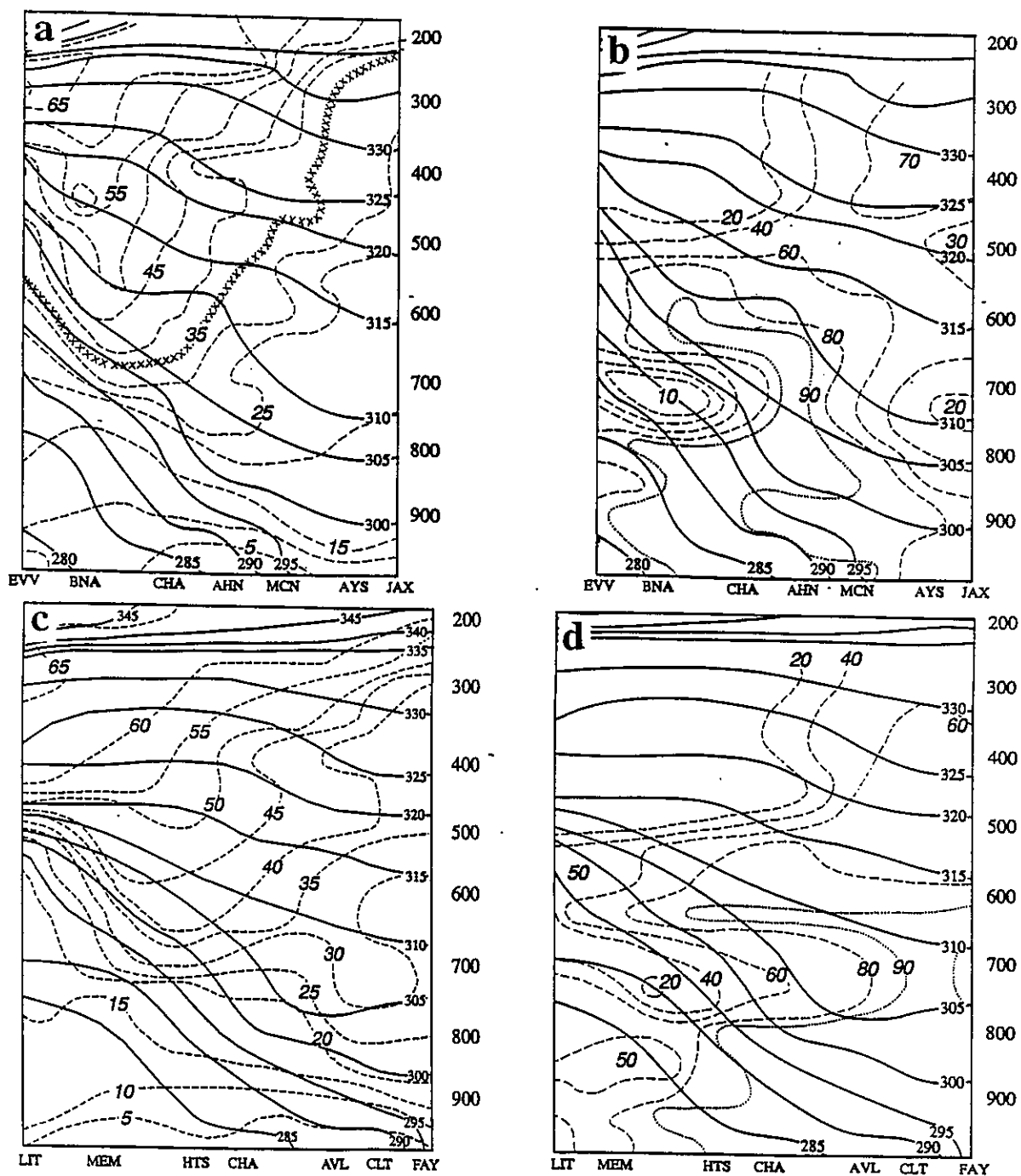


Figure 8. Subjectively analyzed vertical cross sections from Evansville, Indiana (EVV) to Jacksonville, Florida (JAX) of (a) potential temperature (solid lines in K) and isotachs (dashed lines in ms^{-1} except 35 ms^{-1} where crosses are used) and (b) potential temperature (solid lines in K) and relative humidity (dashed lines in %; except 90 % where dots are used) valid at 0000 UTC 28 November 1988. Included in the cross section are the approximate locations of NWS surface observation stations Nashville, Tennessee (BNA), Chattanooga, Tennessee (CHA), Athens, Georgia (AHN), Macon, Georgia (MCN), and Waycross, Georgia (AYS). (c,d) Same as (a,b) except vertical cross section extends from Little Rock, Arkansas (LIT) to Fayetteville, North Carolina (FAY). Additional surface observing stations are Memphis, Tennessee (MEM), Huntsville, Alabama (HTS), Chattanooga, Tennessee (CHA), Asheville, North Carolina (AVL), and Charlotte, North Carolina (CLT).

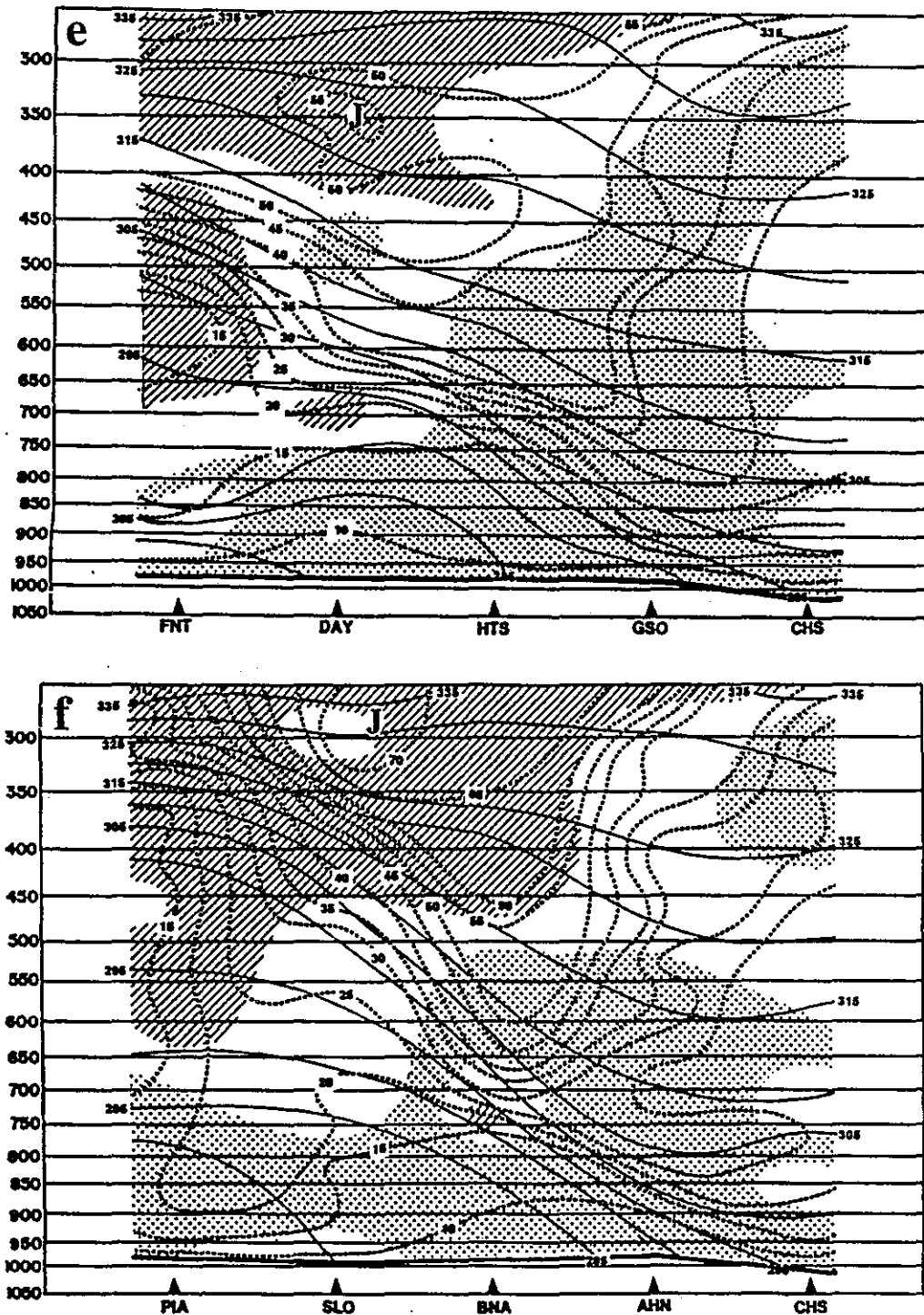


Figure 8 continued. (e) Subjectively analyzed vertical cross section from Peoria, Illinois (PIA) through Charleston, South Carolina (CHS) valid at 0000 UTC 28 November 1988 from rawinsonde data (from Funk, 1991). Isentropes are solid (K), isotachs are dashed (ms^{-1}), dot shaded areas represent dewpoint depressions $\leq 5^{\circ}\text{C}$, and cross hatched areas represent dewpoint depressions $\geq 30^{\circ}\text{C}$. (f) Same as (e) except from Flint, Michigan (FNT) to CHS.

wind shear zones lie well southeast of the polar jet core at 300 mb, which is in actuality beneath the subtropical jet core located above 250 mb in Fig. 8. Additionally, there is an adiabatic layer which slopes southwestward from southeastern West Virginia at ~450 mb to northwestern Georgia at ~650 mb directly within this vertical shear zone. This layer is indicative of a cold front aloft (CFA) which is downstream from the primary baroclinic zone associated with the polar front located over the Mississippi River Valley, and is likely the signal of the thermally indirect circulation about the STJ. A low-level jet cuts underneath and is orthogonal to the STJ's CFA which is located over the western Appalachian Mountains. A region of strong subgeostrophy corresponds with the entrance region of the PJ and the secondary subtropical CFA, particularly at 300 mb.

Furthermore, two layers of dry air can be seen in close proximity to the CFA over the western Appalachians.

Note that the cyclonic side of the STJ at 0000 UTC depicted in Fig. 3 is directly above the anticyclonic side of the PJ depicted in Fig. 5. This results in a layer of very cold air being superimposed upon a layer of very deep warm air yielding a dramatic change in the vertical lapse rate between the middle and upper troposphere. The unique thermodynamic structure which occurs over the Southern Appalachians is directly reflected by the large temperature lapse rates within the upper troposphere over the southern Appalachians and Gulf of Mexico coastal regions (Fig. 9). Note that most of the values lie between moist and dry adiabatic (Fig. 10). In other words, the atmosphere

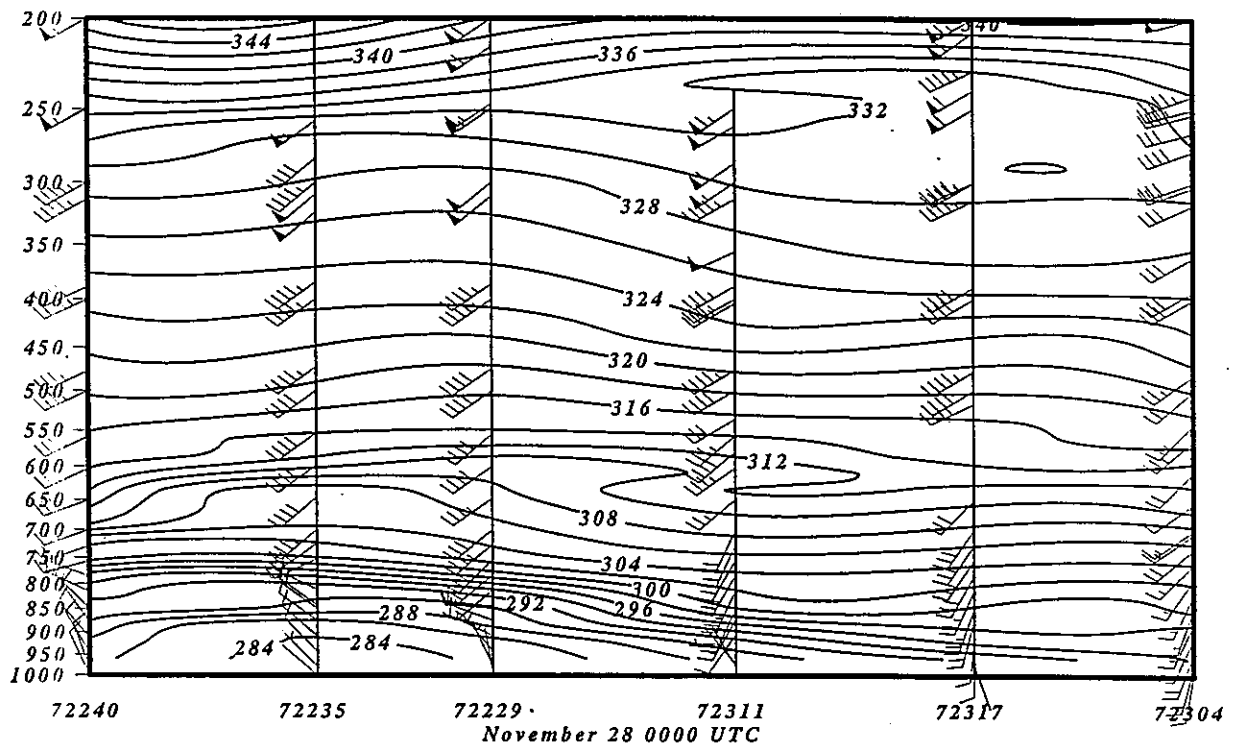


Figure 9. Observed vertical cross section of potential temperature (solid lines in K) and wind velocity (dashed lines in ms^{-1}) for the stations: Lake Charles, La (72240), Jackson, Ms (72235), Centerville, AL (72229), Athens, Georgia (72311), Greensboro (72317), and Cape Hatteras (72304), North Carolina valid at 0000 UTC 28 November 1988.

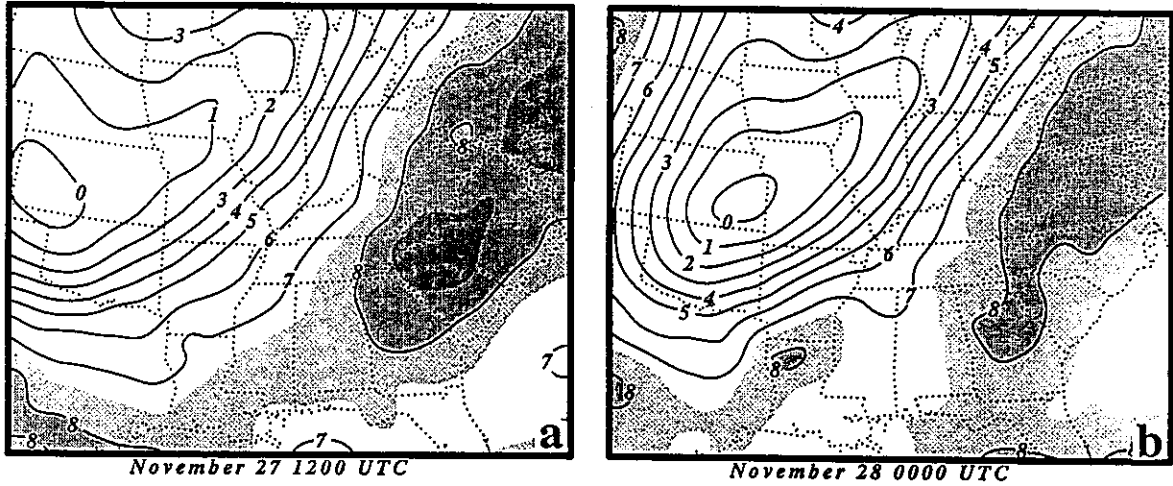


Figure 10. Objectively analyzed average vertical temperature lapse rate analysis (Kkm^{-1}) between 400-250 mb valid at (a) 1200 UTC 27 November 1988 and (b) 0000 UTC 28 November 1988.

is conditionally unstable in these regions. This alteration of the Brunt-Vaisala frequency in conjunction with the mid-upper tropospheric vertical wind shears over the same region indicates a very dramatic vertical variation of the Scorer parameter with height over the southeastern U.S. resulting in a deep wave duct (Lindzen and Tung 1976).

Figure 11 illustrates vertical cross sections of observed relative humidity from Mobile, Alabama (MOB) to GSO and from Tupelo, Mississippi (TUP) to Valdosta, Georgia (VLD) at 1200 UTC. Quite evident is the deep moist layer which extends to nearly 500 mb throughout most of this region, particularly over the Georgia and South Carolina Piedmont. The depth of this layer is evident in the sounding presented in Fig. 12 with near saturated conditions extending from near the surface to near 500 mb. This deep moist layer over Georgia, South Carolina, and North Carolina is still in place at 0000 UTC and is evidence for the likely coupling between the ageostrophic circulations associated with the polar jet entrance and subtropical jet exit regions.

Finally, Figs. 13-14 represent how the strong baroclinic zone accompanying the surface cold front is impeded in its eastward motion after 0000 UTC over the South Carolina, North Carolina, and Georgia Piedmont. Notice that the concentration of

pressure falls primarily between Charlotte, North Carolina (CLT) and Richmond, Virginia (RIC) increase during the period in which the northward transport of subtropical air and northward propagation of convection is occurring ahead of the surface cold front.

3.2 Simulated Duct Structure

Figure 15 depicts simulated cross sections of Richardson number, θ , and critical level from Montgomery, Alabama (MGM) to Richmond, Virginia (RIC) between 2200 UTC and 0200 UTC. The Richardson number is defined here as

$$R_i = \frac{g}{\theta} \frac{\partial \theta}{\partial z} \left\{ \left(\frac{\partial u}{\partial z} \right)^2 + \left(\frac{\partial v}{\partial z} \right)^2 \right\}^{-1} \quad (1)$$

Clearly evident in these vertical cross sections is the presence of a critical level. The critical level helps to maintain and support the simulated gravity waves with the simulated wave duct. The presence of such a pronounced wave duct allows both the

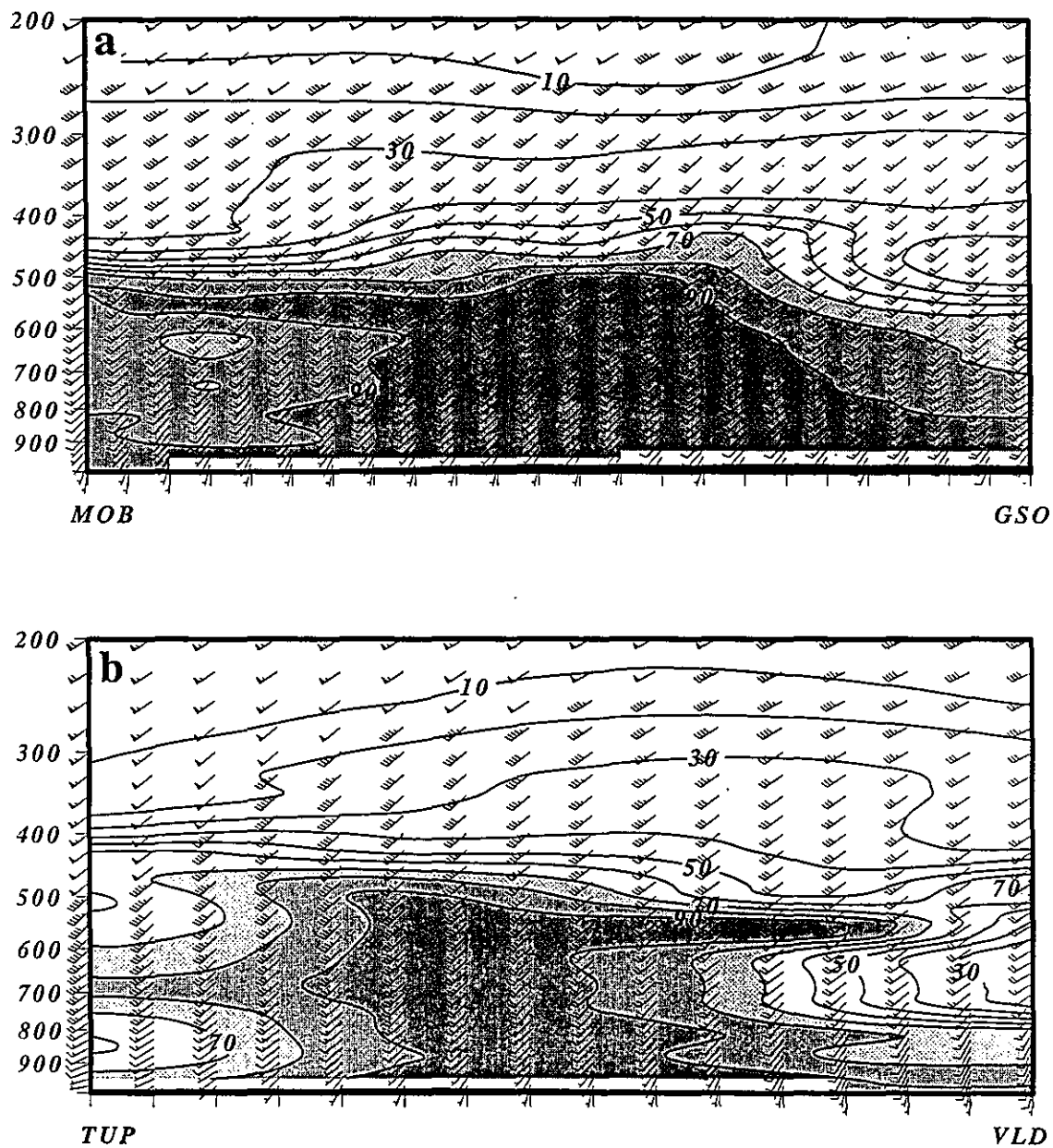


Figure 11. Vertical cross sections of initial state relative humidity (%), with values $\geq 70\%$ shaded, analyzed from observed NWS rawinsonde and surface data valid at 1200 UTC 27 November 1988 between (a) Mobile, Alabama (MOB) and Greensboro, North Carolina (GSO) and (b) Tupelo, Mississippi (TUP) and Valdosta, Georgia (VLD).

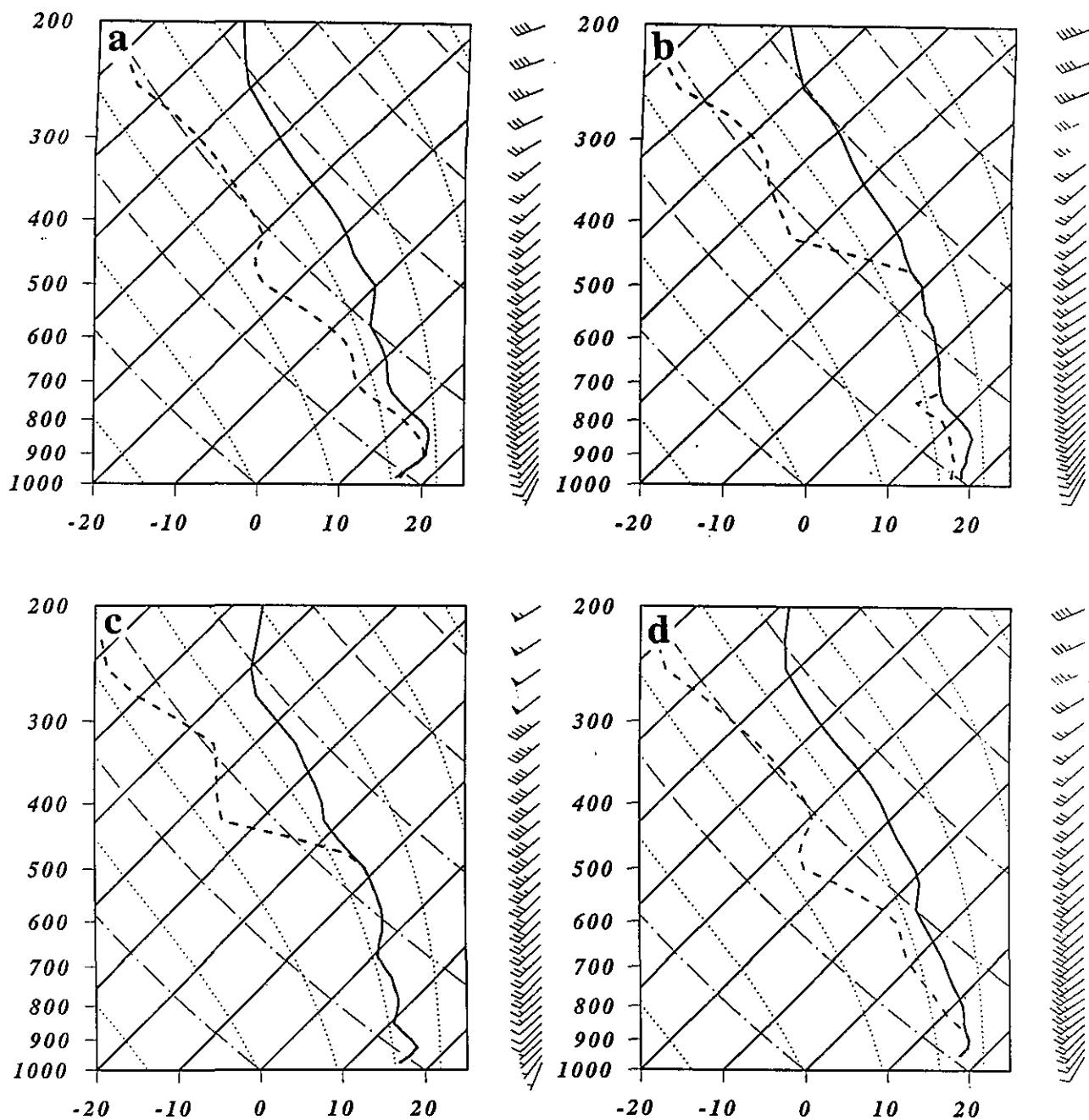


Figure 12. Vertical soundings of model initial data analyzed from observed NWS rawinsonde and surface data valid at 1200 UTC 27 November 1988 for (a) Charlotte, North Carolina (CLT), (b) Greensboro, North Carolina (GSO), (c) Columbia, South Carolina (CAE), and (d) Centerville, Alabama (CKL).

simulated and observed gravity waves to be trapped and therefore not propagate vertically. The wave duct extends over a synoptic scale area which is analogous to that observed from rawinsonde data (Fig. 9). Since both the simulated and observed gravity waves last for many wave cycles, the duct should necessarily meet the four-part criteria outlined by Lindzen and Tung (1976). Necessary for the maintenance of prolonged internal modes there must be proof that the wave energy is, to a large extent, trapped as dictated by the wave dispersion relation from Uccellini and Koch (1987),

$$l^2 = k^2 \left[\left(\frac{N}{\omega} \right)^2 - 1 \right], \quad (2)$$

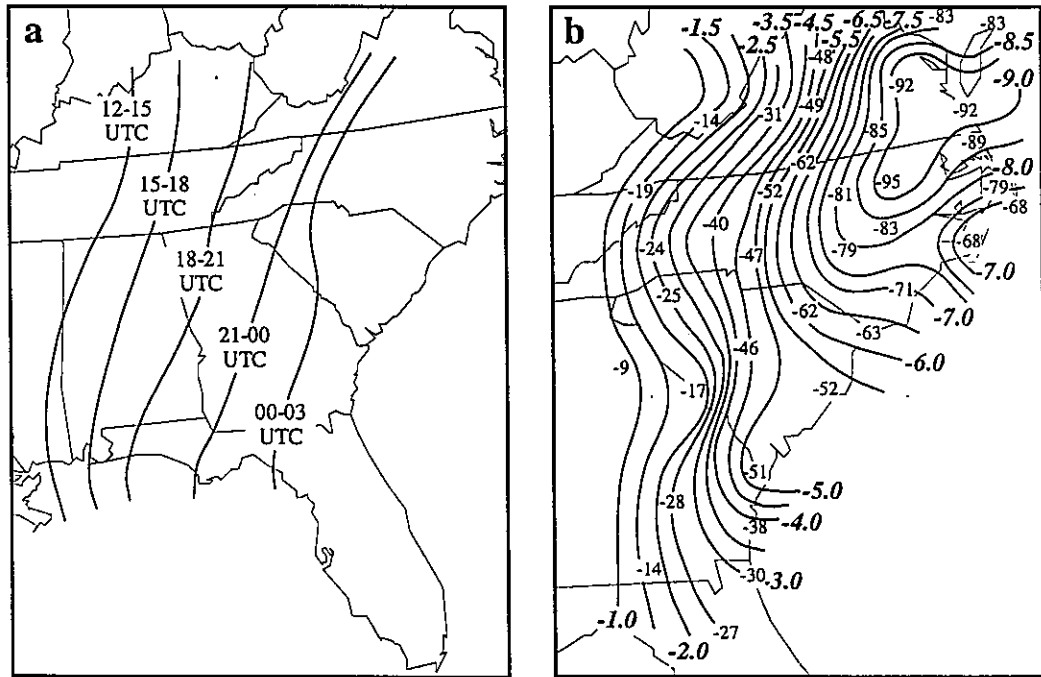
where ω is the intrinsic wave frequency and is

defined by

$$\omega = k(U - c). \quad (3)$$

Here, N is the Brunt-Vaisala frequency and U is the magnitude of the wave motion the wind velocity in the direction of wave propagation. Note that the above equations require values of l be imaginary, $\omega > N$, for evanescent wave modes and real, $\omega < N$, for vertically propagating modes.

We will now examine the simulated stratification and vertical wind shear profiles to determine if they are consistent for the maintenance of a wave duct, thus providing additional proof that the simulated gravity waves are similar in character to those observed in nature. The first criterion requires that a layer of strong static stability exists. This is evident as a stable layer is present along the path of the cross sections depicted in Fig. 15. This very deep layer extends from near 850 mb where θ values are ~ 292 K to near 350 mb where θ



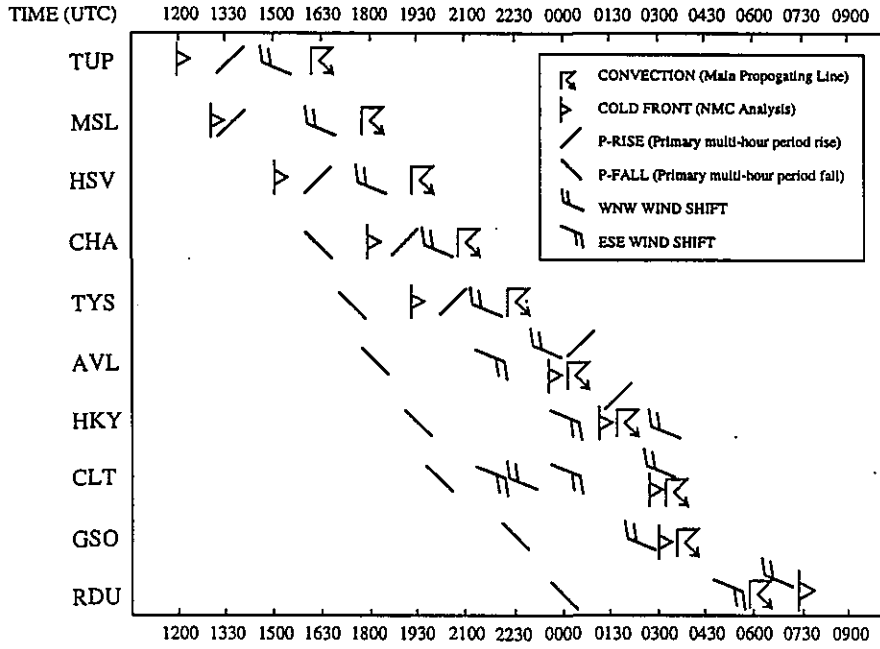


Figure 14. Time line of observed convection, cold front, mean sea level pressure rises and pressure falls as well as surface wind shifts for the region between Tupelo, Mississippi (TUP) and Raleigh-Durham, North Carolina (RDU) for the period from 1200 UTC 27 November 1988 through 0900 UTC 28 November 1988.

values are ~ 330 K. The low-level part of the inversion is even stronger over the western piedmont of the Carolinas and Virginia with low-level theta values ~ 288 K accompanying the dammed pool of cold air. Such a deep inversion with average static stability values $> 8\text{K}/100\text{mb}$ ($N \sim .025\text{s}^{-1}$) and depth values ~ 7 km is favorable for the maintenance of internal gravity waves with high phase velocities as dictated by the following equation from Lindzen and Tung (1976):

$$D > \frac{\pi}{2} \frac{(c - U^*)}{N} \quad (4)$$

where U^* is the wind velocity in the direction of wave propagation. The second necessary criterion is implicitly met because the simulated depth and static stability indicate a wave phase velocity consistent with both simulated and observed waves with a phase velocity of $\sim 30\text{ ms}^{-1}$. This value is

actually a slight underestimate for the faster moving "secondary" modes over the piedmont which propagate at $\sim 35\text{ ms}^{-1}$. Specifically, the second criterion requires that the wave duct be thick enough to contain 25% of the vertical wavelength corresponding to the phase velocity as dictated by the following relation:

$$C_d = \frac{2}{\pi} \left\{ \frac{gD(\theta_T - \theta_B)}{\theta} \right\}^{1/2} \quad (5)$$

where g is the gravitational acceleration, θ refers to potential temperature and θ_T , θ_B , θ refer to top of layer, bottom of layer, and layer mean value, respectively. This duct clearly does pass the test when one assumes values of $c \sim 32.5\text{ ms}^{-1}$, $N \sim .02\text{ s}^{-1}$, and $U^* \sim 20\text{ ms}^{-1}$ producing a minimum value of $D \sim 800\text{ m}$. Since the duct actually exceeds 7 km in depth it is several times deeper than is theoretically

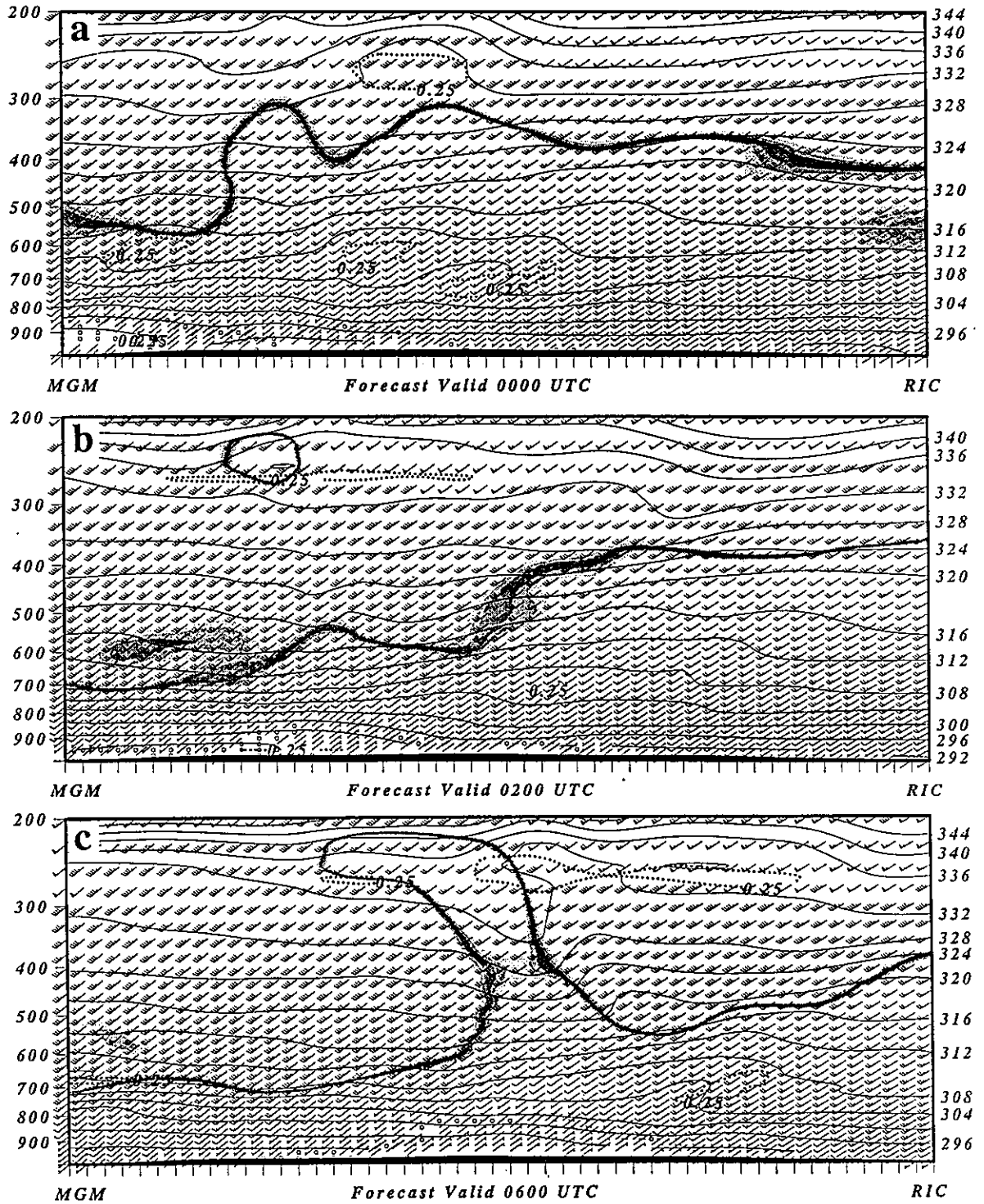


Figure 15. GMASS coarse mesh simulated vertical cross sections of potential temperature surfaces (thin solid lines every 2K), Richardson Number (dotted lines encircling values less than .25), and critical level from 27-28 November 1988. Cross sections are taken in the direction of gravity wave propagation. Shaded contour represents the critical level ($c \sim 31 \text{ ms}^{-1}$).

necessary and would therefore easily accommodate a wide range of U^* values.

In order to determine if the third criterion is met, the deep stable layer should be compared to the average static stability of the unstable upper tropospheric layer extending from ~350 mb to ~225 mb of $\sim 1.5\text{K}/100\text{ mb}$ which is fully less than 20% as stable as the underlying layer. This satisfies the third criterion wherein a conditionally unstable layer above the stable layer significantly aids in the reflection of vertically propagating wave energy. The reflection of wave energy within the unstable layer can be increased even further by the near existence of a critical level where the wave phase velocity (c) is equal to the wind velocity in the presence of low Bulk Richardson Number (values < 1.0 (Schneider, 1990)) (Fig. 15).

These criteria are met for the gravity waves by virtue of the fact that near 325 mb the wind velocity above the inversion is $\sim c$ and the bulk Ri values are $< .3$ within the very unstable layers where the static stability is $\sim 1\text{Kkm}^{-1}$. Furthermore, it should be noted that the "primary" CISK-generated gravity wave acts to aid in the maintenance of the duct by perturbing the mass field thus producing the anomalously slow wind velocities within the upper tropospheric conditionally unstable layer in a manner analogous to that simulated by Clark and Peltier (1984) for standing mountain wave phenomena which they termed "self-induced critical layers".

Finally, the fourth criterion from Lindzen and Tung specifies that a critical level does not exist within the lower stable layer which is true during the period of coherent wave propagation. Wave trapping occurs when the vertical wave numbers are negative. This can only occur when the Brunt-Vaisala Frequency is less than the wave's intrinsic frequency. This is most likely to occur within the upper tropospheric layer of extremely low values of static stability where the Brunt-Vaisala Frequency is extremely low, i. e., $\sim < .004$. Calculations employing values of horizontal wave number assuming a wavelength of $\sim 200\text{ km}$, N values simulated within the upper troposphere, and U values within the upper troposphere indicate that

the intrinsic frequency is greater than the Brunt-Vaisala Frequency in the upper troposphere indicating a favorable environment for wave trapping.

3.3 Summary of Synoptic Scale Structure

In summary, the synoptic scale environment as defined by 12 hourly rawinsonde observations 6-18 hours preceding the Raleigh tornado outbreak contain the following key features:

- 1) A polar jet streak (PJS) entrance region and anticyclonic shear zone is located over the southeastern U. S., and is juxtaposed to the exit region of a STJ.

- 2) A transverse thermally-direct (indirect) circulation extends throughout much of the troposphere (stratosphere) with cross-stream subgeostrophic (supergeostrophic) flow over the Tennessee River Valley and Gulf of Mexico (southern Appalachian Piedmont).

- 3) Virtually no positive vorticity advection occurs over the southeast within the middle troposphere. However, increasing positive vorticity advection (PVA) does occur within the upper troposphere and lower stratosphere.

- 4) Deep relatively weak warm air advection, weak directional vertical wind shear, and substantial vertical wind velocity shear occurs over the southeast.

- 5) Deep moisture advection over much of the southeastern U. S. accompanies a strong low-level southerly ageostrophic jet.

- 6) The cyclonic side of the STJ is collocated with the anticyclonic side of the PJ.

- 7) A pronounced wave duct which extends from Louisiana to North Carolina is in place where the polar and subtropical jet streaks merge. The wave duct meets all four necessary criteria for gravity wave maintenance as proposed by Lindzen and Tung (1976) over a synoptic-scale region.

8) A cold front aloft (CFA) is suggested in close proximity to the ageostrophic flow accompanying the STJ and is accompanied by substantial vertical wind shear over and just west of the Appalachian Mountains.

9) Wedges of dry air exist in proximity to the cold front aloft.

4. Hydrostatic Mesoscale Dynamics

In this section of the report we will take advantage of both asynoptic observations and mesoscale numerical simulation output to define a four-stage process which organized the meso- β scale environment for tornadogenesis over North Carolina and Virginia after 0600 UTC on 28 November 1988. These four stages include: 1) Stage A - Genesis of the Georgia mesocyclone. 2) Stage B - A mesoscale wind surge/mass flux divergence region forced by geostrophic adjustment. 3) Stage C - Propagation and intensification of the Georgia mesolow/low-level jet via wave-CISK mechanism. 4) Stage D - Rear inflow jet descent, buoyancy, and the development of rotation near RDU.

4.1 Stage A - Genesis of the Georgia Mesocyclone: Observations

Figure 16 depicts high resolution mean sea level pressure (MSLP) subjectively analyzed from NWS surface analyses valid at 1200, 1500, and 1800 UTC, 27 November 1988. This sequence illustrates the organization of four mesoscale pressure perturbations into a surface mesolow over southwestern Georgia which is discernible by 1900 UTC. The first mesotrough (P_1) accompanies the strong primary cold front located between northern Mississippi and western Kentucky at 1200 UTC. This feature propagates eastward at 20-25 ms^{-1} and is not strongly connected with the active convection located behind the cold front around approximately 1500 UTC. Perturbation P_1 moves from northeastern Mississippi into north central Alabama and east central Tennessee during the six-hour period between 1200 UTC and 1800 UTC, and is associated with strong northwest to southeast low-level wind shear across the front. Mesotrough P_2 is located over southeastern Louisiana at 1200 UTC and represents a wave on a second, weaker

cold front which is only very slowly propagating eastward over the western Appalachian Mountains. P_2 is associated with convection for the entire period as it propagates northeastwards at $\sim 20 \text{ ms}^{-1}$, and is located over southeastern Alabama near Dothan (DHN) at 1800 UTC. Northerly (southerly) surface flow to the north and west (south and east) of P_2 produce a region of concentrated surface vorticity along the Alabama and Florida Gulf Coasts by 1800 UTC. P_3 is associated with an east-west oriented mesotrough which is located over southeastern Alabama and southwestern Georgia at 1200 UTC. It represents the leading edge of the cold air outflow from convection accompanying the secondary slow-moving cold front pressing southeastward across eastern Alabama and western Georgia between 1200 UTC and 1500 UTC. By 1500 UTC, new convection develops over the Florida Panhandle accompanying this outflow boundary which results in heavy rainfall at Tallahassee, Florida (TLH). This feature acts to increase the southerly flow ahead of P_2 . Finally, by 1500 UTC, a mesohigh (P_4) forms accompanying the cold air outflow from convection located ahead of the weak secondary cold front in northwestern Georgia. This mesohigh builds southwestwards acting as a block to the eastward propagation of features over Georgia as well as producing cool northeasterly surface flow, thus increasing the lower tropospheric vorticity and surface frontogenesis ahead of P_1 , P_2 , and P_3 . P_4 represents the southern extension of a cool surface ridge which builds southwestwards from the North Carolina Piedmont as it strengthens due to evaporative cooling associated with overrunning precipitation. Eastward advancement of the shallow pool of cool air is prohibited by the dominant south/southeasterly flow around a synoptic scale high pressure area located off the Carolina coast. The quasi-stationary front is analyzed as the cold front located over central Georgia at 1800 UTC in the NWS analyses. All four mesoscale pressure perturbations either accompany or are associated with pre-existing frontal convection as is apparent from the 1735 UTC NWS radar analysis (Fig. 17). Figure 18 shows surface streamline analyses valid from 1700 UTC through 2000 UTC. One notes a defined

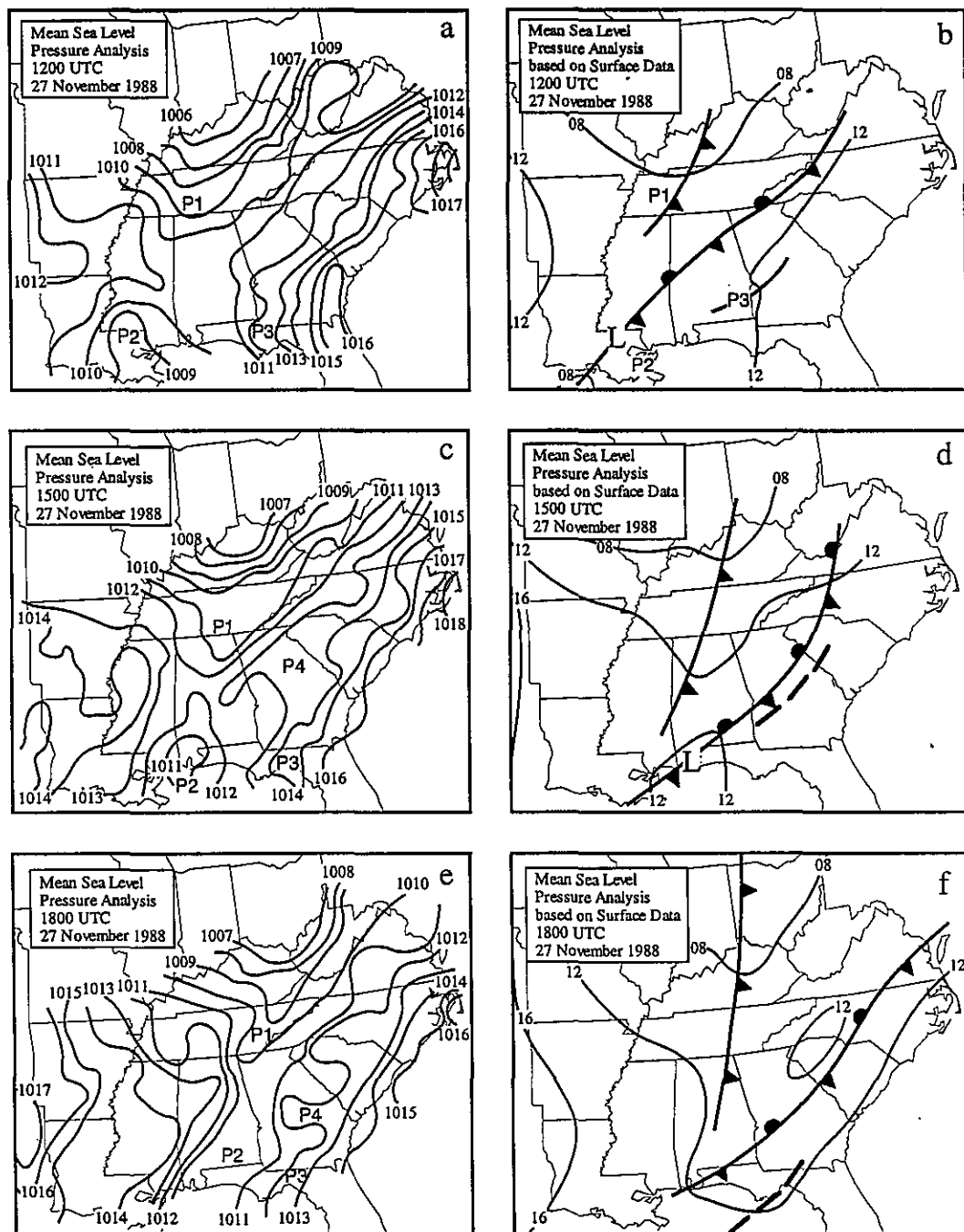


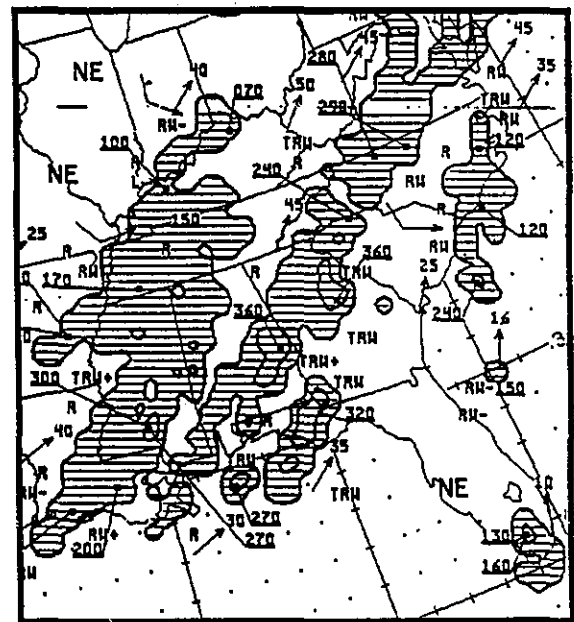
Figure 16. NWS surface three-hourly mean sea level pressure analysis charts valid at (a) 1200, (c) 1500, and (e) 1800 UTC 27 November 1988 and high resolution mean sea level pressure (mb) analyses based on three-hourly NWS surface data valid at (b) 1200, (d) 1500, and (f) 1800 UTC 27 November 1988. Frontal positions denoted by conventional symbols. Dashed lines in figures (d) and (f) represent outflow boundaries.

consolidation of the four mesoscale pressure perturbations by 2000 UTC near Fort Benning, Georgia (LSF). Present in Fig. 19 is a well-defined mesocyclone located over southwestern Georgia by 2000 UTC southwest of the strong thermal/moisture boundary accompanying the stalled cold front. The confluent circulation represents the center of several different air masses including: 1) Maritime tropical air over east-central Georgia and the Atlantic Coastal Plain with temperatures greater than 25°C and dewpoints in excess of 20°C. 2) Dammed cool moist air to the northwest of the well-defined surface front, covering northeastern Georgia, western South Carolina, and western North Carolina with temperatures ~15°C and dewpoints ~10°C. 3) Cool dry air located to the northwest of the Georgia mesocyclone over southeastern Tennessee, northwestern Georgia, and southeastern Alabama with temperatures ~15°C and dewpoints ~5°C, and 4) Relatively hot and somewhat dryer air most likely of Mexican origin located over extreme southern Georgia.

An interesting feature is the shallow surface ridge behind the piedmont front extending from southwestern Virginia through northeastern Georgia. This feature essentially acts as a formidable block which must be removed if the Georgia mesocyclone is to propagate northeastwards towards RDU. Additionally, two distinct mesoscale convergence regions are established by the intersection of: 1) the northerly surface flow associated with P_2 and the southerly surface flow associated with P_3 and 2) the westerly surface flow associated with P_1 and the easterly surface flow associated with P_4 resulting in confluence maxima within the Georgia mesocyclone.

4.2 Stage A - Genesis of the Georgia Mesocyclone: Simulation Results

Figure 20 depicts the time evolution of the coarse mesh 850 mb wind vectors, isotachs, and



1735Z 27 NOV 1988 RADAR SUMMARY

Figure 17. NWS MDR summary valid at 1735 UTC 27 November 1988.

MSLP from 1600 to 2000 UTC. At 1600 UTC, during the genesis of simulated precipitation, weak signals of all four analyzed mesoscale perturbations can be seen. These include two weak confluent zones in the 850 mb wind fields over Mississippi and Alabama corresponding to P_1 and P_2 , as well as pressure troughs corresponding to P_1 , P_2 , and P_3 and a mesoridge over northern Georgia corresponding to P_4 . Also apparent is the north-south variation in southerly wind flow and pressure over the Florida Panhandle accompanying P_3 . By 1800 UTC the convectively-induced mass adjustments have amplified the wind and pressure perturbations. Most notable are the deepening of all three mesotroughs accompanying P_1 , P_2 , and P_3 resulting in increased ageostrophic low-level flow, particularly the north-northwesterly flow behind P_1 and P_2 and the southerly flow ahead of P_2 and accompanying P_3 . The primary effect of P_4 is to increase the easterly flow north of the surface mesotroughs, thus producing two low-level jet maxima, one over the westernmost part of the Florida Panhandle which is comprised primarily of

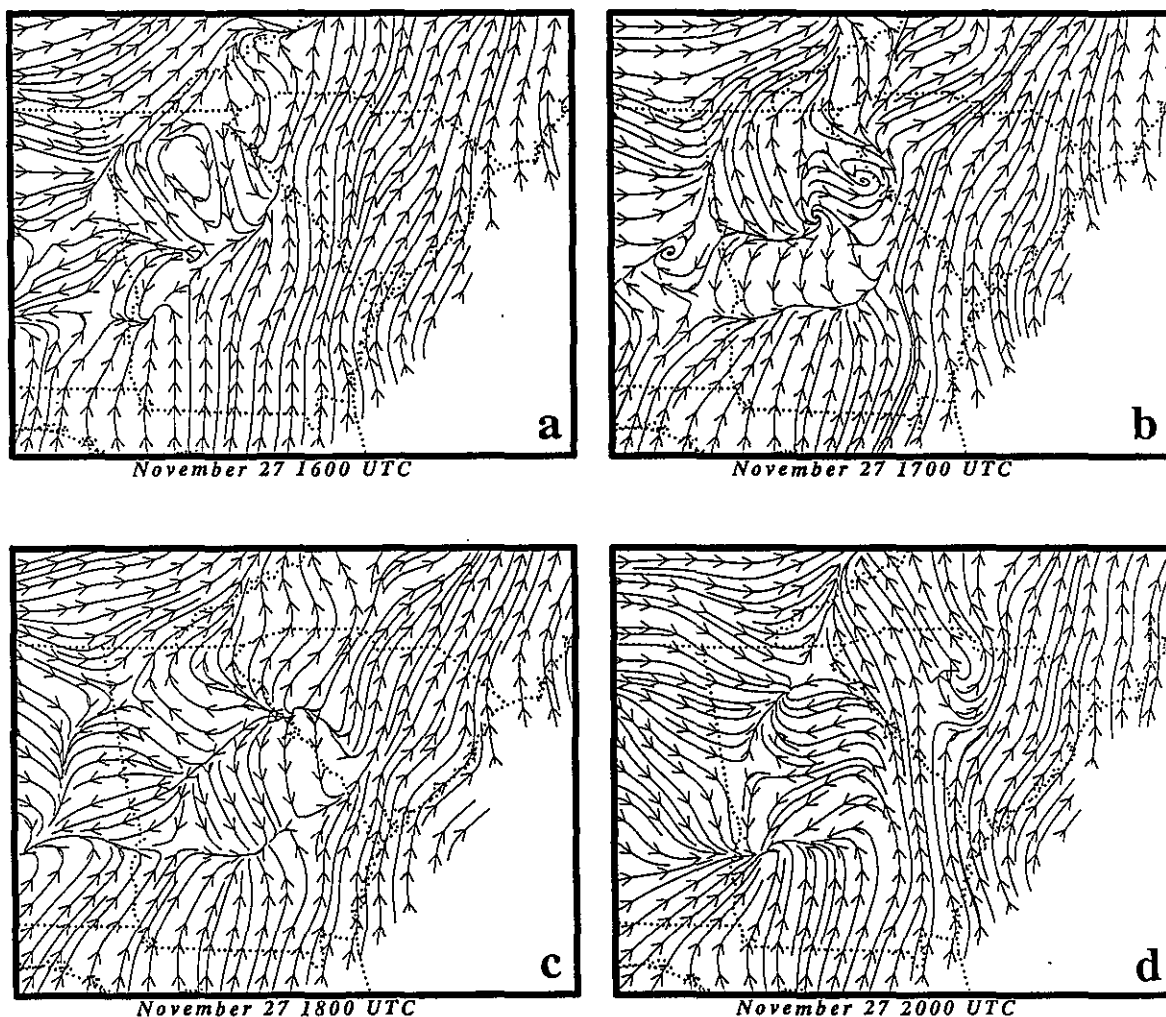


Figure 18. Objective surface streamline analyses based upon hourly NWS surface data valid at (a) 1600, (b) 1700, (c) 1800, and (d) 2000 UTC 27 November 1988.

southerly momentum and a second just west of Columbia, South Carolina which is comprised of both southerly and easterly momentum. By 2000 UTC, these two low-level jet maxima become the forcing mechanisms for the genesis of propagating wave-CISK features which move northeastwards along the piedmont front after the mesoridge (P_4) weakens. These features eventually move orthogonal to the pressure perturbations responsible for their genesis. Additionally, by 2000 UTC, the mass adjustments generated by wave-CISK have intensified the meso circulations

accompanying P_1 , P_2 , and P_3 across northeastern Mississippi, all of Alabama, southeastern Louisiana, northwestern Florida, and southwestern Georgia resulting in a well-organized cyclonic circulation which becomes the simulated analog to the analyzed Georgia mesocyclone.

The process by which wave-CISK amplifies these pressure perturbations and produces a low-level vorticity maximum can be better illustrated through vertical cross sections of the simulated convectively-induced mass adjustments occurring along the Gulf Coast (Fig. 21). At 1600 UTC the

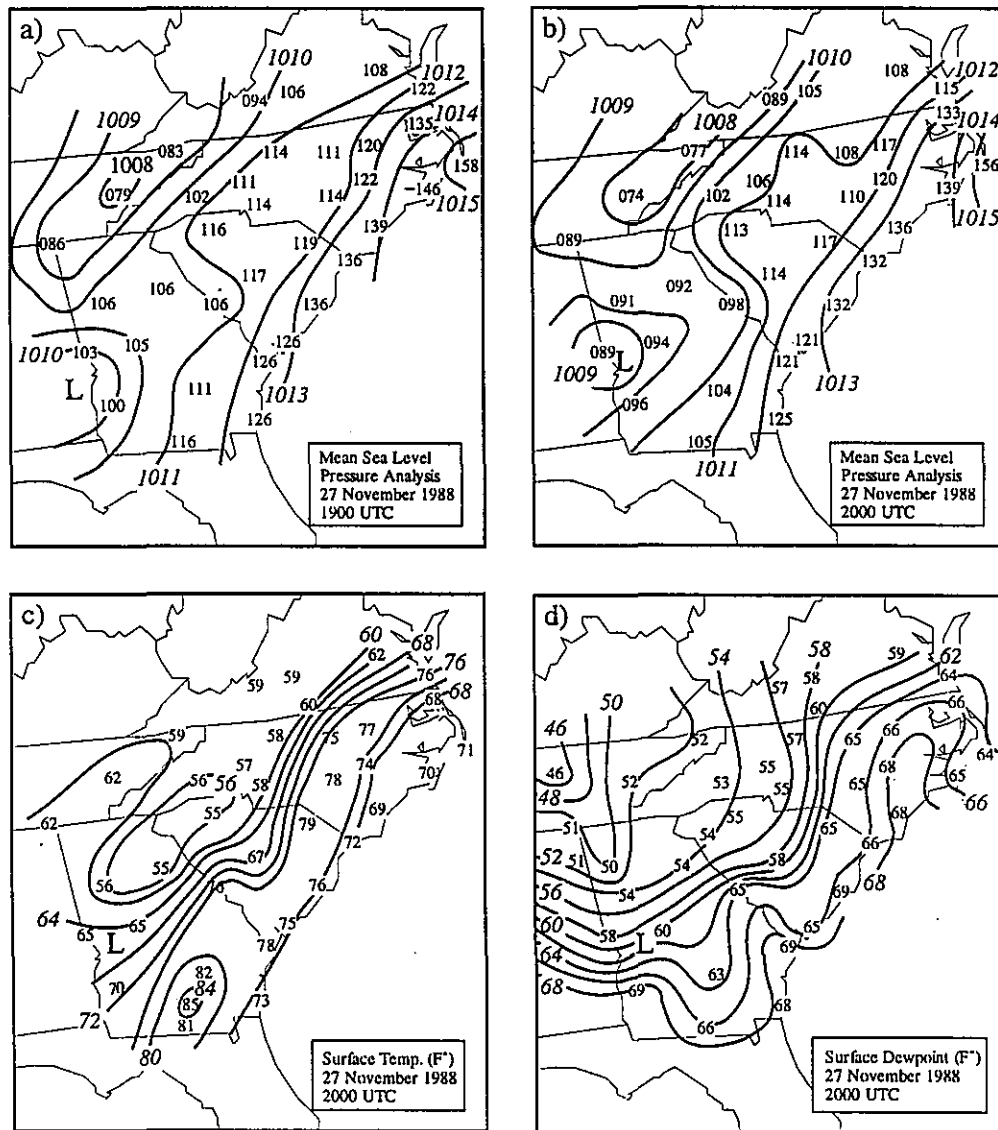


Figure 19. High resolution mean sea level pressure analyses (mb) based on NWS hourly surface data valid at (a) 1900 and (b) 2000 UTC 27 November 1988. High resolution (c) surface temperature (°C) analysis and (d) surface dewpoint (°C) analysis based on NWS hourly surface data valid at 2000 UTC 27 November 1988.

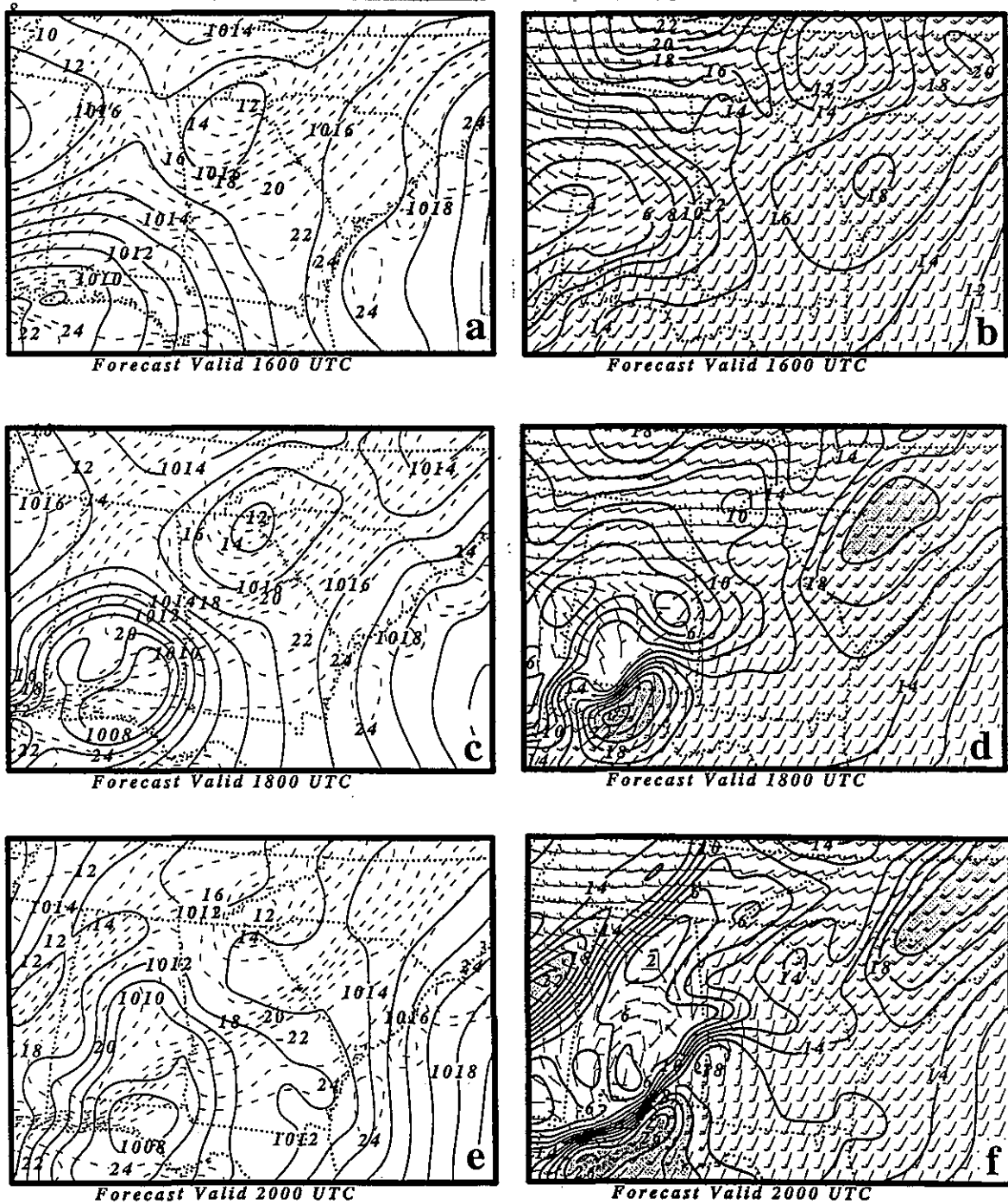


Figure 20. GMASS coarse mesh simulated mean sea level pressure (mb) and temperature (°C) valid at (a) 1600, (c) 1800, and (e) 2000 UTC 27 November 1988. GMASS coarse mesh simulated 850 mb wind vectors and isotachs (ms⁻¹) valid at (b) 1600, (d) 1800, and (f) 2000 UTC 27 November 1988.

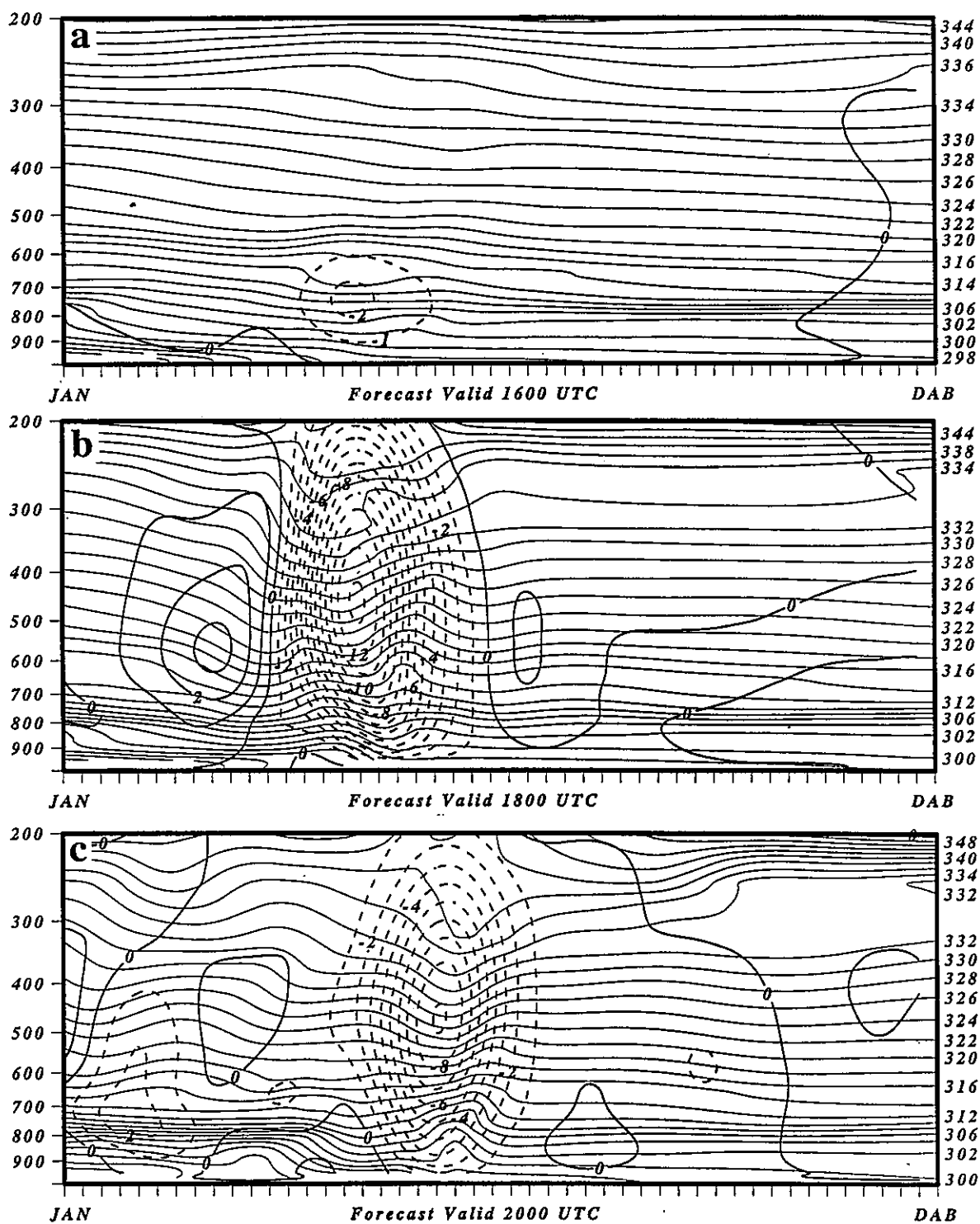


Figure 21. GMASS coarse mesh simulated vertical cross sections of potential temperature (thin solid lines in K) and vertical velocity (positive values are thick solid lines and negative values are thick dashed lines in 10^{-2} mb^{-1}) from Jackson, Mississippi (JAN) to Daytona Beach, Florida (DAB) valid at (a) 1600, (b) 1800, and (c) 2000 UTC 27 November 1988. Same for horizontal wind velocity (thick lines with shading of values greater than 40 ms^{-1}) valid at (d) 1600, (e) 1800, and (f) 2000 UTC 27 November 1988.

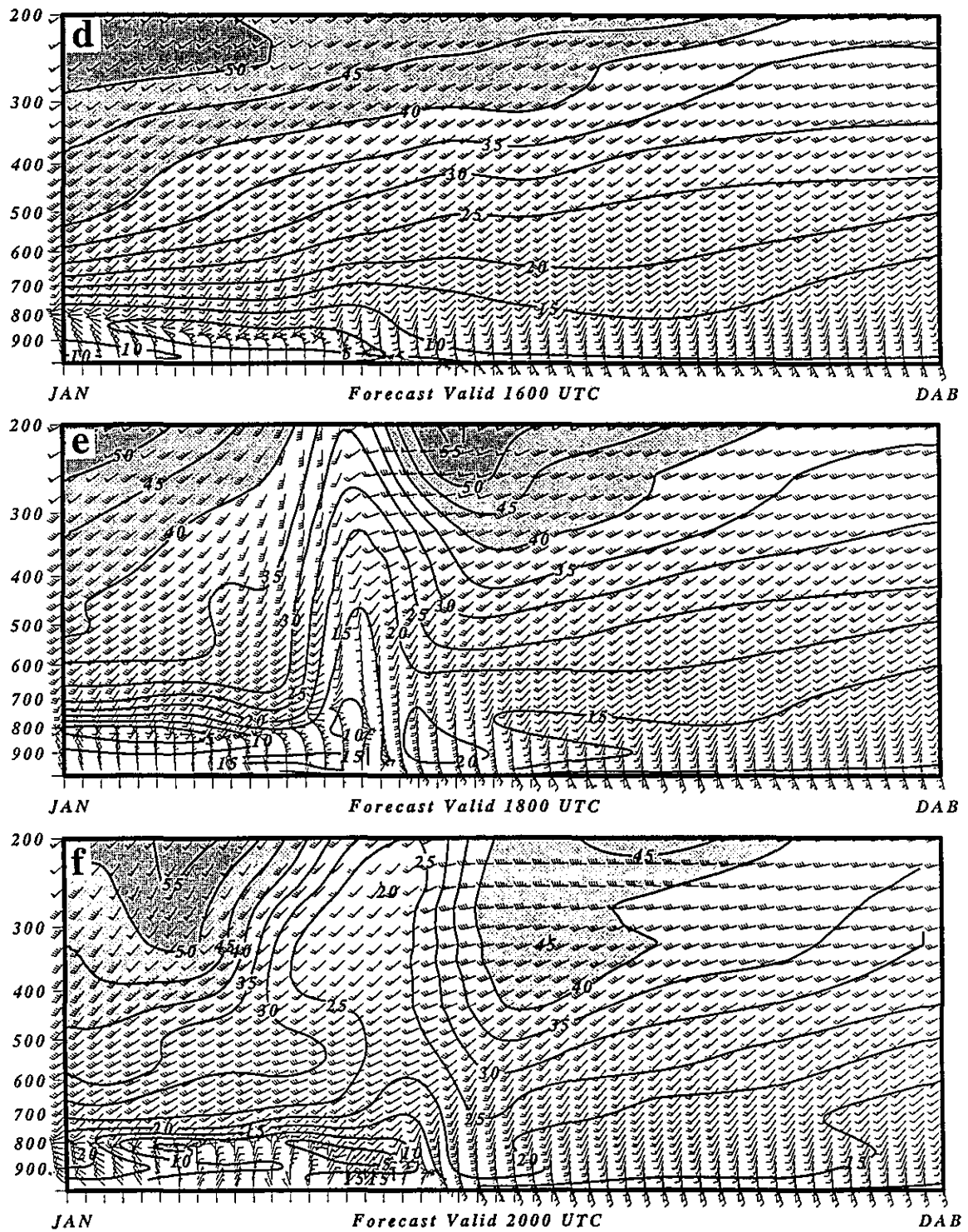


Figure 21 (Continued)

isentropes over the western part of the cross section from eastern Mississippi to western Alabama slope downward within a region of relatively weak ascent which is representative of the thermally-direct entrance region circulation of the PJS. Along the leading edge of this circulation, incipient convectively-induced ascent maxima are developing over southern Alabama and the Florida Panhandle. By 1800 UTC the diabatic heating becomes deeper and stronger, thus perturbing the wind field throughout much of the model troposphere. This induces a very strong mass flux divergence aloft, several internal gravity waves, and low-level mass flux convergence accompanying evaporative cooling. By 2000 UTC the vertical cross section indicates that as the primary ascent maximum propagates eastward across Alabama and the Florida Panhandle, a new ascent maxima forms over eastern Mississippi accompanying P_1 . These simulated cross sections clearly indicate many of the features which one would expect to see accompanying wave-CISK, i. e., deep perturbations in the velocity fields, very strong low-level convergence ahead of an evaporatively-cooled air mass controlling low-level frontogenesis, and a quadrature relationship between the vertical ascent maxima and the isentropes indicating the existence of an internal gravity wave. These features are consistent with the many numerical and theoretical studies of wave-CISK (Hayashi 1970; Raymond 1975; Davies 1979; Raymond 1983, 1984; Xu and Clark 1984; Nehrkorn 1986; Raymond 1987; Raymond and Rotunno 1989; Cram 1990; Raymond and Jiang 1990 and Powers and Reed 1993).

4.3 Summary of Stage A

The key processes which occur during Stage A include:

- 1) The rapid eastward movement of the primary cold front/trough (P_1) from Mississippi to Georgia.

- 2) The slow and eventual stalling of the secondary cold front in the Carolina Piedmont as a mesolow (P_2) propagates northeastward from southern Louisiana into Alabama and Georgia.

- 3) The meso ridge (P_4) caused by rain-cooled air accompanying the secondary piedmont cold front builds southwestward into central Georgia.

- 4) The cold air outflow from convection accompanying the piedmont front produces an east-west mesoscale pressure trough (P_3) which strengthens through convection taking place near the Alabama/Florida/Georgia border.

- 5) Wave-CISK fortifies three meso-troughs through latent heating/evaporative cooling.

- 6) The merging of the low-level circulations accompanying each CISK-amplified pressure perturbation over southeastern Alabama and southwestern Georgia.

- 7) The increase of surface vorticity where air parcel trajectories merge and the surface pressure features intersect over southwestern Georgia.

- 8) The development of two low-level confluence maxima within the Georgia mesocyclone, which become the genesis mechanism for strong northeastward-propagating meso-circulations associated with wave-CISK.

4.4 Stage B: Mid-Upper Level Mesoscale Wind Surge/Mass Flux Divergence Forced by Convectively Driven Geostrophic Adjustment Processes: Observations

A time series of subjectively analyzed sea-level pressure is presented in Fig. 22. By 2100 UTC the Georgia mesocyclone as well as the primary and secondary cold fronts are nearly in phase. The trough in the eastern Tennessee River Valley and the low over southwestern Georgia are almost collocated, producing a region of low

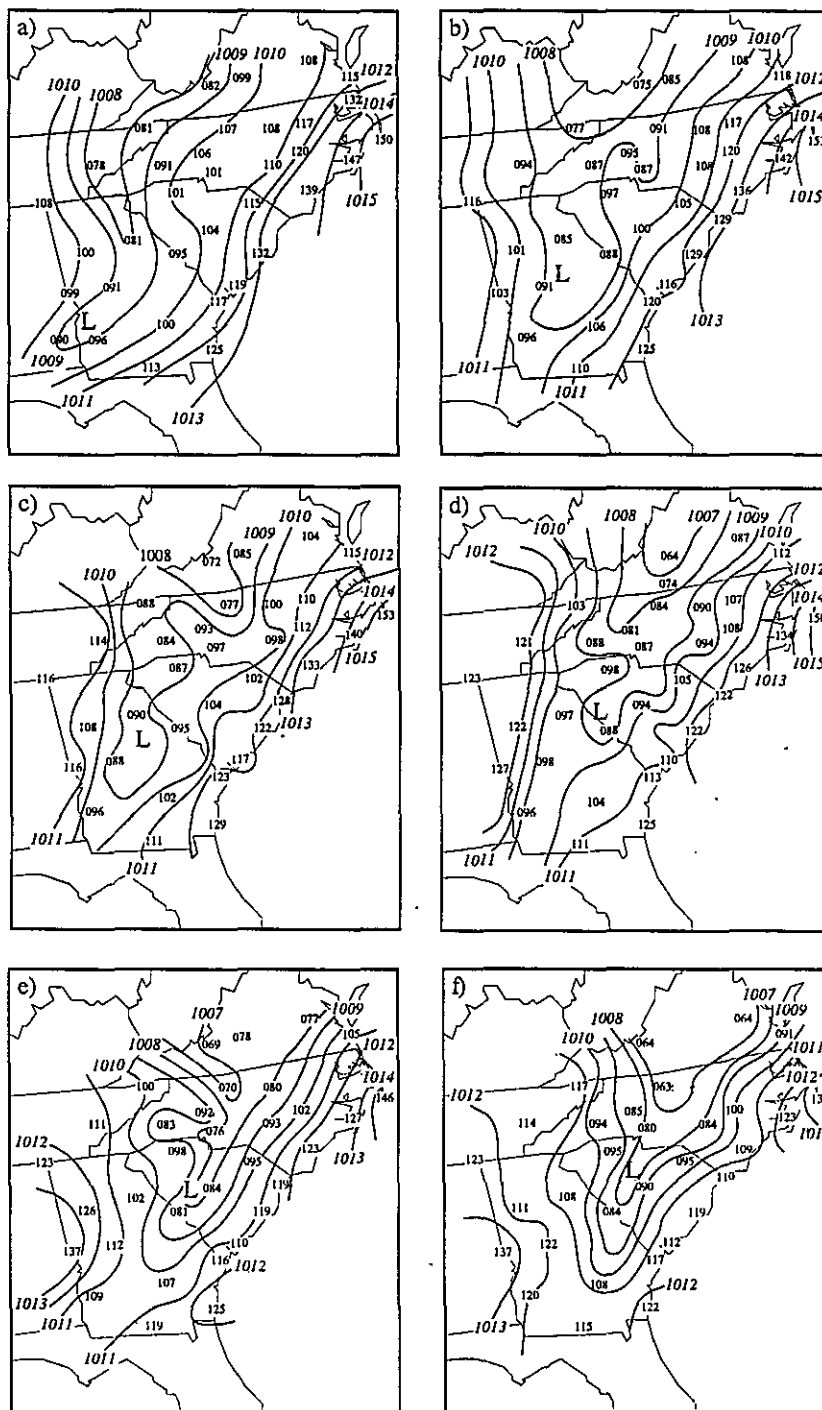


Figure 22. High resolution mean sea level pressure analyses (mb) based on NWS hourly surface data valid at (a) 2100, (b) 2200, (c) 2300, (d) 0000, (e) 0100, and (f) 0200 UTC 27-28 November 1988.

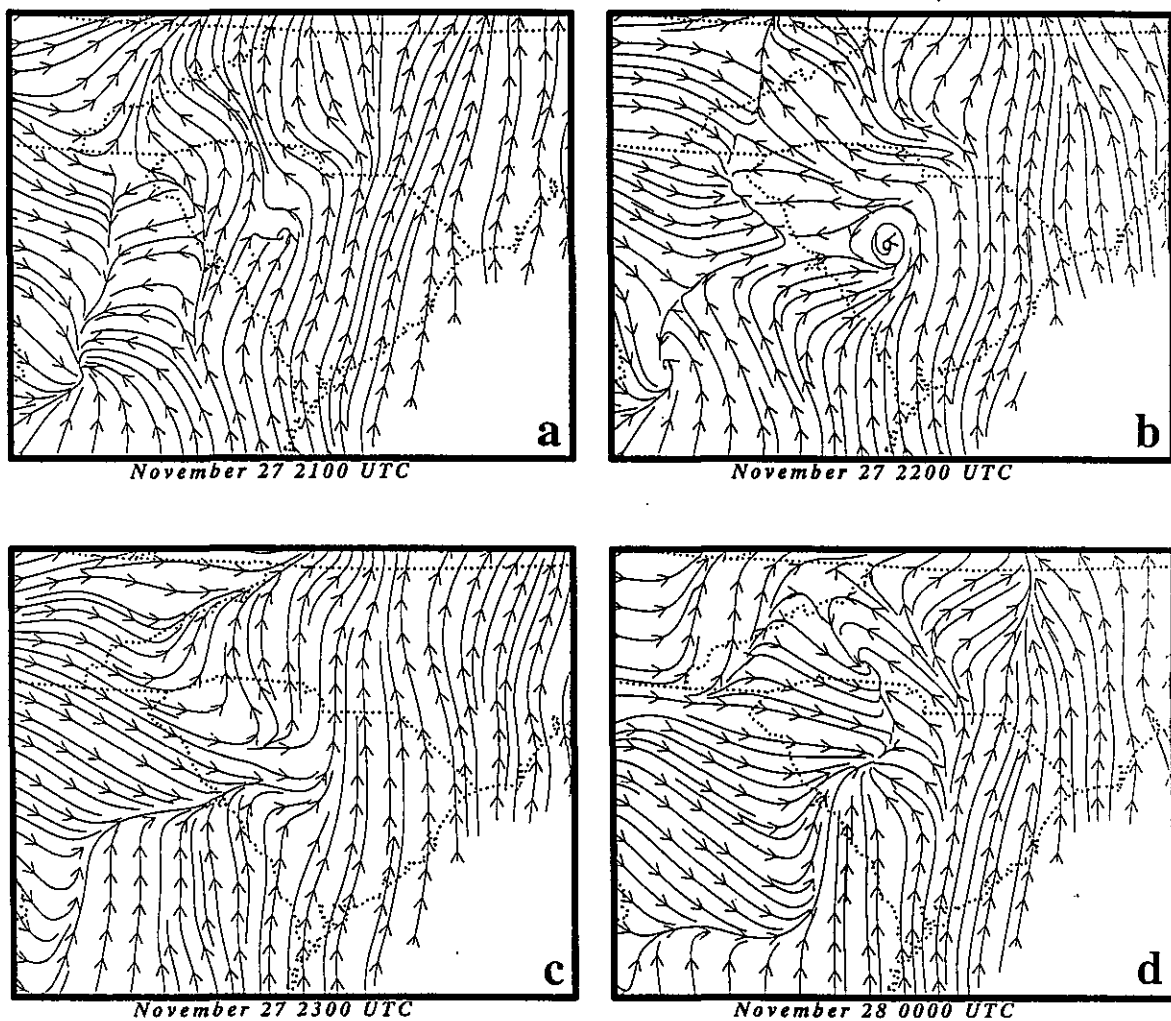


Figure 23. Objective surface streamline analyses based on NWS hourly surface data valid at (a) 2100, (b) 2200, (c) 2300 UTC, (d) 0000, (e) 0100, (f) 0200, (g) 0300, and (h) 0400 UTC 27-28 November 1988.

pressure and surface confluence from southeastern Kentucky to the Florida Panhandle. Shortly after this time a series of mesoscale pressure and surface wind perturbations develop from the Georgia piedmont to the Virginia Piedmont. These waves of depression have a wavelength of about 150 km and propagate east-northeastwards ahead of P_1 and the Georgia mesocyclone at a velocity of $\sim 30 \text{ ms}^{-1}$ during the period from 2200 through 0200 UTC. At least three distinct pressure troughs can be analyzed ahead of and in conjunction with the Georgia mesocyclone during this period.

Moreover, the surface pressure perturbations are generally accompanied by confluence of the surface wind field indicating gravity wave phenomena (Fig. 23).

The *unfiltered* microbarograph records for this period are displayed in Fig. 24 and Table 1. Here the high temporal resolution pressure signals from nine Piedmont stations will be heuristically described emphasizing the period from 1700 through 0500 UTC. These stations include; Asheville (AVL), Greensboro (GSO), Hickory (HKY), Charlotte (CLT) and Raleigh-Durham

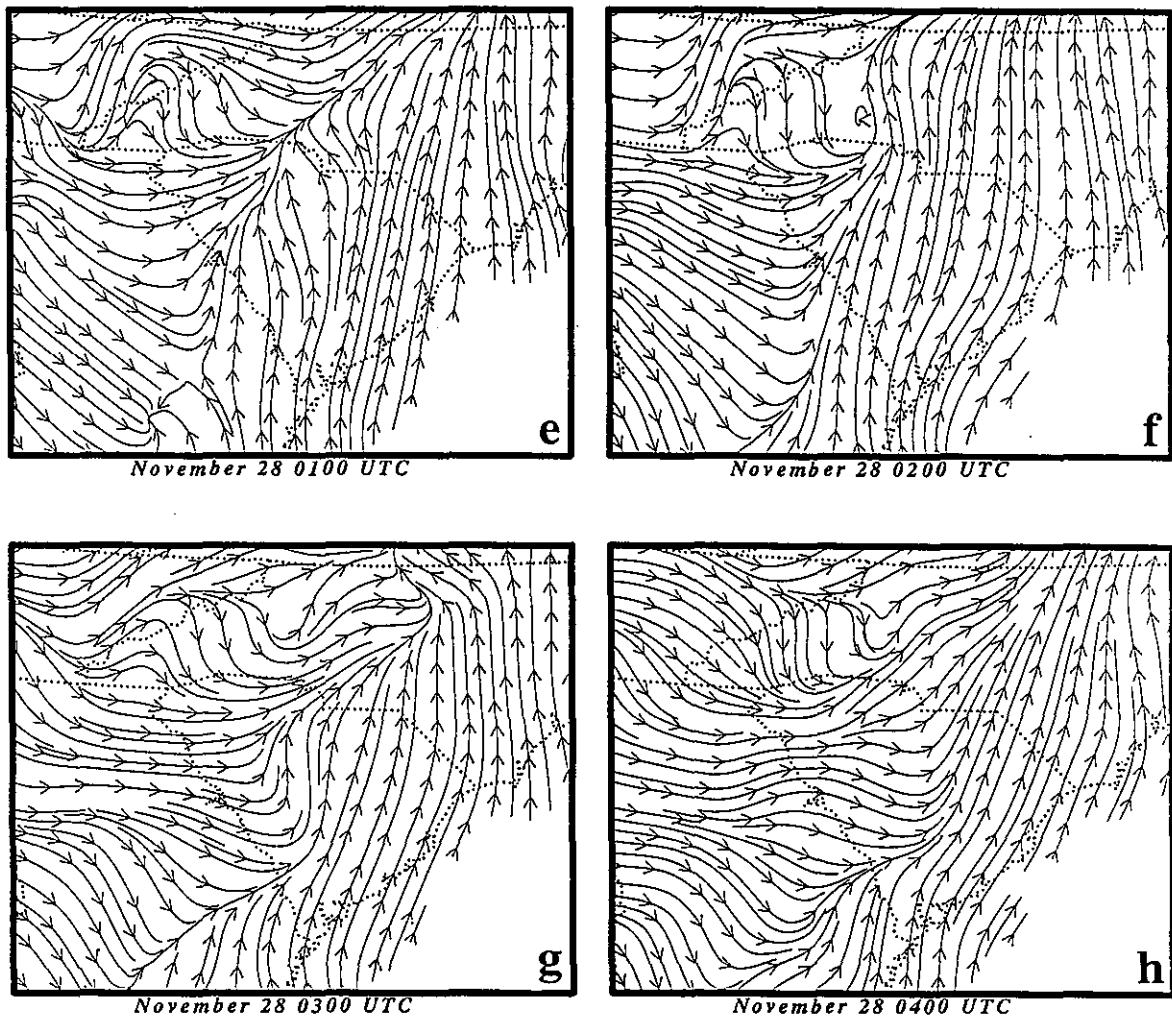


Figure 23. (continued)

(RDU), North Carolina; Athens (AHN), Georgia; and Greenville (GSP), South Carolina. While all stations indicate at least three and up to five wave episodes with periods ~ 1 hour, stations northeast of AHN indicate a second pressure fall signal with a period of ~ 6 hours. The longer and the shorter period signals generally overlap each other during the period from 1800 UTC to 0200 UTC, with both signals producing maximum hourly pressure falls ~ 1 mb. Hence, all stations show evidence of coherent gravity wave signals, all but AHN show the slower mode pressure fall signal, and one

station, RDU, strongly indicates the presence of a very strong mesocyclone signature of greater than 2 mb in ~ 30 minutes but at a much later time, accompanying the tornado on or about 0600 UTC. Thus, the microbarographs indicate the coexistence of two periods of pressure perturbations preceding and accompanying the Georgia mesocyclone in its northeastward journey from southwestern Georgia to upstate South Carolina from 2200 through 0200 UTC. These pressure perturbations preceding the mesolow act to destroy the low-level blocking mesoridge resulting in the transition from a surface

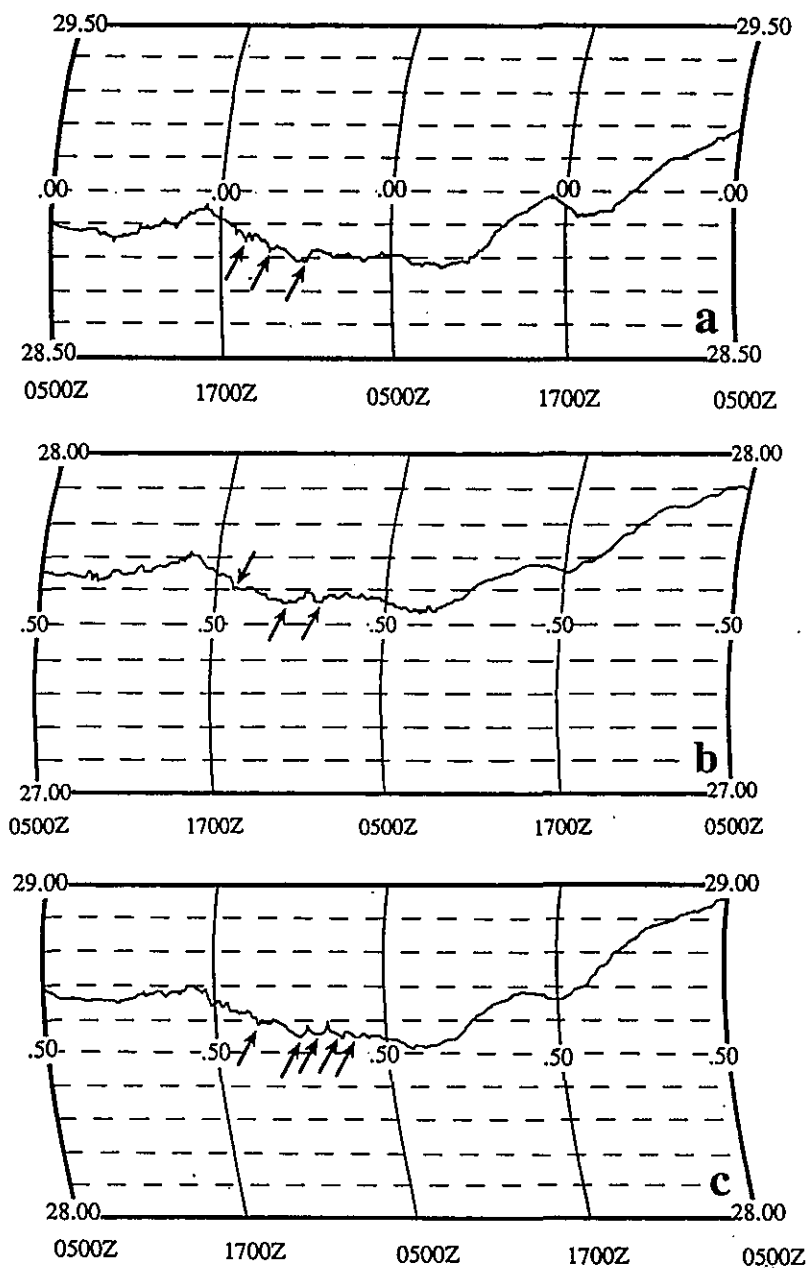


Figure 24. Unfiltered microbarograph traces from (a) Greenville-Spartanburg, South Carolina (GSP), (b) Asheville, North Carolina (AVL), (c) Hickory, North Carolina (HKY), (d) Charlotte, North Carolina (CLT), (e) Greensboro, North Carolina (GSO), and (f) Raleigh, North Carolina (RDU) valid from 1700 UTC 27 November through 0500 UTC 28 November 1988.

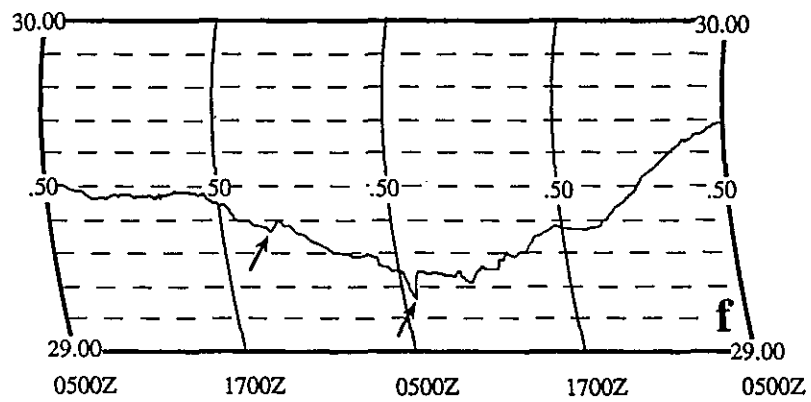
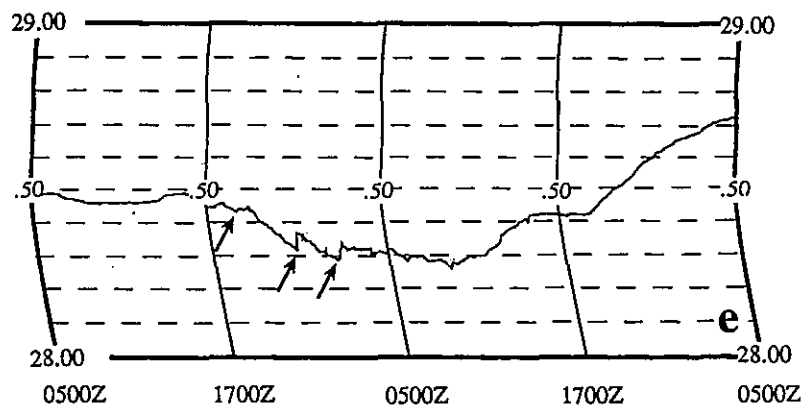
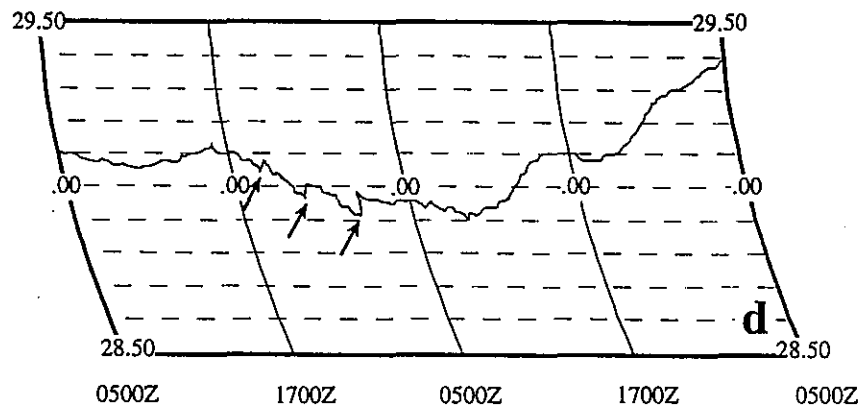


Figure 24. (Continued)

UNFILTERED GRAVITY WAVE CHARACTERISTICS OBSERVED FROM MICROBAROGRAPHS

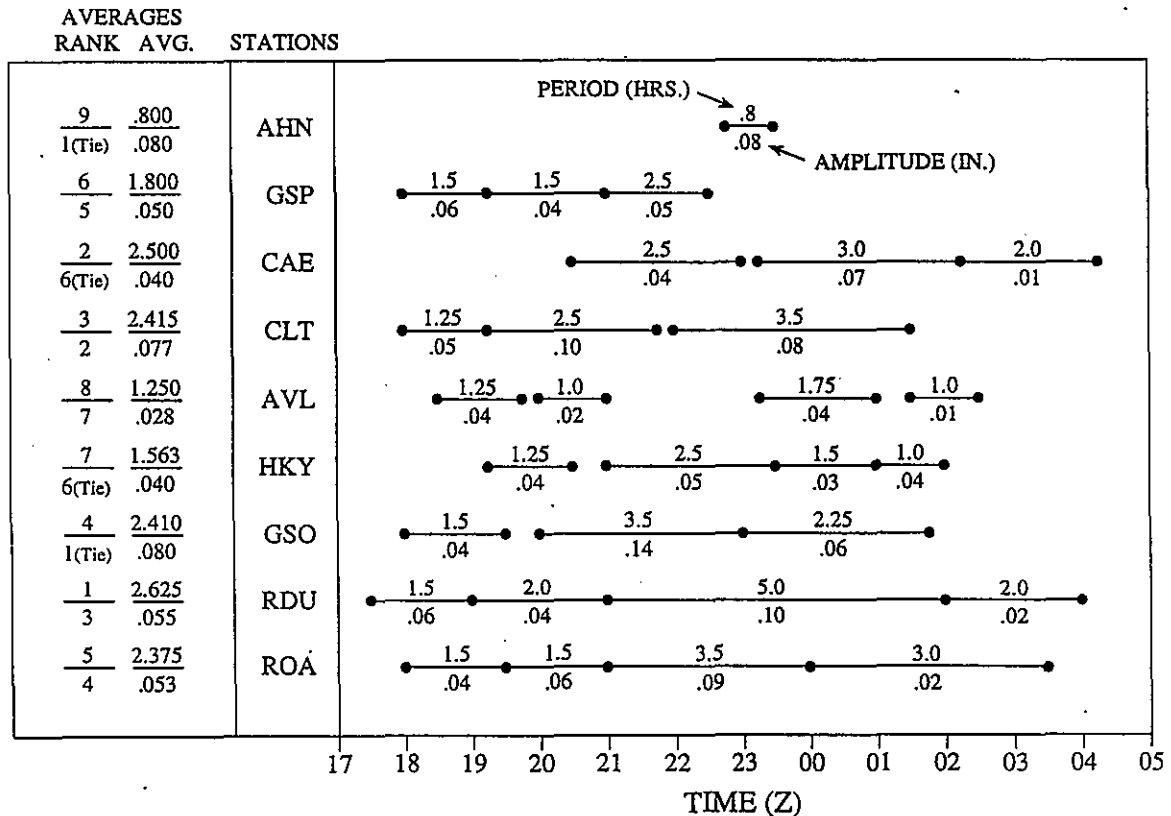


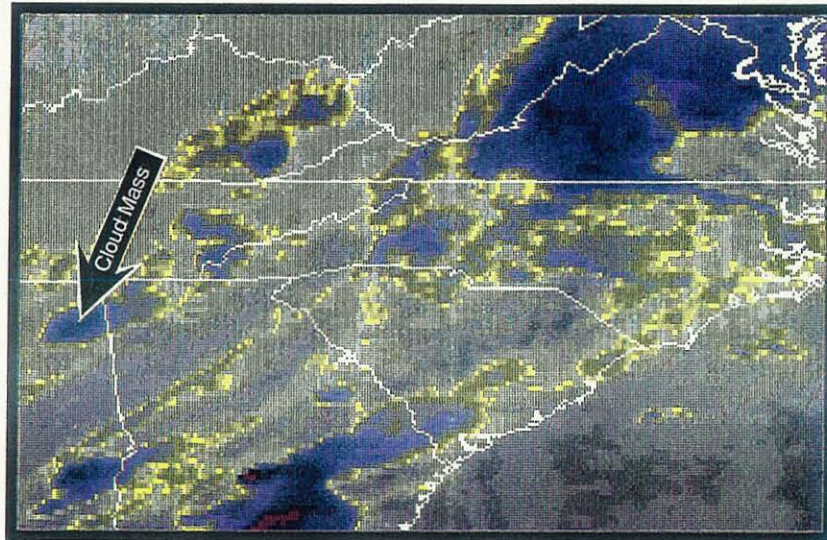
Table 1 Detailed analysis of surface gravity waves detected from barograph traces at selected observing stations in Georgia, South Carolina, North Carolina, and Virginia. The rightmost column summarizes the individual waves periods (above horizontal line in hours) and amplitude during that period (below line in inches) Leftmost column illustrates the average period and amplitude for all wave events at a particular station as well as the relative rank among all the stations listed.

wedge of high pressure behind the piedmont front which was evident at 2100 UTC to a mesocyclone/surface confluence zone extending from northeastern Georgia to southwestern Virginia by 0200 UTC. The strong surface pressure falls along the piedmont, particularly in North Carolina and Virginia between CLT, ROA, and RIC during the 2100-0300 UTC period as depicted in Fig. 27, attest to the destruction of the shallow ridge.

GOES satellite observations from both the infrared and moisture channels are pictured in Fig. 25 and indicate that just upstream from the pressure fall is a rapidly moving cloud mass which

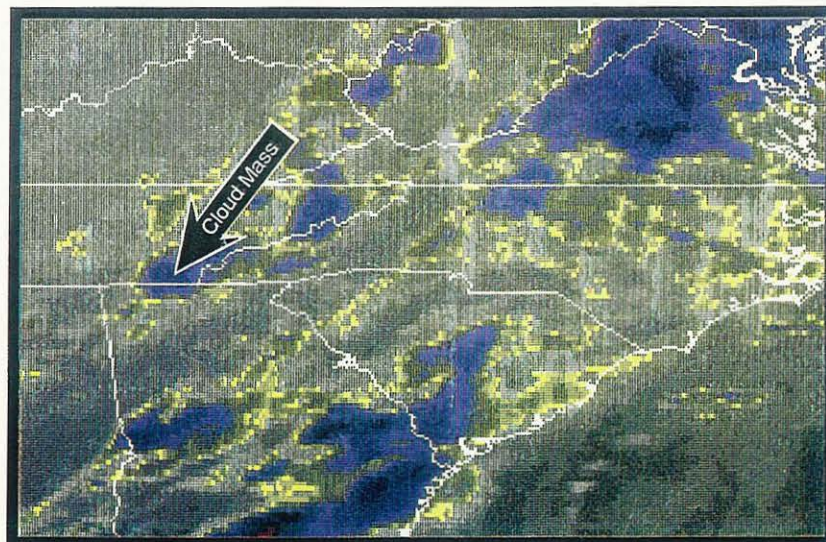
propagates from northeastern Alabama to southwestern Virginia between 2100 and 0000 UTC. This cloud mass moves at $\sim 40 \text{ ms}^{-1}$ and is located between the polar jet entrance region and the convection accompanying the Georgia mesocyclone at 2035, 2235, and 0035 UTC as diagnosed from NWS radar data (Fig. 26). This feature directly follows the propagating gravity waves and pressure falls over the North Carolina and Virginia piedmont which occurs between 2100 and 0000 UTC. Furthermore, the water vapor imagery indicates that a dry slot intensifies just behind and to the right of this cloud mass between 2100 and 0000 UTC over the Georgia piedmont

a



27 Nov 88 2100 UTC

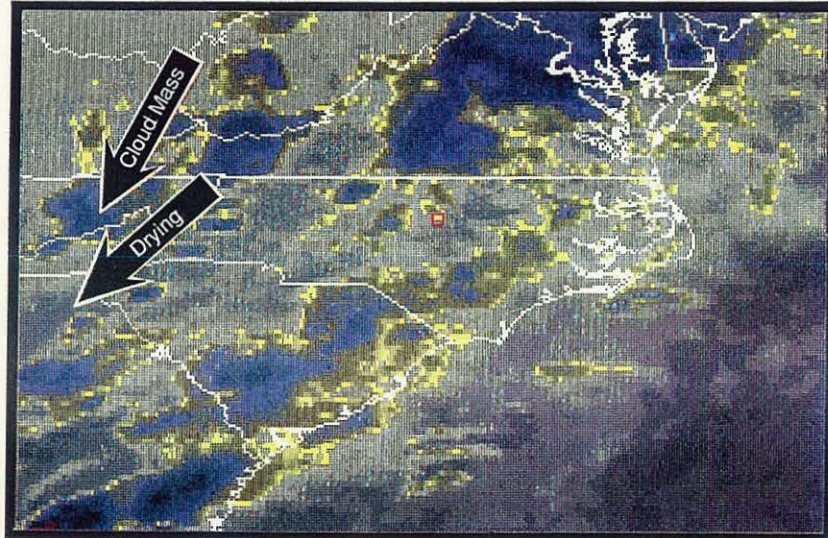
b



27 Nov 88 2200 UTC

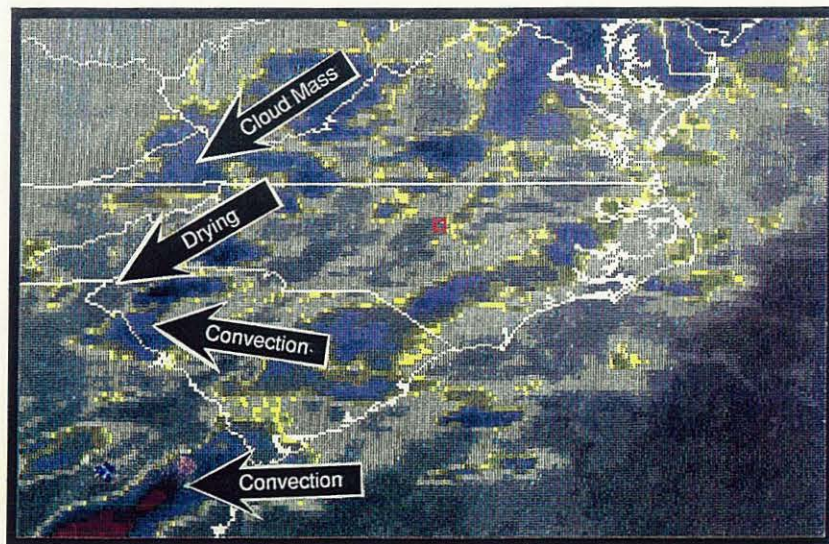
Figure 25. GOES infrared satellite imagery valid at (a) 2100, (b) 2200, (c) 2300, and (d) 0000 UTC 27-28 November 1988. Goes water vapor imagery valid at (e) 2100, (f) 2200, (g) 2300, and (h) 0000 UTC 27-28 November 1988

c



27 Nov 88 2300 UTC

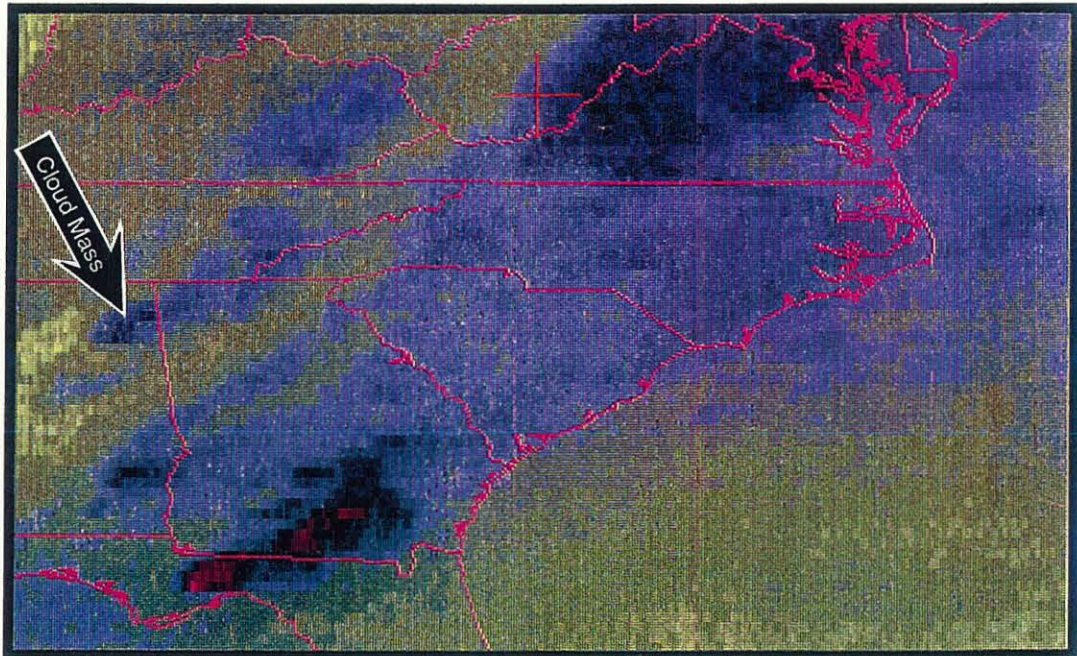
d



28 Nov 88 0000 UTC

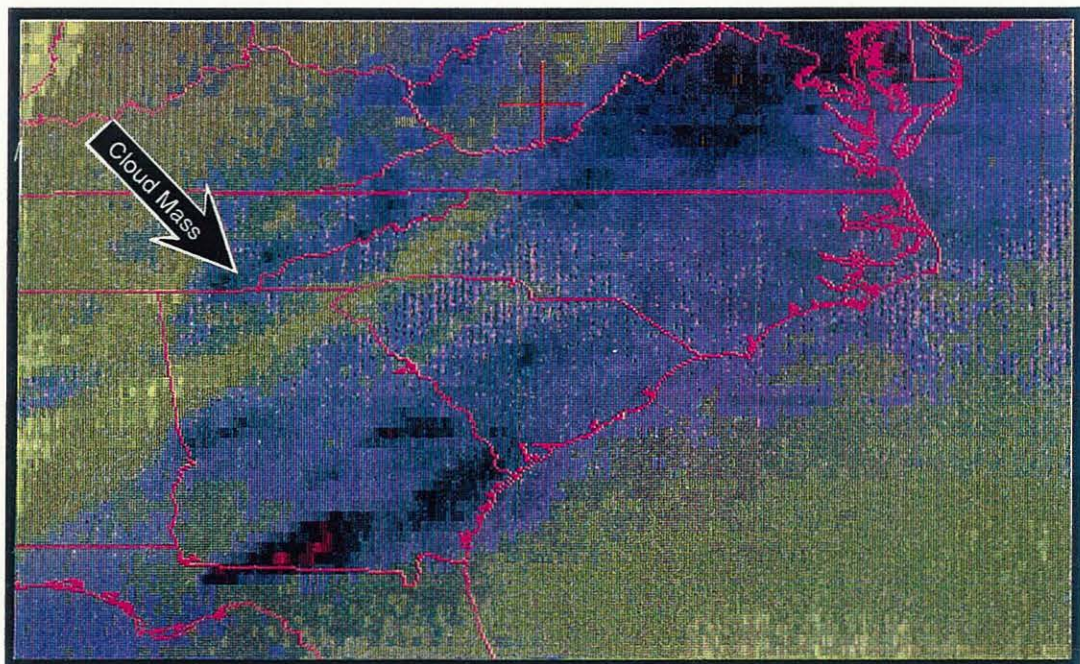
Figure 25. (Continued)

e



27 Nov 88 2100 UTC

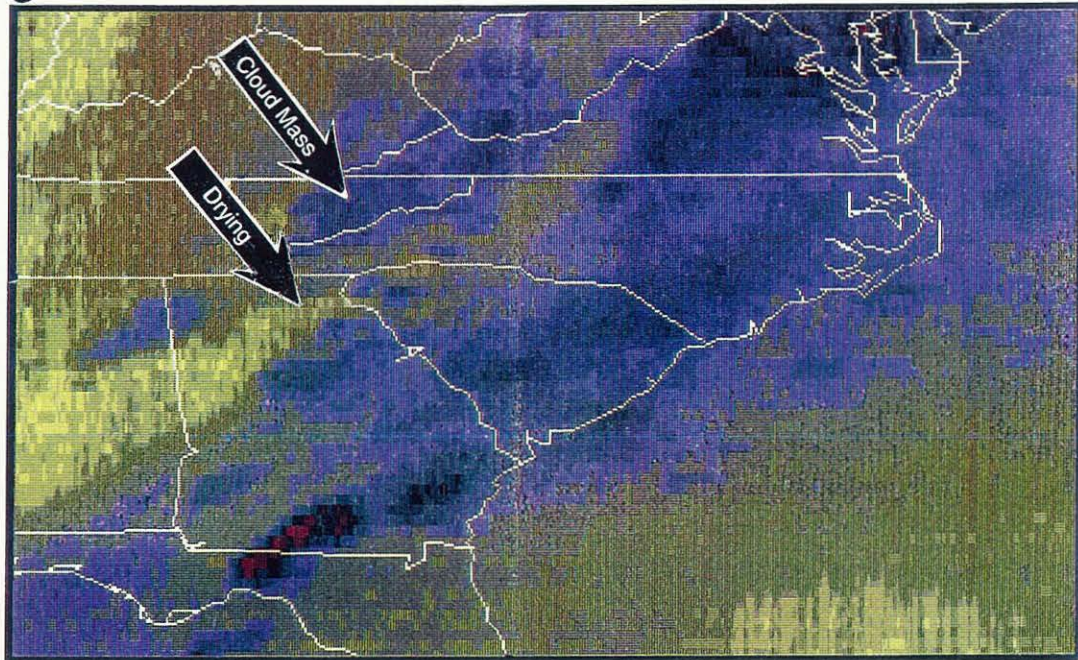
f



27 Nov 88 2200 UTC

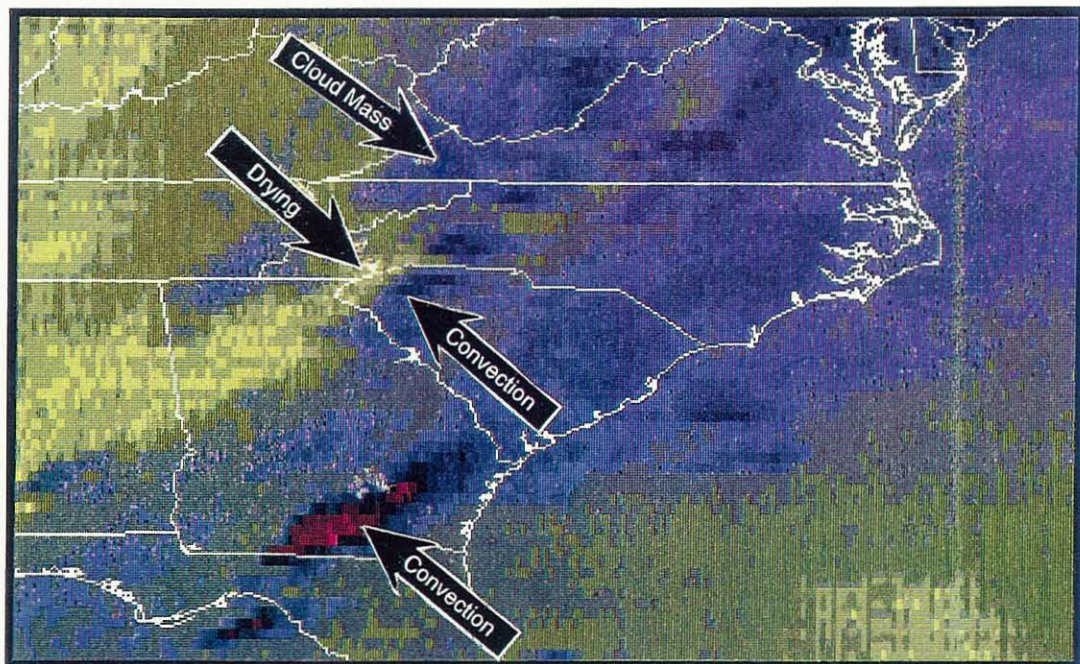
Figure 25. (Continued)

g



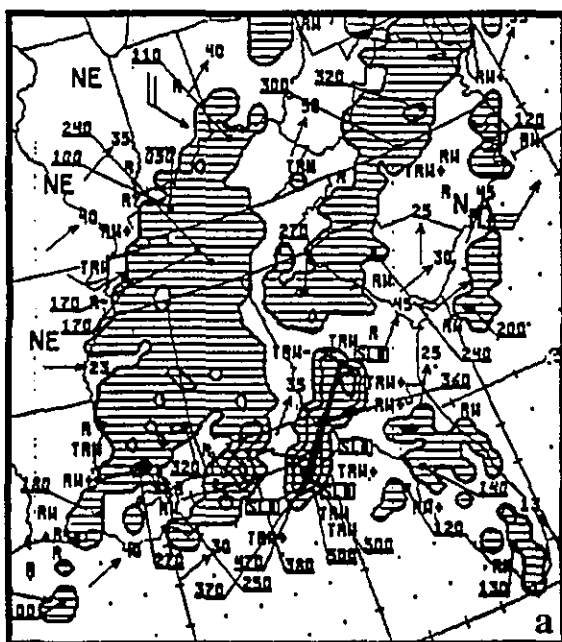
27 Nov 88 2300 UTC

h

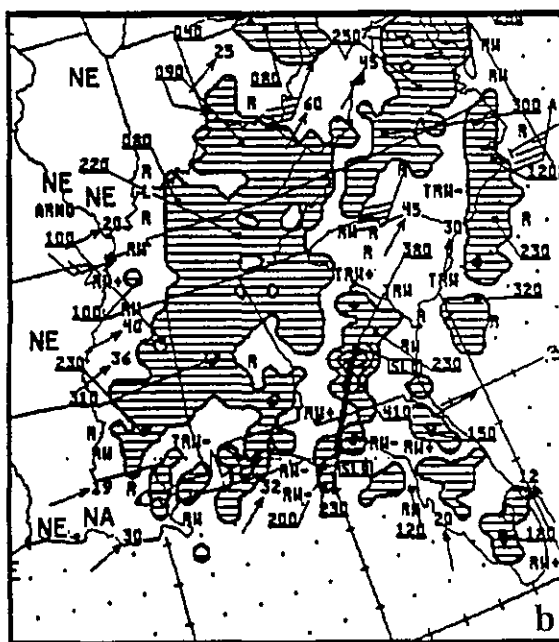


28 Nov 88 0000 UTC

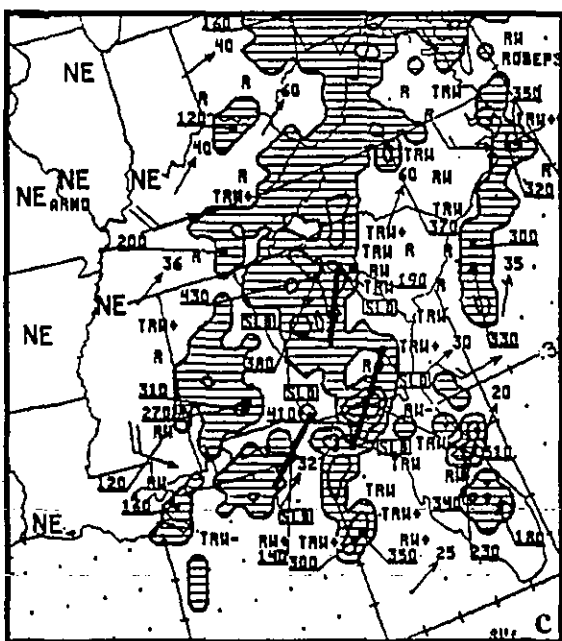
Figure 25. (Continued)



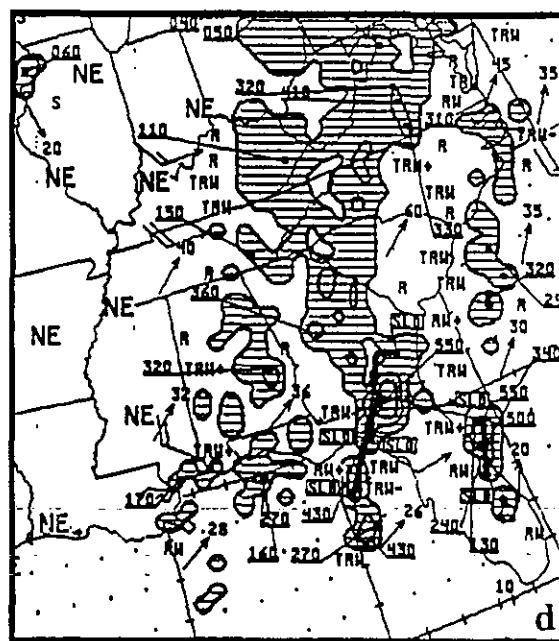
1935Z 27 NOV 1988 RADAR SUMMARY



2135Z 27 NOV 1988 RADAR SUMMARY



0035Z 28 NOV 1988 RADAR SUMMARY



0135Z 28 NOV 1988 RADAR SUMMARY

Figure 26. NWS MDR summaries valid at (a) 1935, (b) 2135, (c) 0035, and (d) 0135 UTC 27-28 November 1988.

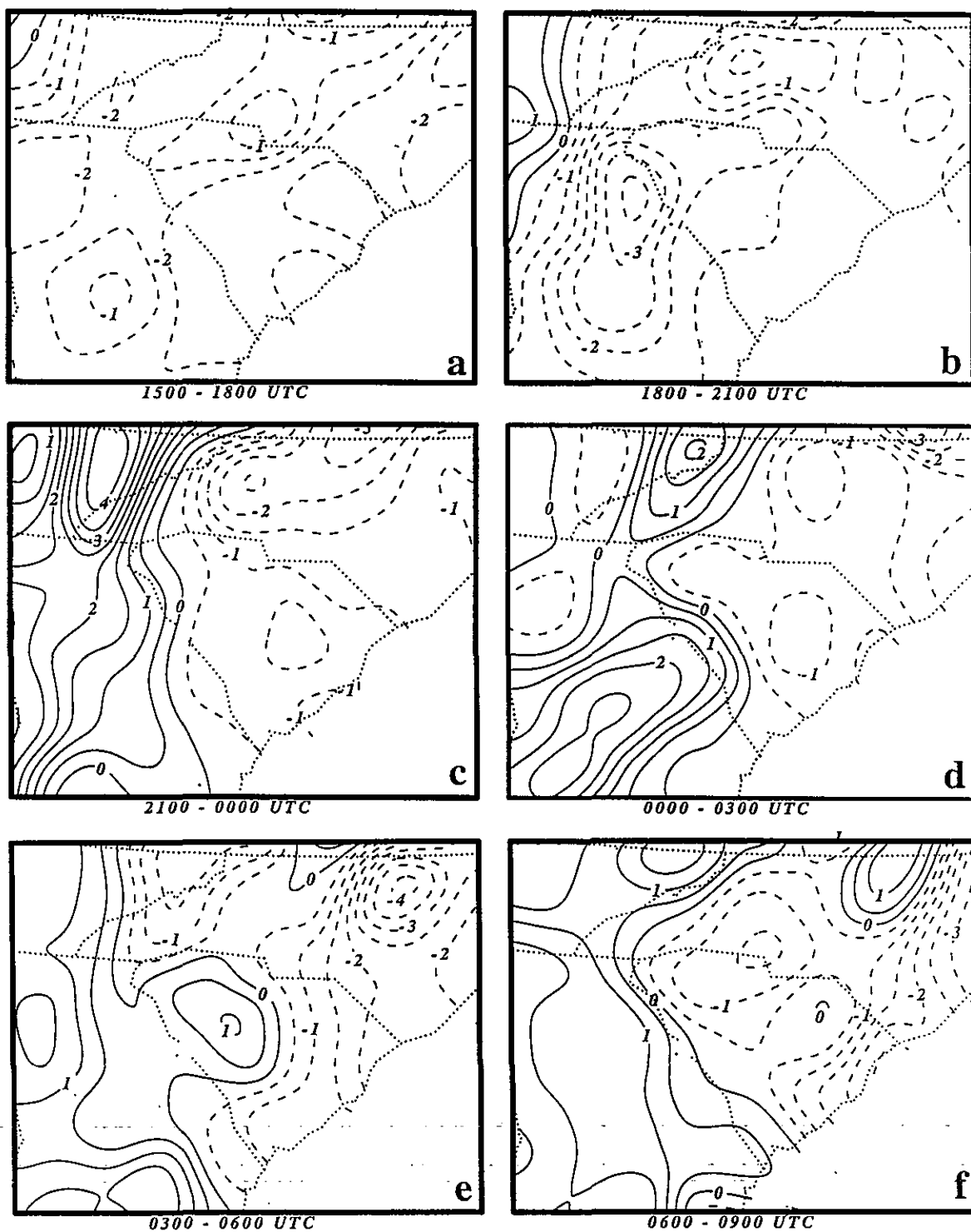


Figure 27. Objective analyses of mean sea level pressure change (mb) based on NWS three-hourly surface data for the time periods valid between (a) 1500 and 1800 UTC, (b) 1800 and 2100 UTC, (c) 2100 and 0000 UT, (d) 0000 and 0300 UTC, (e) 0300 and 0600, and (f) 0600 and 0900 UTC 27-28 November 1988.

and in upstate South Carolina. Therefore, this feature is apparently associated with mass flux divergence which forms between the convection and the polar jet. Additionally, this feature seems to play a role in reducing the amplitude of the blocking ridge by gravity wave generation, and the generation of the slow-mode pressure fall over the piedmont as well as injecting drier air over the region just northwest of the Georgia mesocyclone. This dry slot is consistent in location and timing with the subtropical CFA/dry tongue analyzed aloft derived from rawinsonde data between northwestern Georgia and southeastern West Virginia at 0000 UTC as earlier depicted in the analyzed cross sections (Fig. 8).

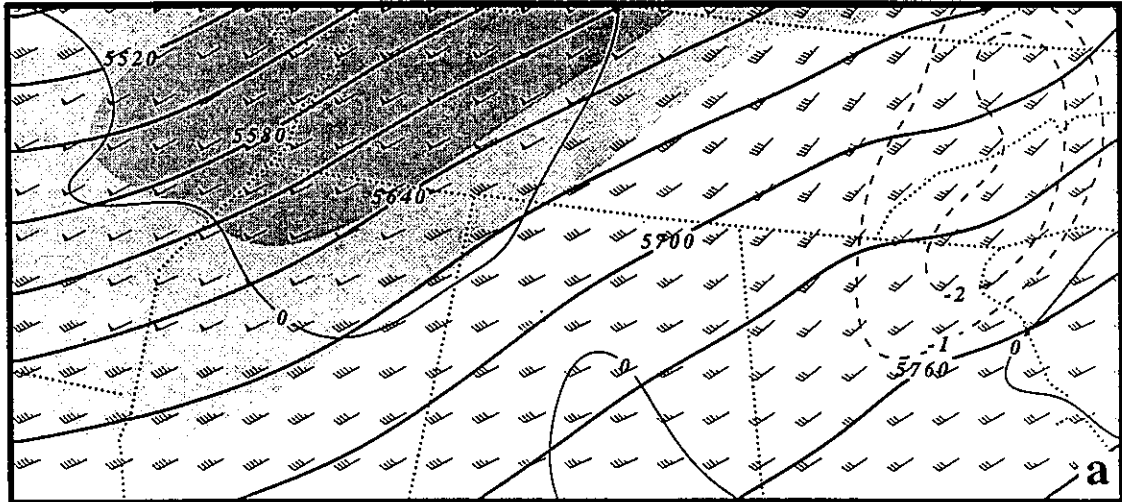
4.5 Stage B - Simulation Results

Figure 28 shows the coarse mesh 500 mb simulated height, wind vectors, and vertical motions over northern Mississippi, Alabama, and Georgia as well as southern Tennessee. This region represents the interface between the polar jet entrance region and the simulated convection over southern and central Mississippi, Alabama, and Georgia. Hence, the juxtapositioning between the largest simulated jet streak wind velocities and mesoscale latent heat release occur between JAN; BNA, and AHN during the 1600-2000 UTC time period. Clearly evident in Fig. 28 at 1600 UTC is the southernmost flank of the jet max entrance region at 500 mb, and the height field over northern Mississippi and southwestern Tennessee. Here, wind vectors whose magnitudes are in excess of 50 ms^{-1} are nearly parallel to the simulated isoheights at this time. By 1800 UTC simulated stratiform and convective latent heating have increased the isoheights over northern and central Mississippi by $\sim 10\text{m}$. This height rise increases the northwestward-directed pressure gradient force by nearly 40% between Central Mississippi and the Tennessee border, resulting in an increase in the leftward-directed cross stream ageostrophic flow. Wind vectors are directed to the left of the height field by nearly 30 degrees, thereby increasing the magnitude of the southerly wind component relative

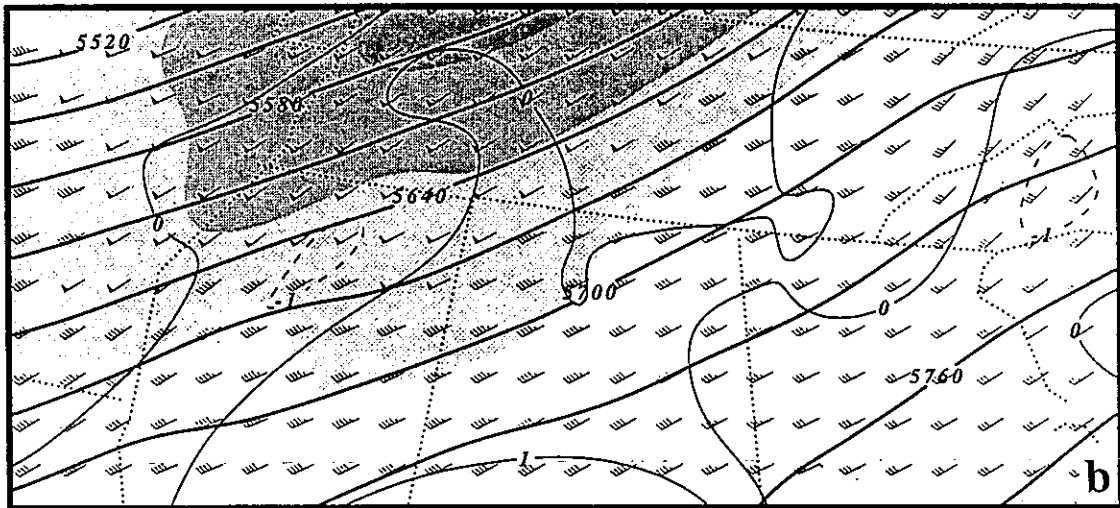
to the preexisting westerly wind component. This is the same region wherein subgeostrophic flow between the polar and subtropical jet streaks was observed to exist at 0000 UTC (Fig. 6).

Between 1600 and 2000 UTC, the 5 ms^{-1} increase in the ageostrophic meridional wind component is sufficient to result in a geostrophic adjustment in the zonal wind component of nearly the same magnitude thus, turning the wind field back to the right accompanying a cross-stream inertial-advective adjustment. Hence, the flow just downstream from the leftward-directed ageostrophic perturbation turns to the right in response, resulting in a propagating mesoscale velocity maximum over northern Alabama by 2000 UTC. This new mesoscale jet maximum and its exit region begins to rapidly propagate away from its source region producing mass flux divergence (convergence) to the northeast (southeast) and ascending (descending) motion as it propagates over northwestern Georgia and southeastern Tennessee by 2200 UTC (Fig. 28). Its subsequent movement will be to follow and intensify (due to differential adiabatic and diabatic heating) the subtropical CFA between southeastern Tennessee and southeastern West Virginia. This simulated geostrophic adjustment process is analogous to that hypothesized to be important in gravity wave generation by Kaplan and Paine (1977); Zack and Kaplan (1987); Uccellini and Koch (1987); and Koch and Dorian (1988) except that the pressure perturbation here is primarily convectively-induced and does not exist prior to the generation of wave-CISK. This represents an unbalanced thermally direct circulation and amplifying jetlet.

Figures 29 and 30 depict the simulated 500 and 300 mb wind vectors and isotachs over the piedmont between 2300 and 0200 UTC respectively. The 500 mb flow splits as the mesoscale jetlet (S_1) and its exit region propagate away from southeastern Tennessee over northwestern North Carolina and southwestern Virginia, placing the region from AVL to ROA within the right front exit region of the unbalanced mesojlet. This would result in pressure falls due to inertial-advective mass flux divergence occurring where the observed gravity waves and slow mode

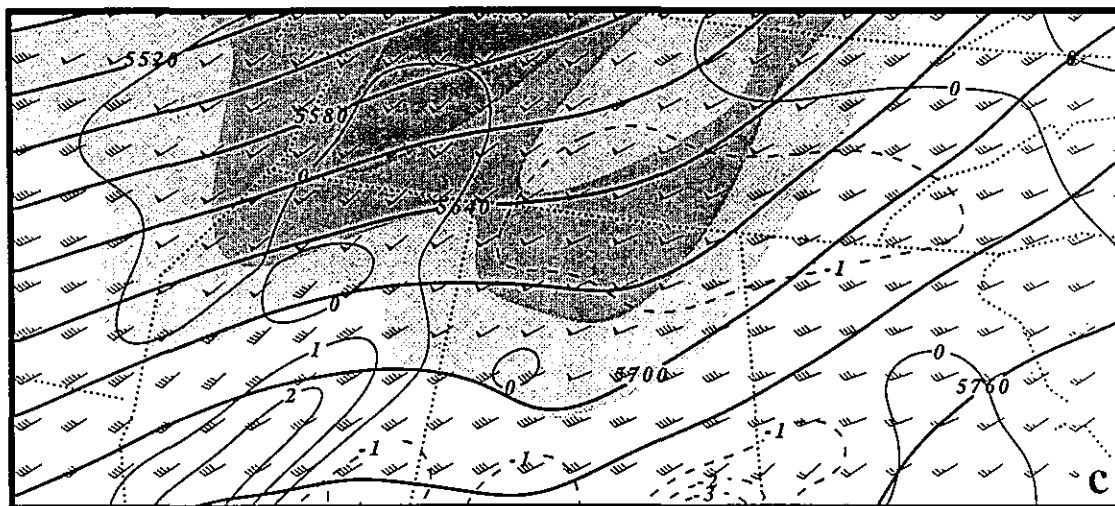


Forecast Valid 1600 UTC

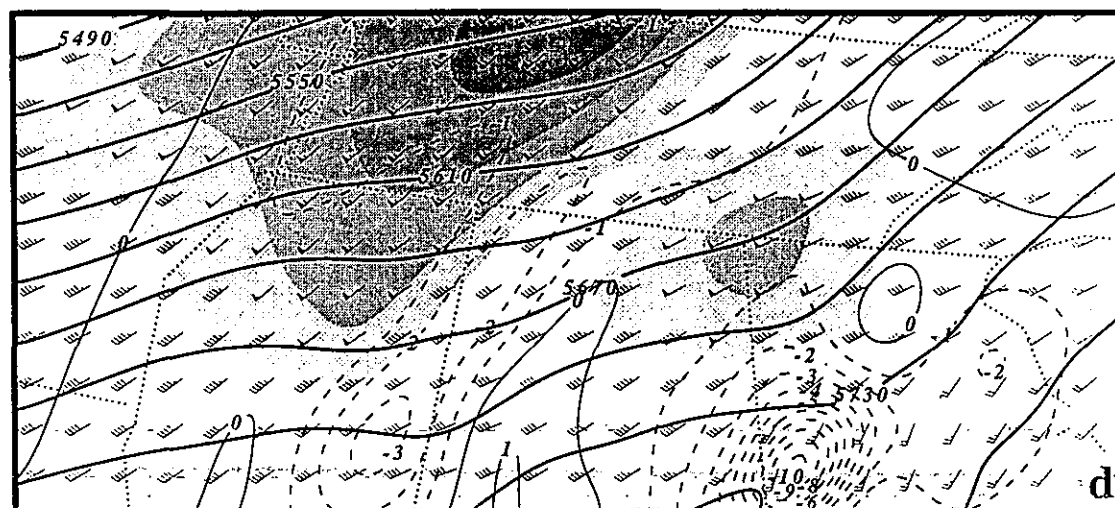


Forecast Valid 1800 UTC

Figure 28. GMASS coarse mesh simulated 500 mb height (thick solid lines in m), horizontal wind vectors (barb 10 ms^{-1} , half barb 5 ms^{-1} , triangle 50 ms^{-1} , shaded every 5 ms^{-1} over 45 ms^{-1}), and omega (thin solid lines reflect descent, dashed lines ascent in 10^{-2} mbs^{-1}) valid at (a) 1600, (b) 1800, (c) 2000, and (d) 2200 UTC 27 November 1988.



Forecast Valid 2000 UTC



Forecast Valid 2200 UTC

Figure 28. (Continued).

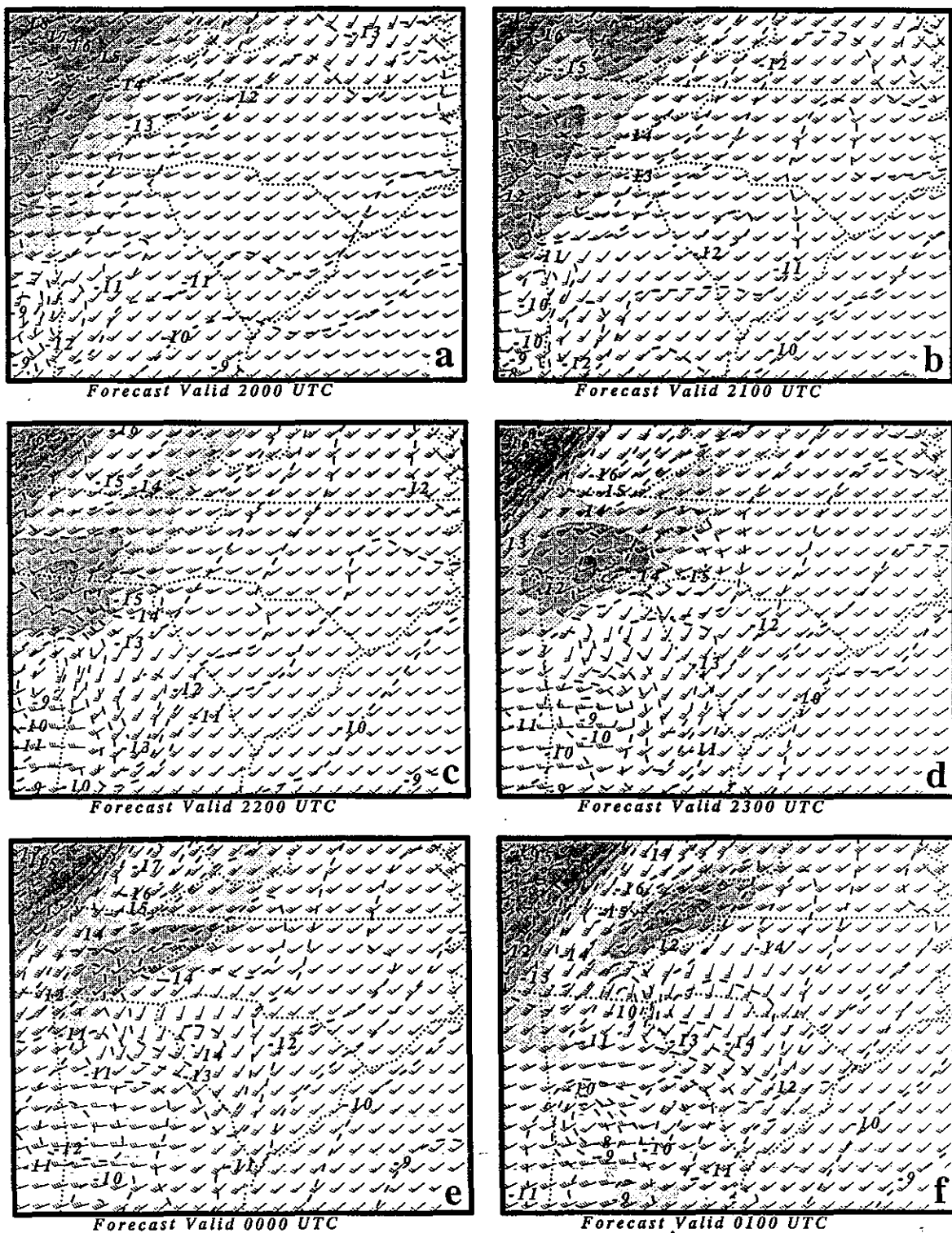


Figure 29. GMASS coarse mesh simulated 500 mb wind vectors and temperature (dashed lines in $^{\circ}\text{C}$) valid at (a) 2000, (b) 2100, (c) 2200, (d) 2300, (e) 0000, and (f) 0100 UTC 27-28 November 1988. (Shaded regions represent wind velocities in excess of 40 ms^{-1})

pressure fall signals were observed thereby destroying the surface blocking mesoridge located northwest of the piedmont front (Figs. 24 and 27). At 300 mb there are also indications that a "lobe" of kinetic energy has been extracted from the primary core of the PJS and has passed directly over the North Carolina and Virginia piedmont during this time period, thus reinforcing the tendency for mid-tropospheric mass flux divergence. Such a pattern of mid-upper tropospheric mass flux divergence would induce vertical ascent over the region from Georgia to Virginia during a three to five hour period, as is observed from satellite imagery (Fig. 25). Additionally, the warm advection accompanying this propagating mesoscale jetlet in its southwestern quadrant and the cold advection in its northeastern quadrant would work against the development of thermal wind balance through differential vertical motions. These baroclinic processes are facilitated by the fact that the subtropical CFA and mesoscale jetlet are closely coupled in space and time, insuring an unbalanced accelerating flow (Fig. 29).

S_1 (depicted in Fig. 36) is clearly not the only wind velocity surge apparent in Fig. 29. Between 2300 and 0200 UTC surges are located upstream from what will be referred to as gravity waves #4 and #5 (W_4 and W_5) located over upstate South Carolina and central Georgia by 0200 UTC. These represent CISK-induced gravity waves which develop over southeastern Alabama and southwestern Georgia as the mesocyclone amplifies from the juxtapositioning of the four mesoscale pressure perturbations. W_4 and W_5 form as the two LLJs amplify between 1800 and 2000 UTC near CSG at the confluence zones formed by the merger of P_1 - P_4 . S_2 and S_3 develop behind W_4 and W_5 in the mid-upper troposphere as descending rear inflow jets. Confluence behind the convectively-induced pressure perturbations results in mid-upper tropospheric velocity convergence and the downward transport of horizontal momentum. They are similar to simulated and observed features described by Brown (1979); Johnson and Hamilton (1988); and Zhang and Gao (1989). These surges accompanying W_4 and W_5 amplify as the disturbed

pressure gradient force which is coupled to the gravity wave crest induces confluent flow behind the wave and diffluent convective heating-induced outflow ahead of the wave. The effect of the upper and lower-level wind surges is to produce relative vorticity maxima which are much stronger than that typically detected on the larger synoptic scale (Fig. 31). Additionally, the juxtapositioning between the simulated upper and lower tropospheric mesoscale jetlets is to produce increased vertical wind shears and helicity values after 0000 UTC over the Carolina Piedmont and Coastal plains.

The juxtapositioning of the mesojets exit region coupled with W_4 and W_5 produces the simulated relative humidity fields at 0000 UTC (Fig. 32), and are quite consistent with the satellite imagery (Fig. 25). Present in the vertical cross section of simulated relative humidity between BNA and CHS is a dry tongue that descends from 300 to 550 mb and is situated over a moist lower tropospheric region in southwestern North Carolina. Both features are consistent with the dry slot and cloud mass over the same regions shown in Fig. 25. Additionally, note the deep moist layer in the upper cross section over AHN indicating the ascent field ahead of W_4 . The corresponding simulated sounding over this area indicates a deep moist adiabatic layer accompanying substantial upper-tropospheric outflow (Fig. 33). Consistent with these are the features depicted in the lower cross section between Tupelo, Mississippi (TUP) and Savannah, Georgia (SAV) where the mesojets' cloud mass is northwest of the mesojets' dry slot and the descending rear inflow jet accompanying W_4 . The ascending side of W_4 and both the ascending and descending sides of W_5 can also be detected in this cross section. Note the simulated Macon, Georgia (MCN) sounding (which is within the ascending part of W_5) and its similarity to the sounding at AHN (which is in the ascending part of W_4) results in deep moist adiabatic layers and large outflow ahead of the wave-CISK simulated convection. Of special significance is that the descending rear inflow jets accompanying W_4 and W_5 are becoming superimposed upon the dry slot accompanying the

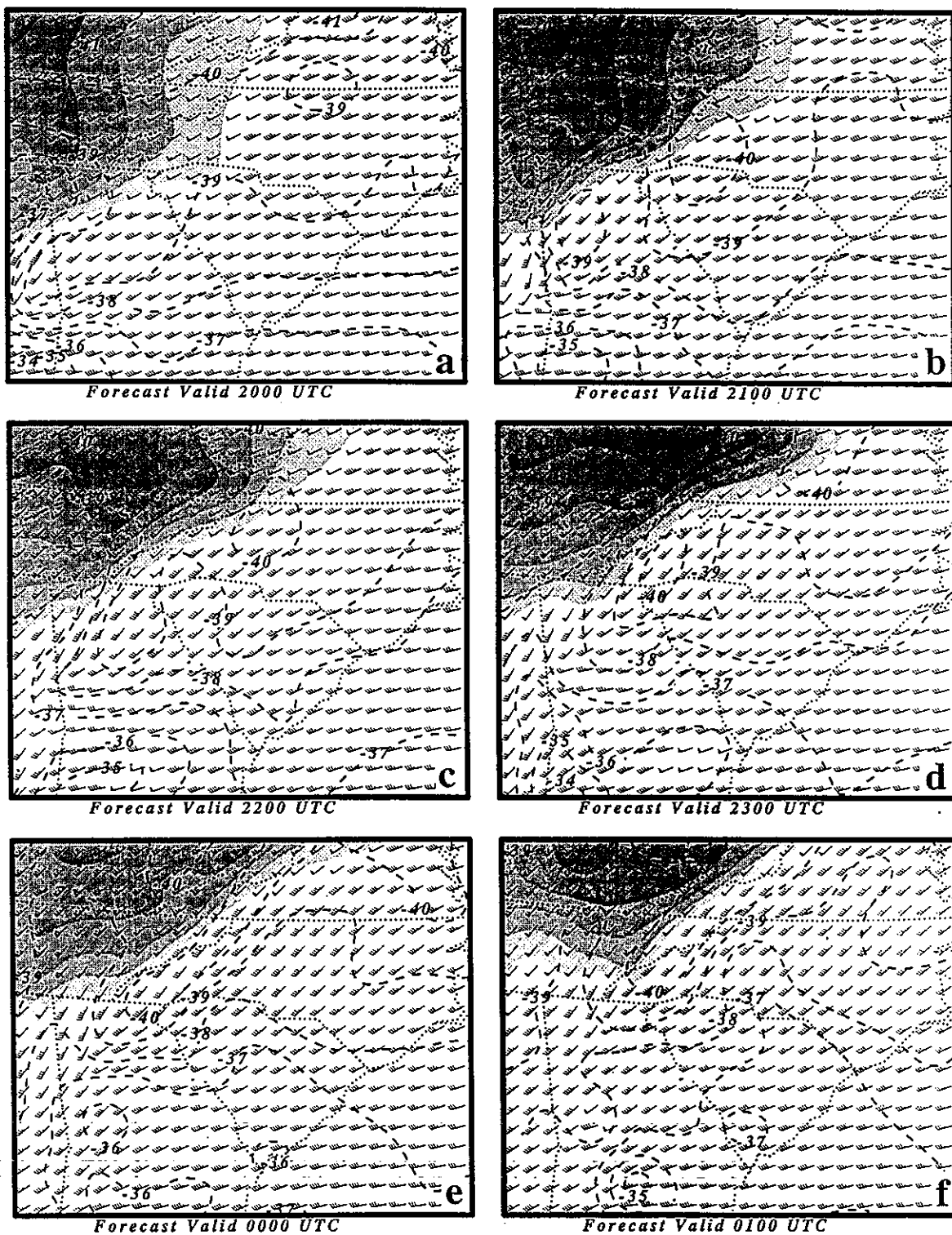


Figure 30. GMASS coarse mesh simulated 300 mb wind vectors, isotachs (shaded every 5 ms^{-1} for values > 50 ms^{-1}), and temperature (dashed lines in $^{\circ}\text{C}$) valid at (a) 2000, (b) 2100, (c) 2200, (d) 2300, (e) 0000, and (f) 0100 UTC 27-28 November 1988.

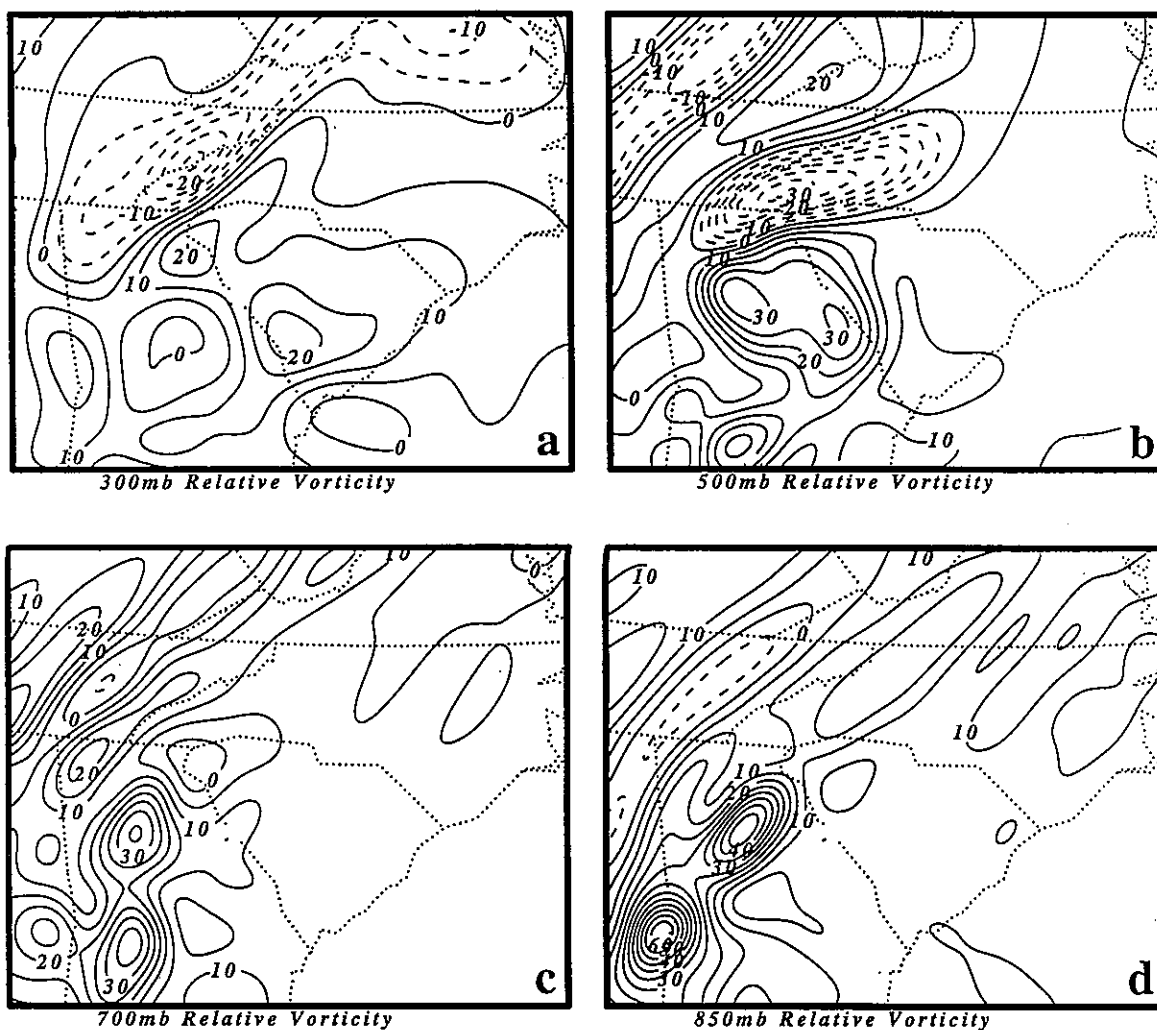


Figure 31. GMASS coarse mesh simulated relative vorticity (10^{-5}s^{-1}) at a) 300mb, b) 500mb, c) 700mb, and d) 850mb valid at 0000 UTC 28 November 1988.

mesoscale jetlet, thus acting to produce an even more concentrated source of dry air as observed in the satellite imagery. These patterns of mesoscale airflow and moisture are similar to other observations of developing mesoscale convective complexes (Maddox, 1980).

The implications of the mesoscale jetlet, its exit region, and gravity waves 4 and 5 for the evolution of the Georgia mesocyclone over the Carolina Piedmont for the 2100 UTC through 0200 UTC period can be seen in the simulated MSLP fields shown in Fig. 34. The surface features

indicate that just as W_4 and W_5 accompanying the mesocyclone become well-organized, a train of at least three gravity waves, W_1 - W_3 , emerges over the Carolina Piedmont and act to eliminate the blocking mesoridge. At 2200 UTC, W_1 and W_2 form under the geostrophic adjustment processes occurring at 500 mb over southeastern Tennessee and northern Alabama, and begin propagating up the Carolina Piedmont ahead of the mid-level mesoscale jetlet. By 0000 UTC, the three waves, which are coupled to the mesojettlet aloft, have propagated into western North Carolina and

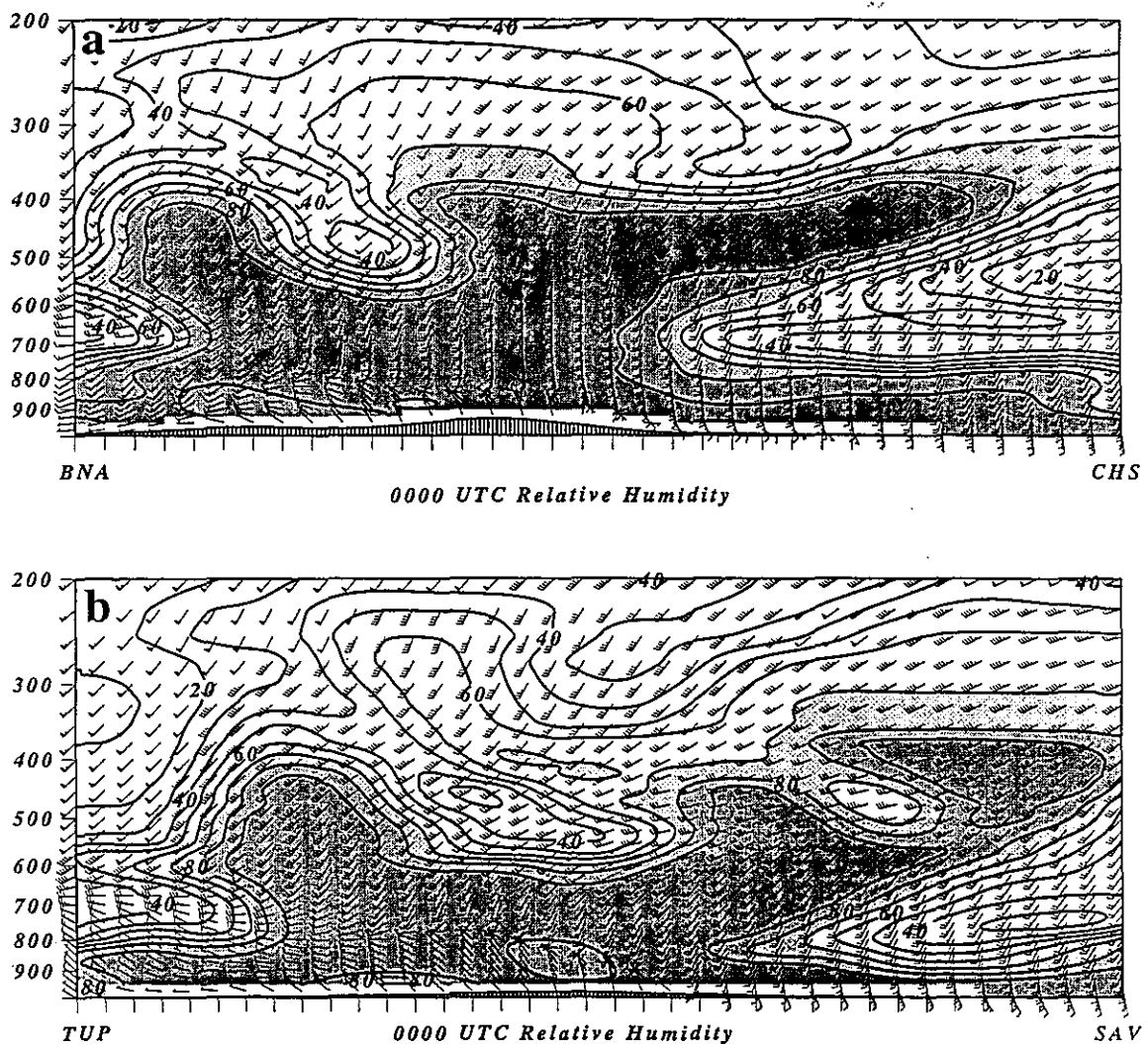


Figure 32. GMASS coarse mesh simulated vertical cross sections of relative humidity (%) with values greater than 70 % shaded (a) from Nashville, Tennessee (BNA) to Charleston, South Carolina (CHS) and (b) from Tupelo, Mississippi (TUP) to Savannah, Georgia (SAV) valid at 0000 UTC 28 November 1988.

Virginia. These "secondary" gravity waves, resulting from geostrophic adjustment accompanying the formation of the mesojettlet aloft, are successful in destroying the blocking ridge over the North Carolina Piedmont. By 0200 UTC, waves 4 and 5 have propagated into upstate South Carolina and northeastern Georgia accompanying simulated convection. Hence, the pressure perturbation and deep velocity perturbations accompanying W_4 and W_5 are much stronger than those accompanying W_1 - W_3 . Gravity waves W_4

and W_5 represent "primary" modes which are essential to the propagation of the numerically simulated mesocyclones and their accompanying LLJs.

The dominance of these primary waves can be seen in their effects on the LLJs during this same time period. Note how distinct 850mb wind and cyclonic vorticity maxima accompany W_4 and W_5 as they propagate northeastwards from western Georgia and the Florida Panhandle into

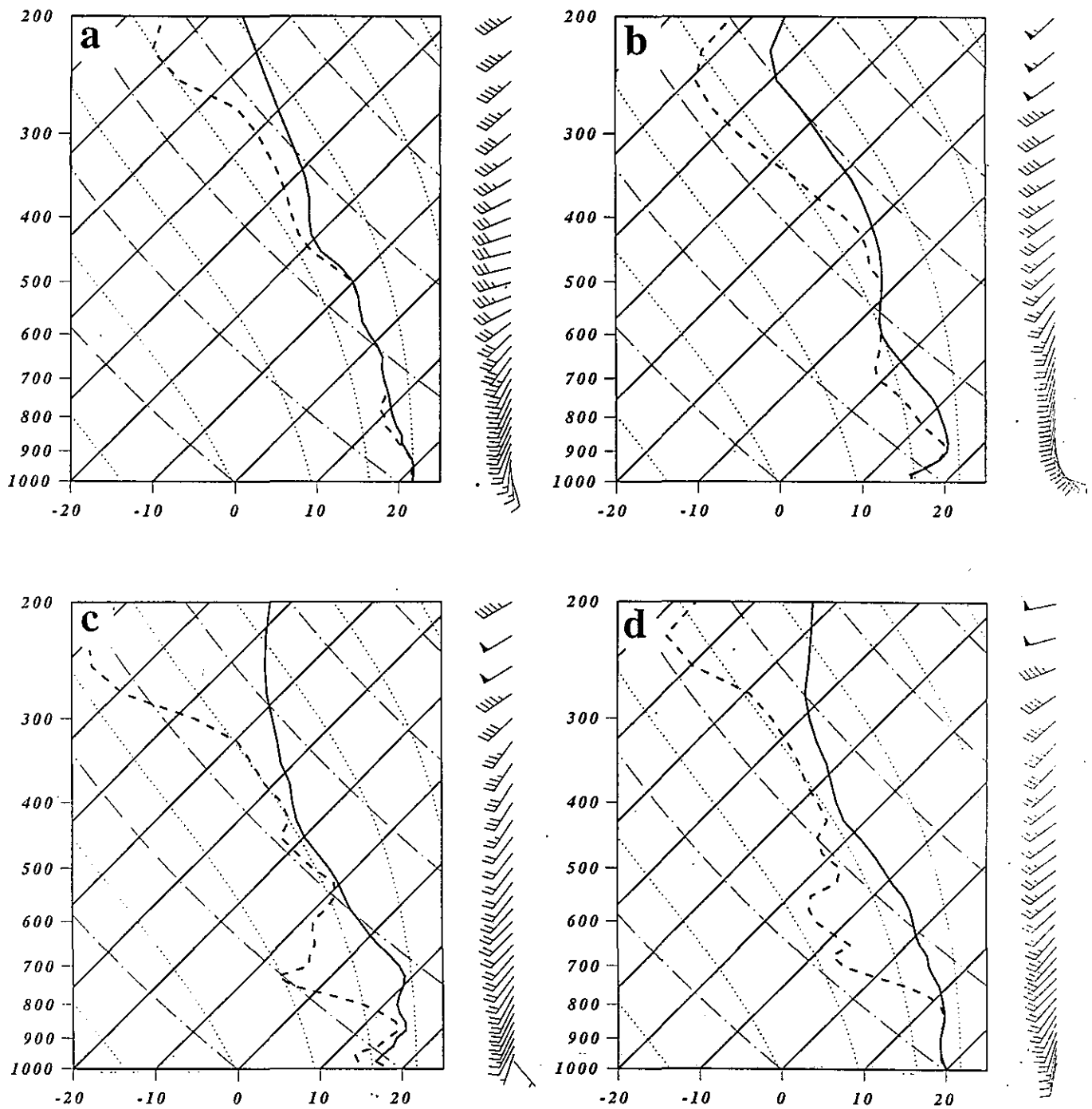


Figure 33. GMASS coarse mesh simulated vertical soundings for (a) Macon, Georgia (MCN), (b) Athens, Georgia (AHN), (c) Charlotte, North Carolina (CLT), and (d) Raleigh-Durham, North Carolina (RDU) valid at 0000 UTC 28 November 1988.

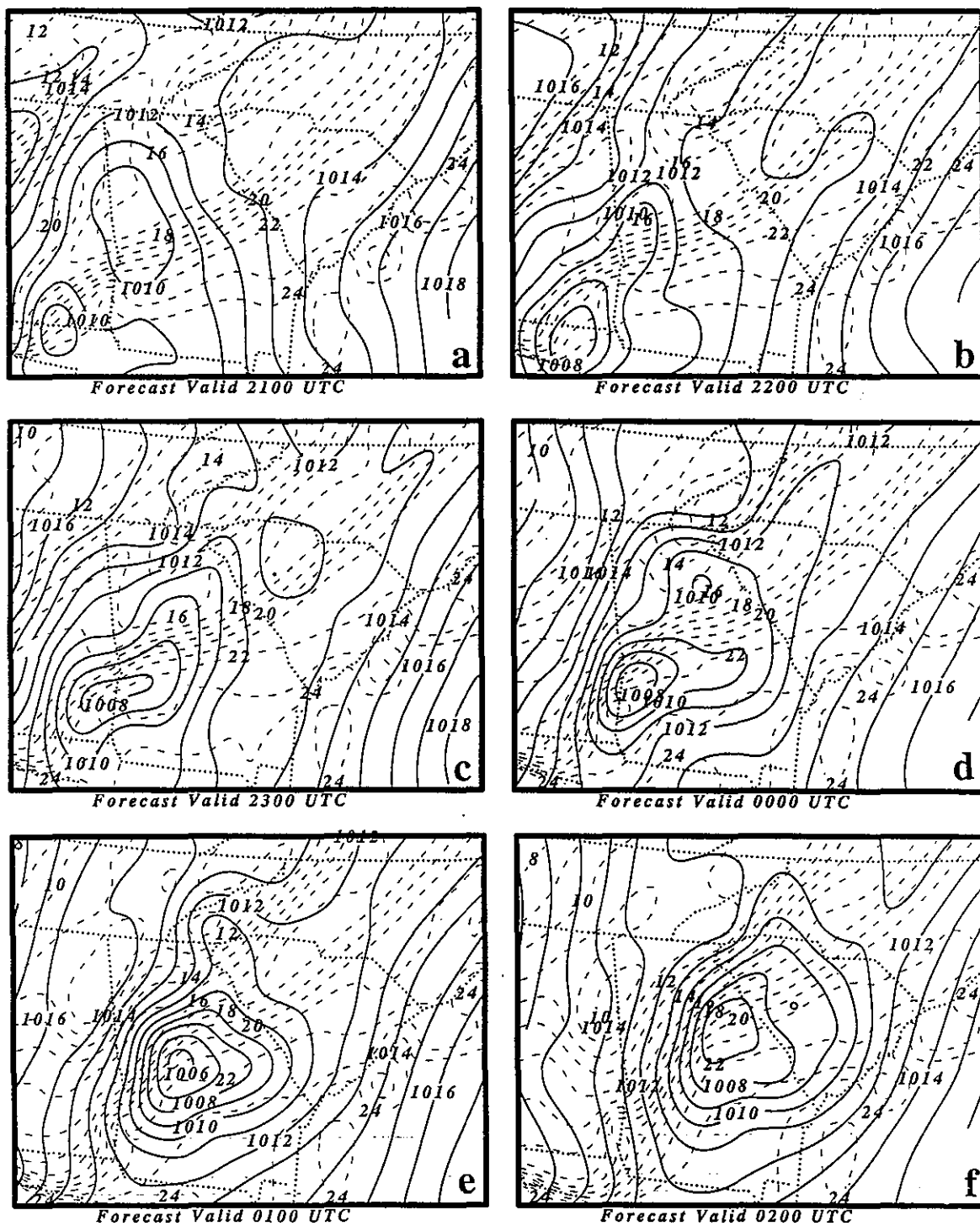


Figure 34. GMASS coarse mesh simulated mean sea level pressure (solid lines in mb) and surface temperature (dashed lines in °C) valid at (a) 2100, (b) 2200, (c) 2300, (d) 0000, (e) 0100, and (f) 0200 UTC 27-28 November 1988.

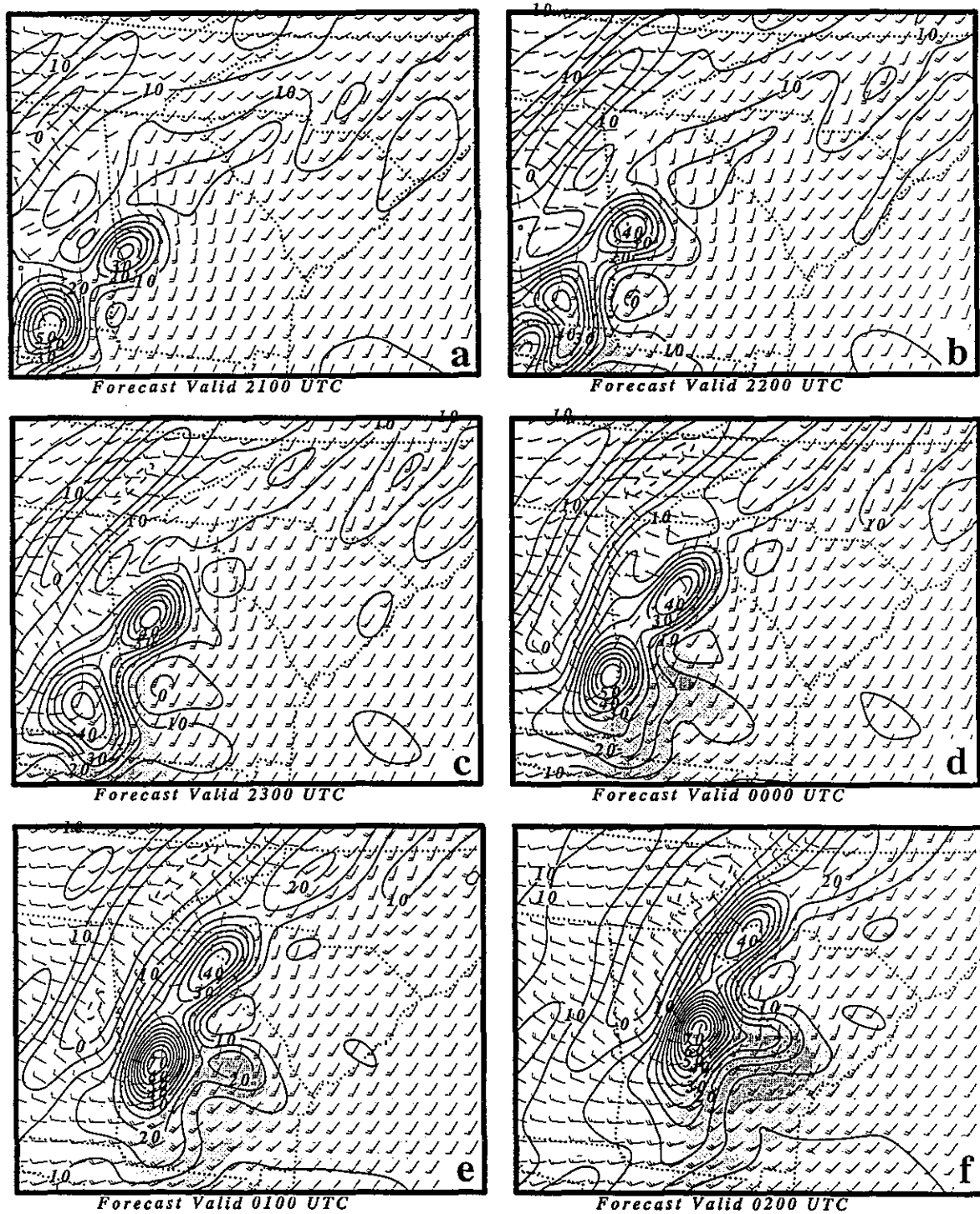


Figure 35. GMASS coarse mesh simulated 850 mb wind vectors (alternate rows and columns except (a), isotachs (shaded every 10 ms^{-1} above 30 ms^{-1}), and absolute vertical vorticity (dashed lines 10^{-5} s^{-1}) valid at (a) 2100, (b) 2200, (c) 2300, (d) 0000, (e) 0100, and (f) 0200 UTC 27-28 November 1988

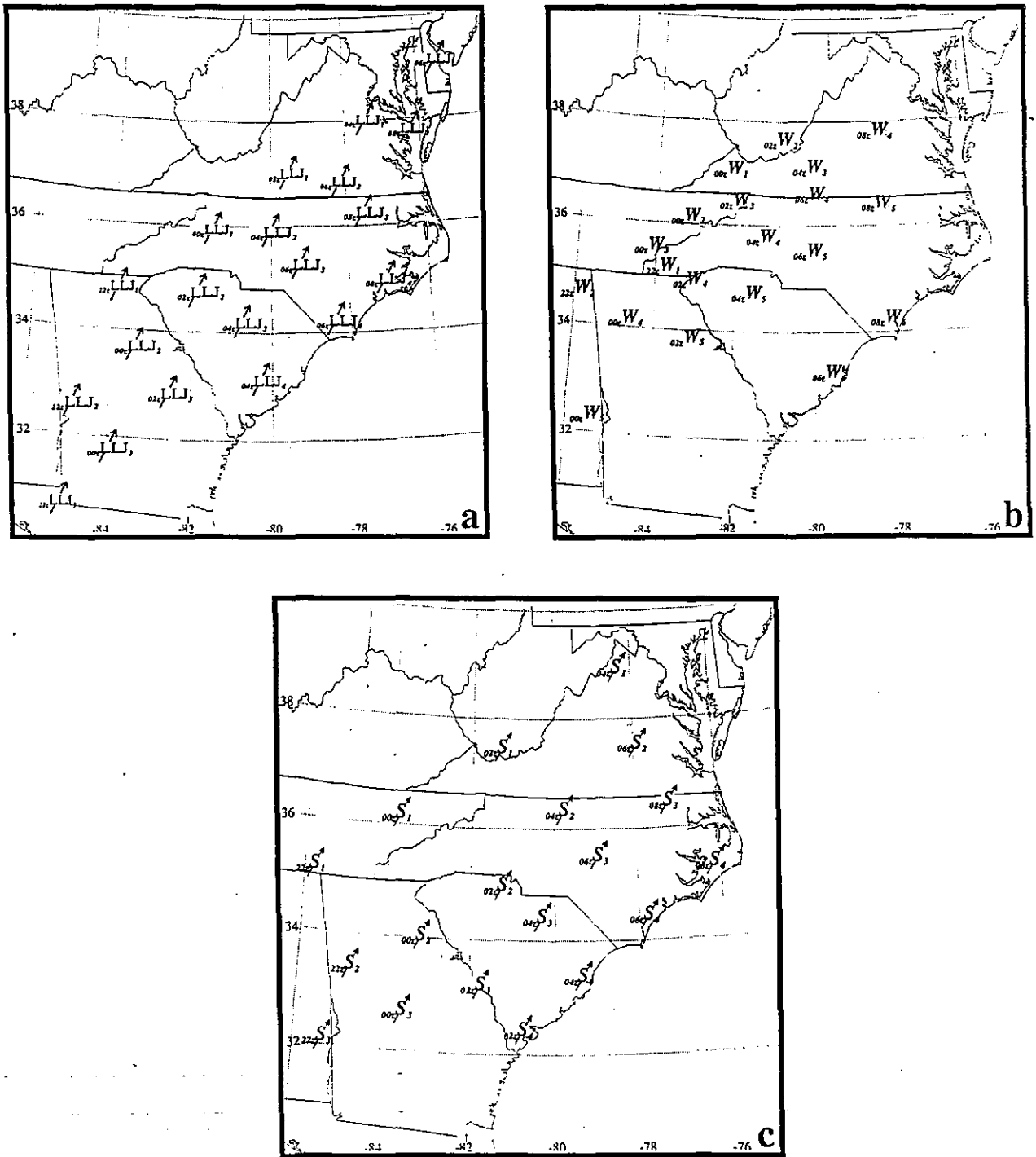


Figure 36. Location of GMASS coarse mesh simulation a) low-level Jet position (J_x), b) gravity wave location (W_x), and c) mid-tropospheric wind surges (S_x) as a function of time during the 2200-0800 UTC 27-28 November 1988 period.

northwestern South Carolina and northeastern Georgia by 0200 UTC (Fig. 35). W_5 , which is accompanied by stronger mean sea level pressure falls, increases its accompanying low-level jet to nearly 38 ms^{-1} by 0200 UTC, while the W_4 jet has diminished slightly to $\sim 24 \text{ ms}^{-1}$ from a maximum value of nearly 30 ms^{-1} . Satellite imagery indicates cloud masses which are observed in close proximity to these simulated features over South Carolina and Georgia at 0100 UTC (Fig. 39).

4.6 Summary of Stage B

The key processes which occur during Stage B include:

- 1) The convection associated with the eastward moving primary cold front perturbs the subgeostrophic entrance region of the PJS located over the Tennessee River Valley.
- 2) The accompanying diabatic heating induces mesoscale height rises which modify the synoptic scale northwestward-directed pressure gradient force, resulting in a northward deflection of the southern part of the polar jet streak entrance region.
- 3) A southeastward deflection of the southern part of the polar jet occurs due to an inertial-advective geostrophic adjustment response to the northward deflection.
- 4) A mesoscale momentum surge and mesoscale exit region form over the Alabama/Georgia/Tennessee border region, resulting in a "split" in the polar jet streak entrance region in close proximity to a secondary CFA.
- 5) This geostrophic adjustment triggers secondary inertial gravity waves over the North Carolina piedmont, downstream from the mesoscale momentum surge which is generated ahead of the primary wave-CISK mode.
- 6) The rapid northeastward movement of the mesojets induces inertial-advective mass flux divergence over the piedmont from Georgia to

Virginia. This mesoscale divergence pattern is sustained in time by baroclinic processes accompanying the coupling of the jetlet to the CFA.

7) The meso-exit region pressure falls break down the surface mesoscale blocking ridge.

8) The subsequent pressure falls allow the Georgia mesoscale/LLJ/vorticity maximum to propagate northeastward while undergoing intensification.

4.7 Stage C : Propagation and Intensification of the Georgia Mesoscale/LLJ Via Wave-CISK: Observations

The satellite, surface, and radar observations depicted in Figs. 37-40 indicate a close relationship between surface mesocyclones/vorticity maxima and propagating mesoscale convective systems between 0300 and 0600 UTC. To the north and south of the mesocyclone are propagating troughs and cloud clusters. These features are embedded within a trough located from southwestern Virginia through south-central Georgia at 0300 UTC. From 0300 to 0600 UTC, the Georgia mesocyclone (L_1) advances from the region between AHN, CAE, and GSP towards RDU following a path southeast of CLT and just northwest of Pope Air Force Base (POB). A weak mesocyclone (L_2) situated over southwestern Virginia at 0300 UTC propagates to the vicinity of RIC by 0600 UTC. Finally, a third mesocyclone/trough system (L_3) located over the area between Alma, Georgia (AMG) and Augusta, Georgia (AGS) at 0300 UTC propagates to near CHS by 0600 UTC. These features are all moving/developing to the right of the rawinsonde-derived mid-tropospheric wind vector averaged at 0000 UTC and 1200 UTC over the region including Virginia through Georgia.

These mesotroughs/confluence zones defined from the surface observations are closely coupled to satellite and radar-derived images of mesoscale cloud systems (Figs. 39, 40). Three key cloud complexes can be identified during this period, two over the North Carolina Piedmont which are well-developed throughout the period, and one along the

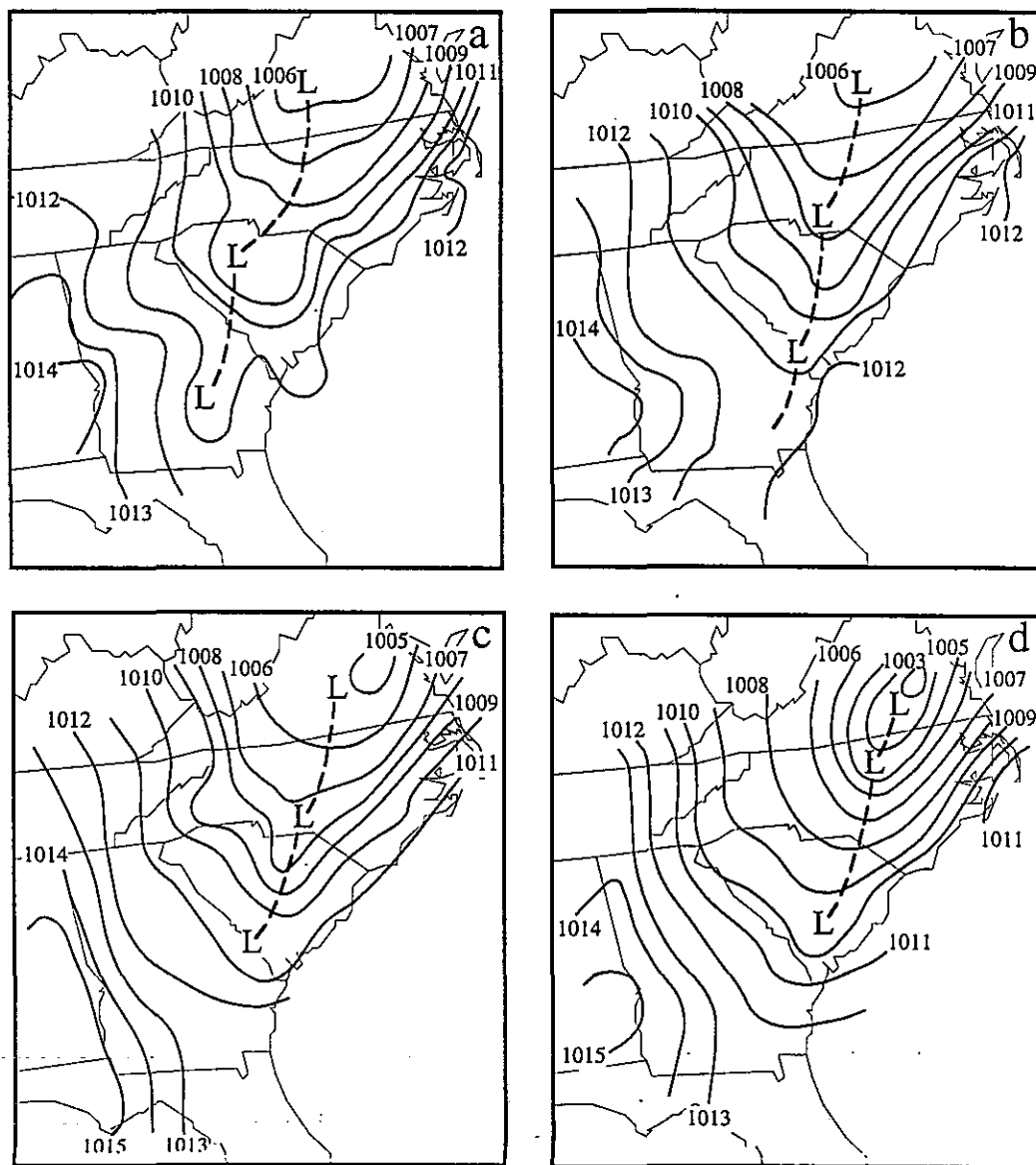


Figure 37. High resolution mean sea level pressure analyses (mb) based on NWS hourly surface data valid at (a) 0300, (b) 0400 (c) 0500, and (d) 0600 UTC 27-28 November 1988.

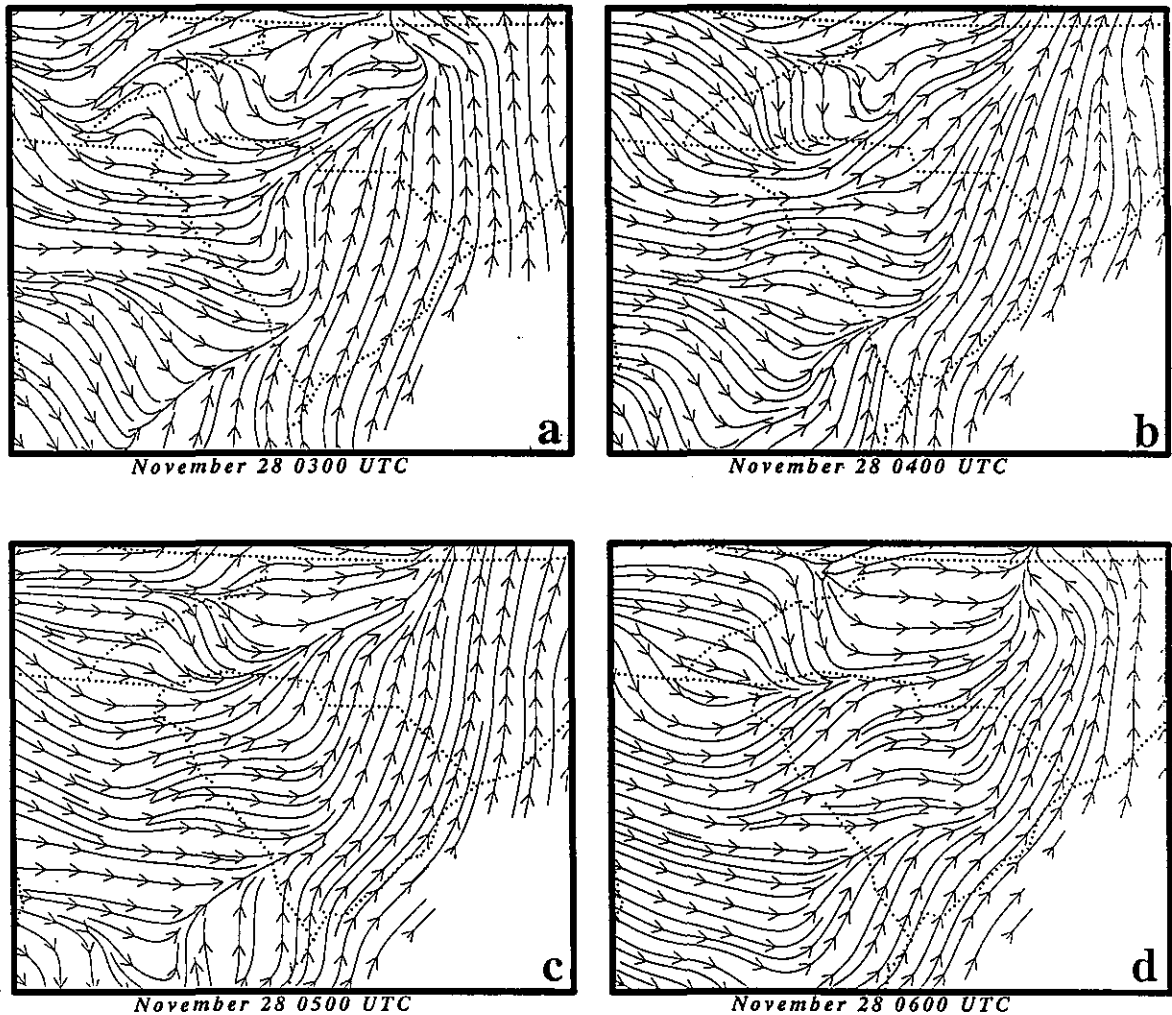
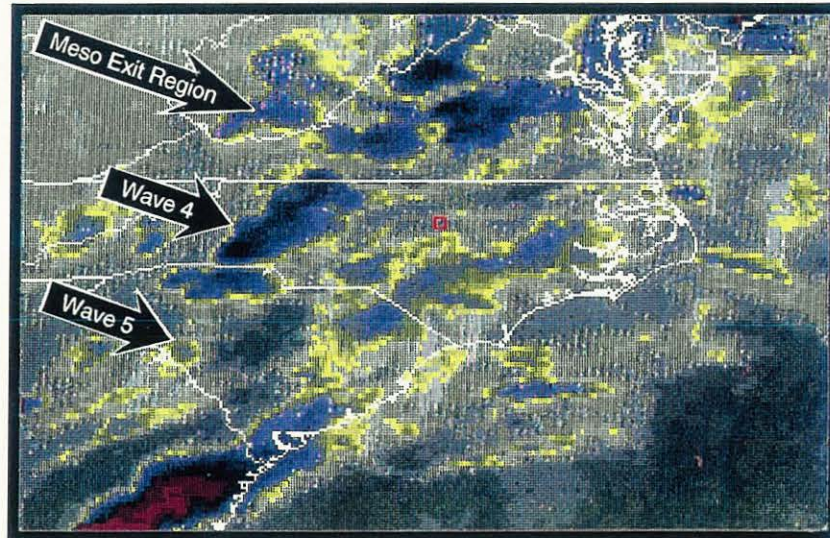


Figure 38. Objective streamline analysis based on NWS surface data valid at (a) 0300, (b) 0400 (c) 0500, and (d) 0600 UTC 28 November 1988.

Atlantic coast which develops close to the end of the period. Between 0300 UTC and 0600 UTC one MCS propagates from south-central Virginia to the Chesapeake Bay, a second MCS propagates from upstate South Carolina to a location between RDU and the Virginia border, while a third MCS develops over southeastern North Carolina by 0600 UTC. Just southwest of each system is a signal of column drying during this period located over southwestern Virginia, west central North Carolina, and just east of the northern part of the South Carolina coast. It is of interest that each observed

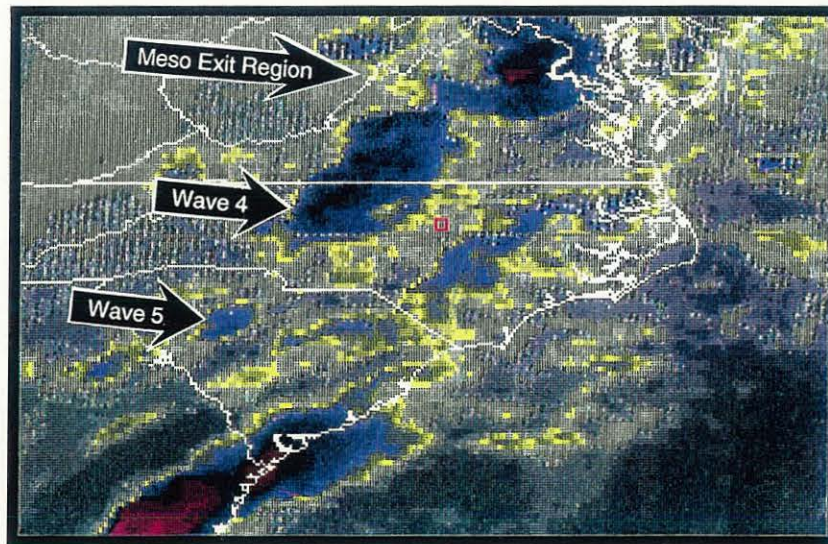
and numerically simulated surface mesocyclone, surface confluence center, mesoscale convective system, and developing dry slot is in close proximity to the three observed clusters of tornadoes around the 0600 UTC time period.

a



28 Nov 88 0100 UTC

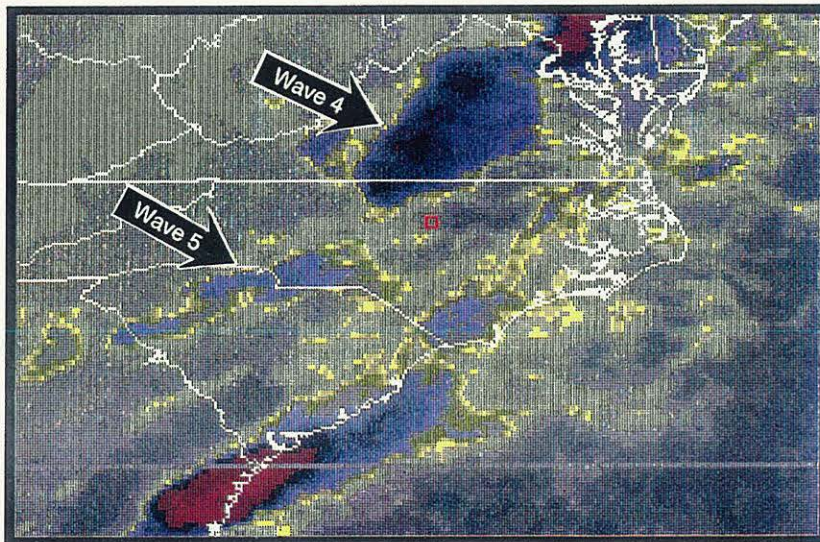
b



28 Nov 88 0200 UTC

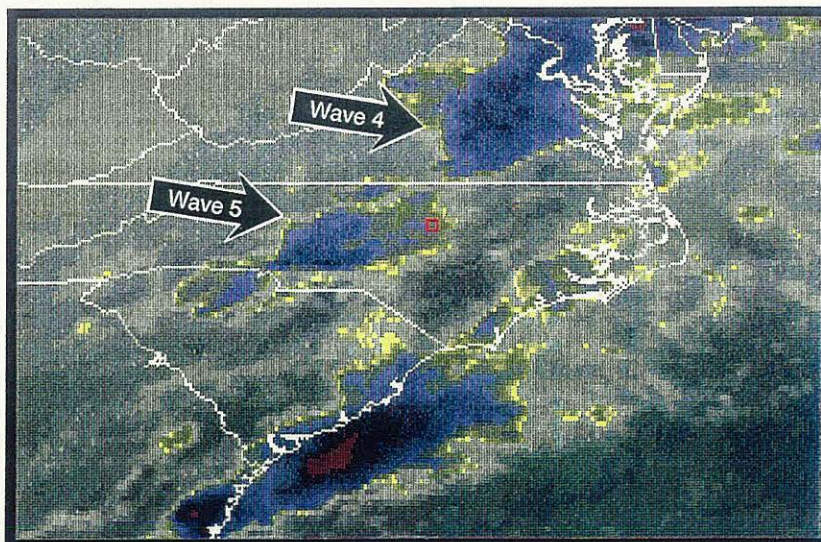
Figure 39. GOES infrared satellite imagery valid at (a) 0100, (b) 0200, (c) 0300, (d) 0400, (e) 0500, and (f) 0600 UTC 28 November 1988. GOES water vapor channel satellite imagery valid at (g) 0100, (h) 0200, (i) 0300, (j) 0400, (k) 0500, and (l) 0600 UTC 28 November 1988.

c



28 Nov 88 0300 UTC

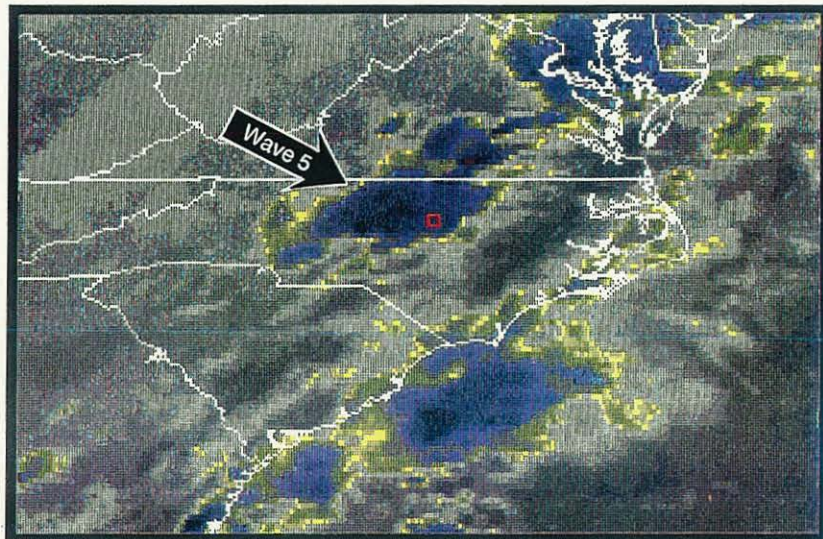
d



28 Nov 88 0400 UTC

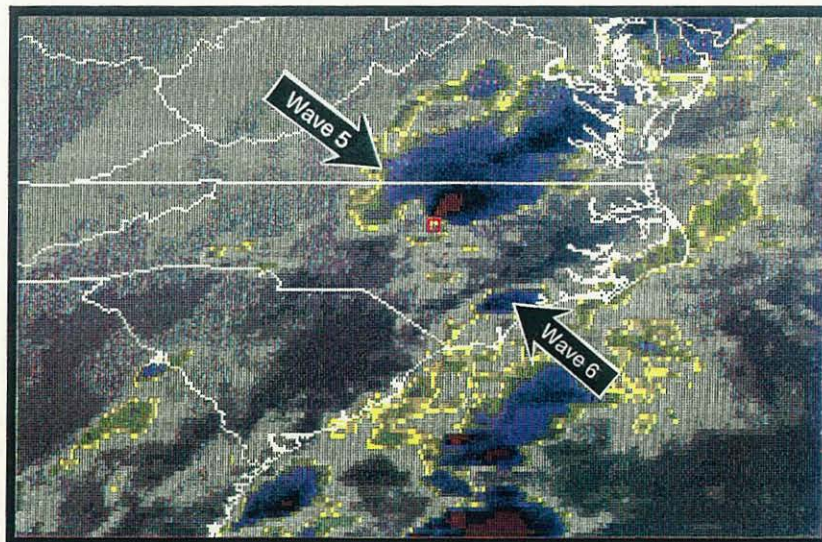
Figure 39. (Continued)

e



28 Nov 88 0500 UTC

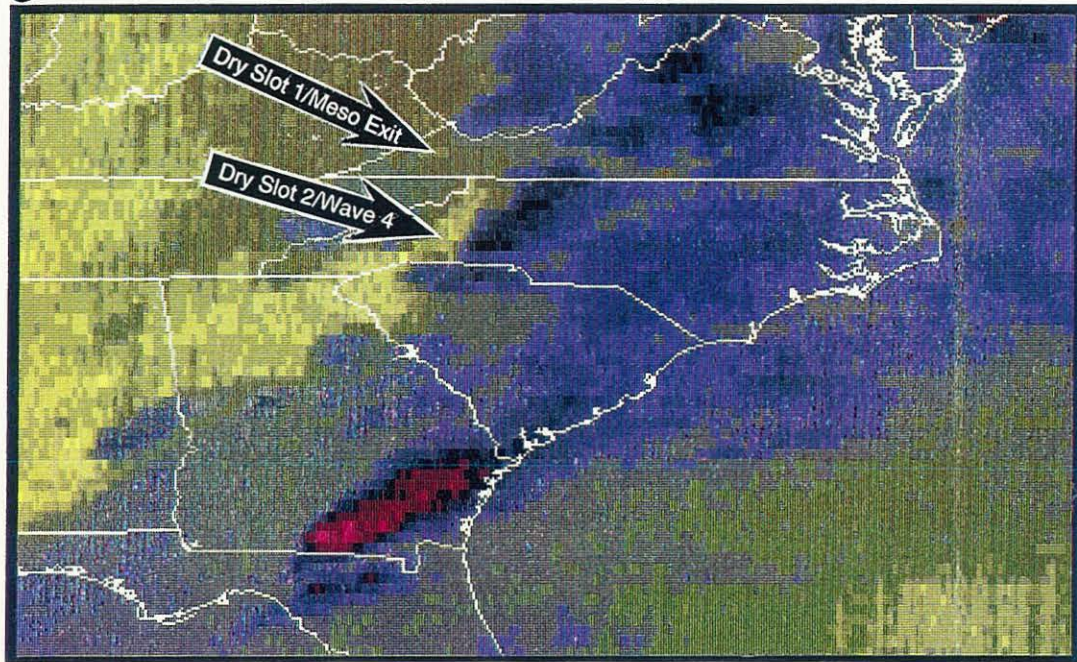
f



28 Nov 88 0600 UTC

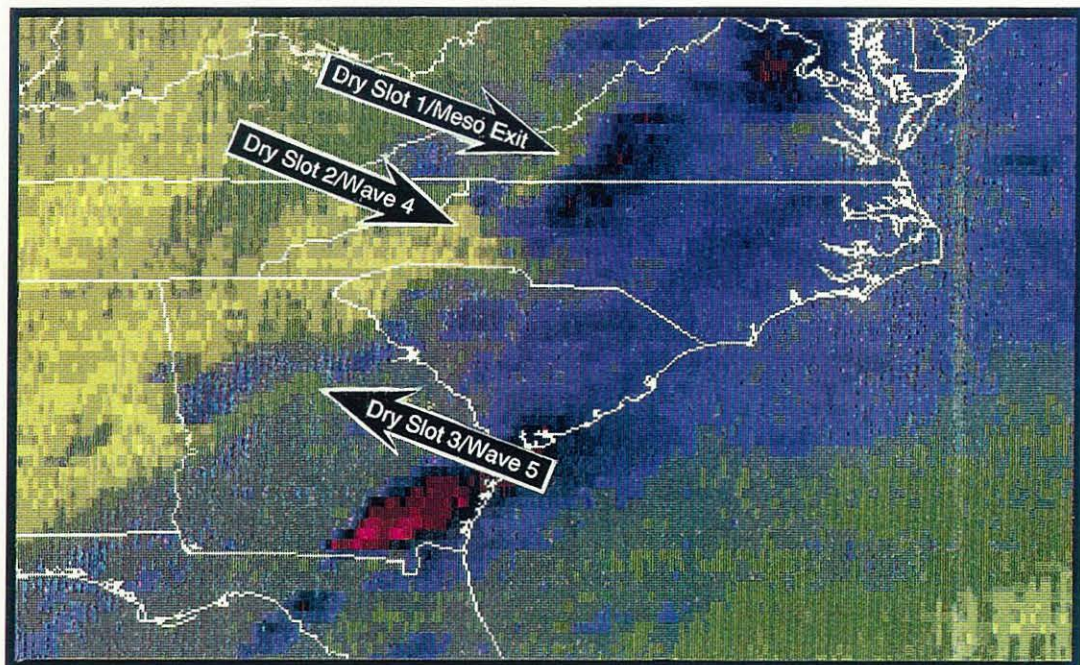
Figure 39. (Continued)

g



28 Nov 88 0100 UTC

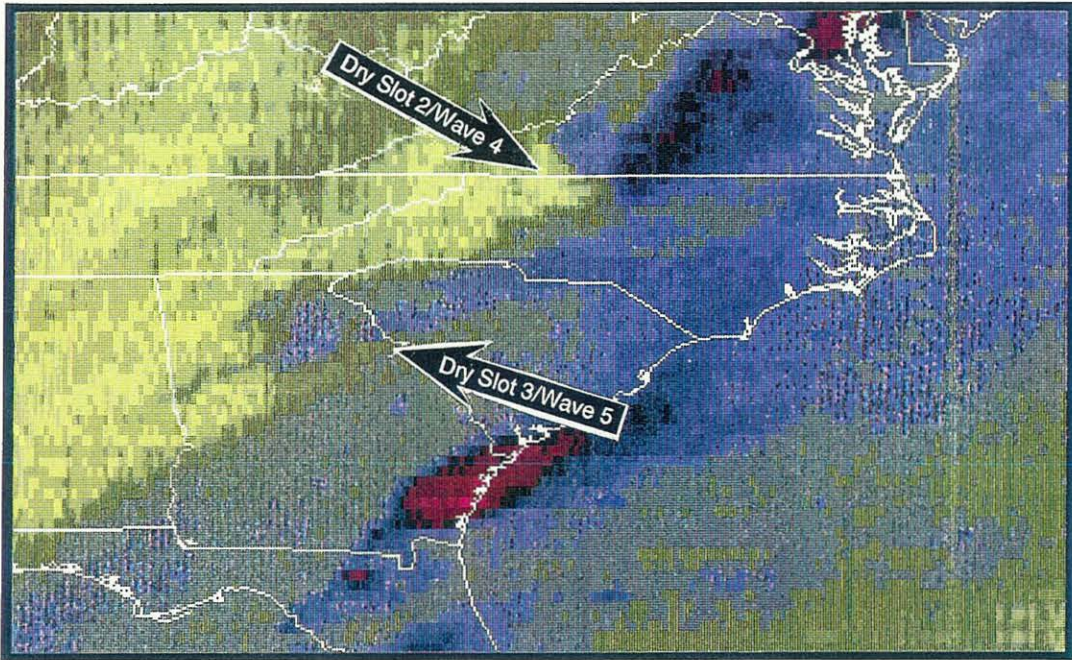
h



28 Nov 88 0200 UTC

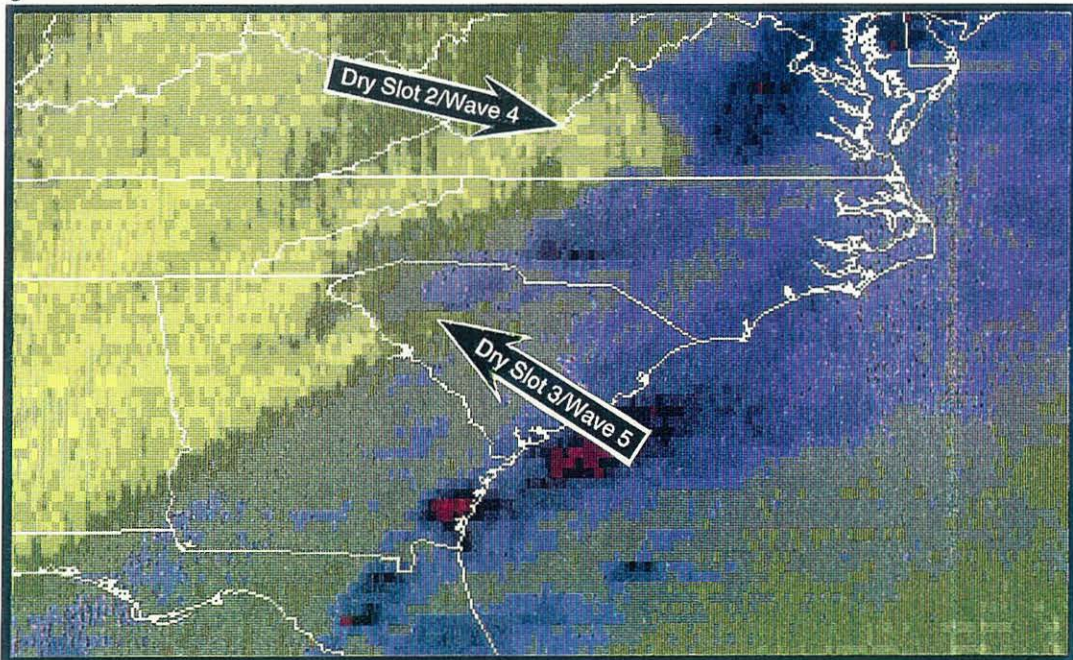
Figure 39. (Continued)

i



28 Nov 88 0300 UTC

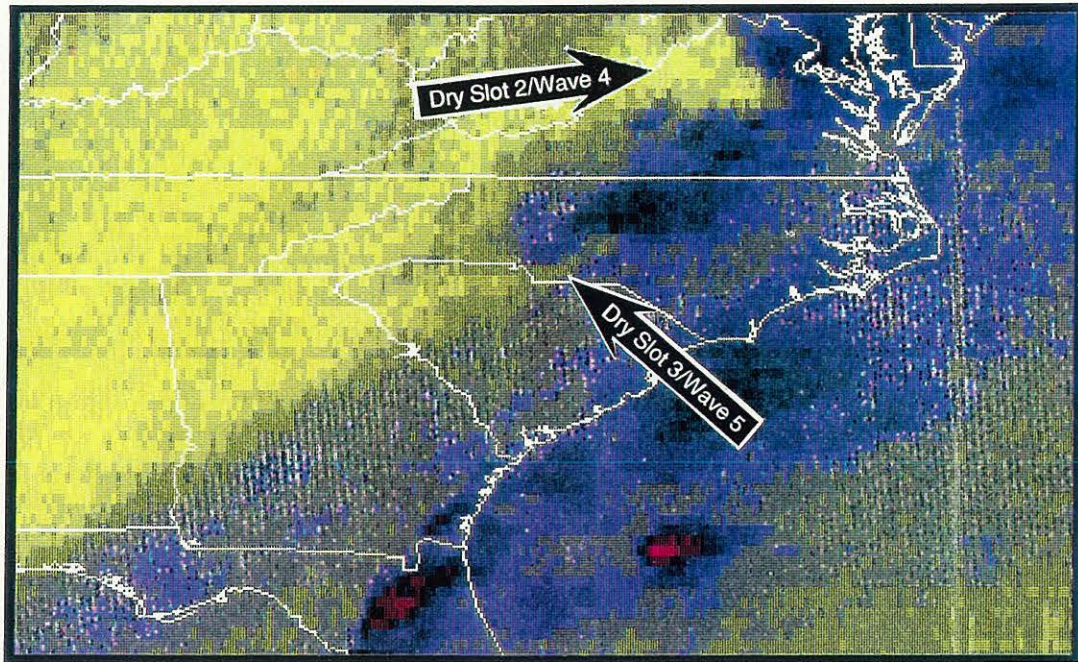
j



28 Nov 88 0400 UTC

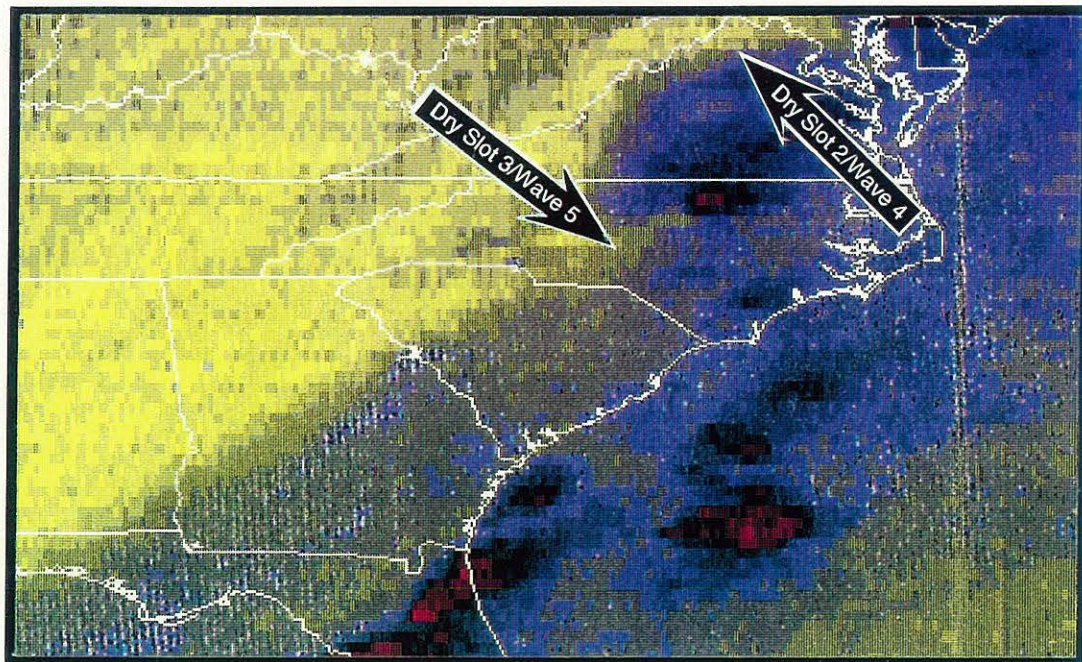
Figure 39. (Continued)

k



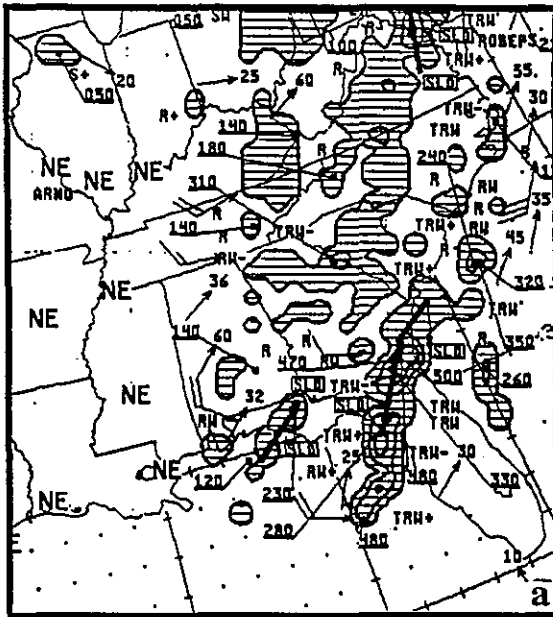
28 Nov 88 0500 UTC

l

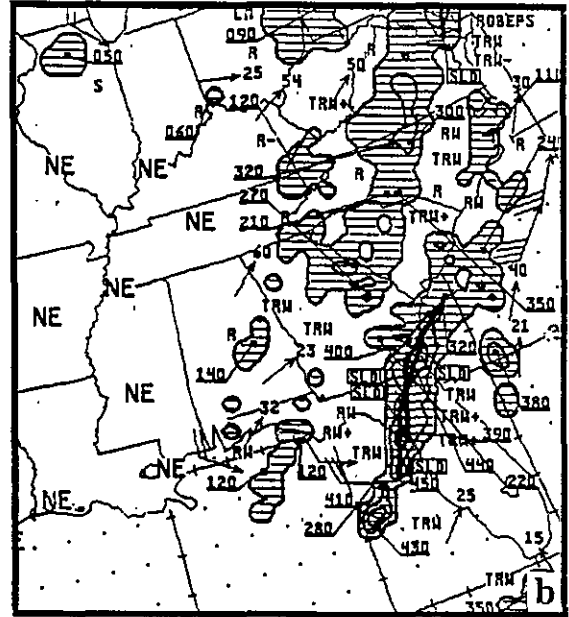


28 Nov 88 0600 UTC

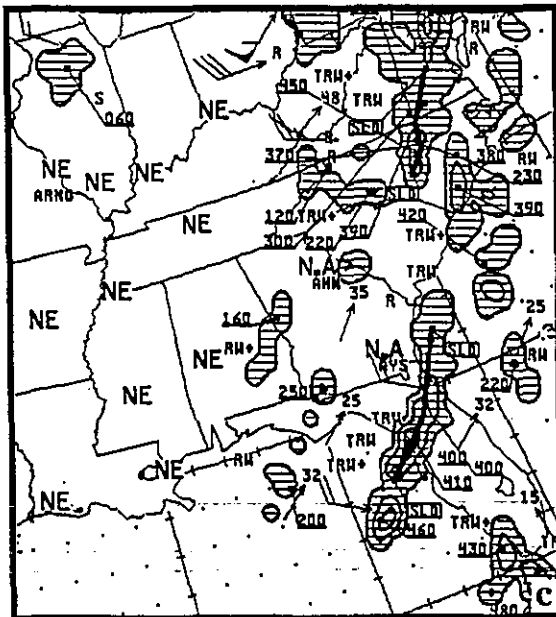
Figure 39. (Continued)



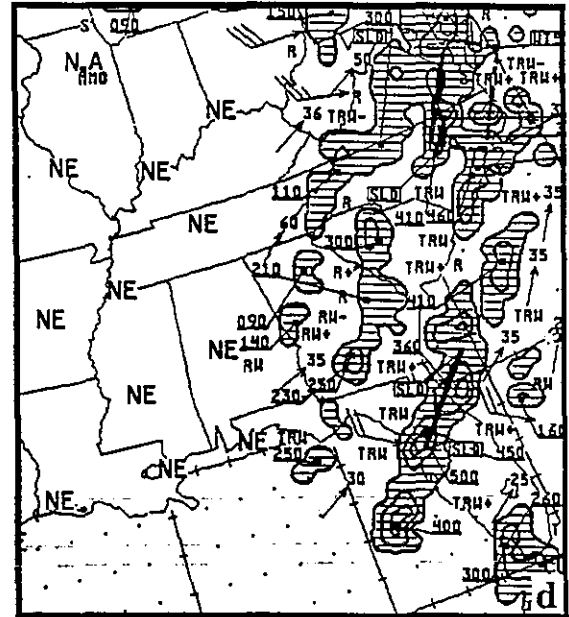
0335Z 28 NOV 1988 RADAR SUMMARY



0435Z 28 NOV 1988 RADAR SUMMARY



0635Z 28 NOV 1988 RADAR SUMMARY



0735Z 28 NOV 1988 RADAR SUMMARY

Figure 40. NWS MDR summaries valid at (a) 0335 (b) 0435, (c) 0635, and (d) 0735 UTC 28 November 1988.

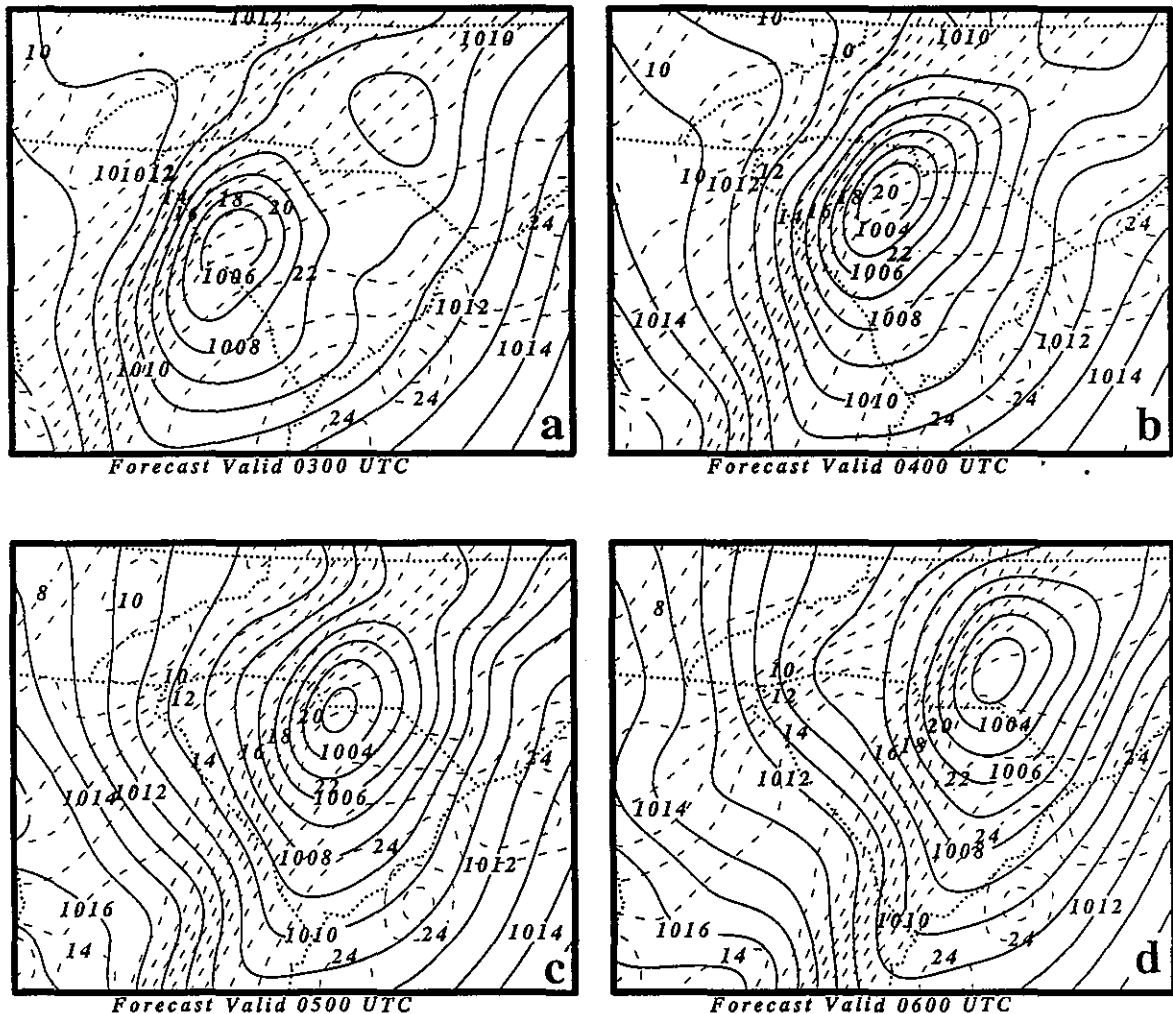


Figure 41. GMASS coarse mesh simulated mean sea level pressure (solid lines in mb) and surface temperature (dashed lines in $^{\circ}\text{C}$) valid at (a) 0300, (b) 0400 (c) 0500, (d) 0600, (e) 0700, (f) 0800, and (g) 0900 UTC 28 November 1988.

4.8 Stage C - Simulation Results

The coarse mesh simulation strongly suggests that each mesocyclone/convective system described in the previous subsection is coupled to a propagating wave-CISK feature. Figure 41 depicts the numerically simulated MSLP fields over the southeastern and middle Atlantic regions from 0300 to 0900 UTC. Evident is a northeast-southwest oriented surface pressure trough which

gradually drifts east-northeastwards. Embedded within this trough are mesoscale areas of low pressure, which are coupled to waves W_4 , W_5 , and, by 0800 UTC wave W_6 . Between 0300 and 0600 UTC, W_4 and its companion mesolow propagate from just northeast of CLT to northwest of RIC, while W_5 intensifies significantly and propagates from just east of AHN to between FAY and RDU. The distance traveled represents a uniform average velocity of $\sim 30 \text{ ms}^{-1}$, which is quite close to the phase velocity supported by the duct as described earlier in section 3.2. W_6 develops just ahead of

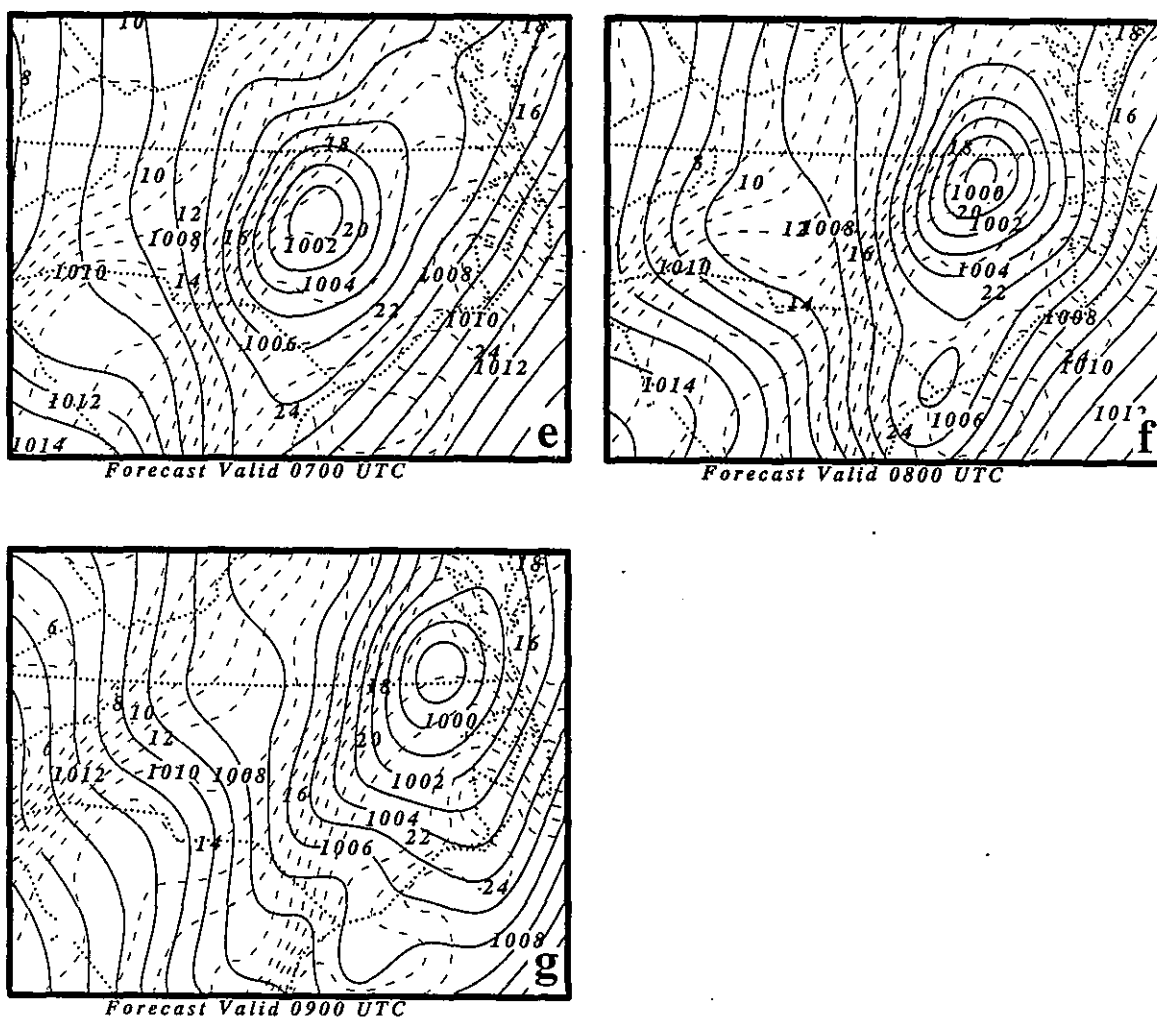


Figure 41 (Continued)

the cold frontal trough near the North/South Carolina border along the Atlantic Coastal Plain after 0700 UTC and continues to propagate northeastwards at $\sim 30 \text{ ms}^{-1}$ towards the Outer Banks region of North Carolina.

Figure 42 illustrates the 850 mb wind vectors and isotachs for the 0300-0900 UTC time period. Clearly evident are low-level jet maxima which are coupled to each mesocyclone and gravity wave as they propagate northeastward along the shallow frontal trough. By 0900 UTC, a new LLJ accompanying W_6 develops along the southeastern

North Carolina Coastal Plain. Each LLJ is comprised primarily of southerly momentum with the strongest jet and strongest ageostrophic wind component being associated with W_5 . Additionally, W_5 is associated with the strongest MSLP falls and largest 850 mb absolute vorticity ($\sim 10^{-3} \text{ s}^{-1}$). As can be seen in Fig. 43, the progression of the simulated low-level jet maximum accompanying W_5 is slightly, approximately 20-30 degrees, to the right of the observed 500 mb wind vector. This rightward cross-stream shift is consistent with observations of the movement of the mesoscale

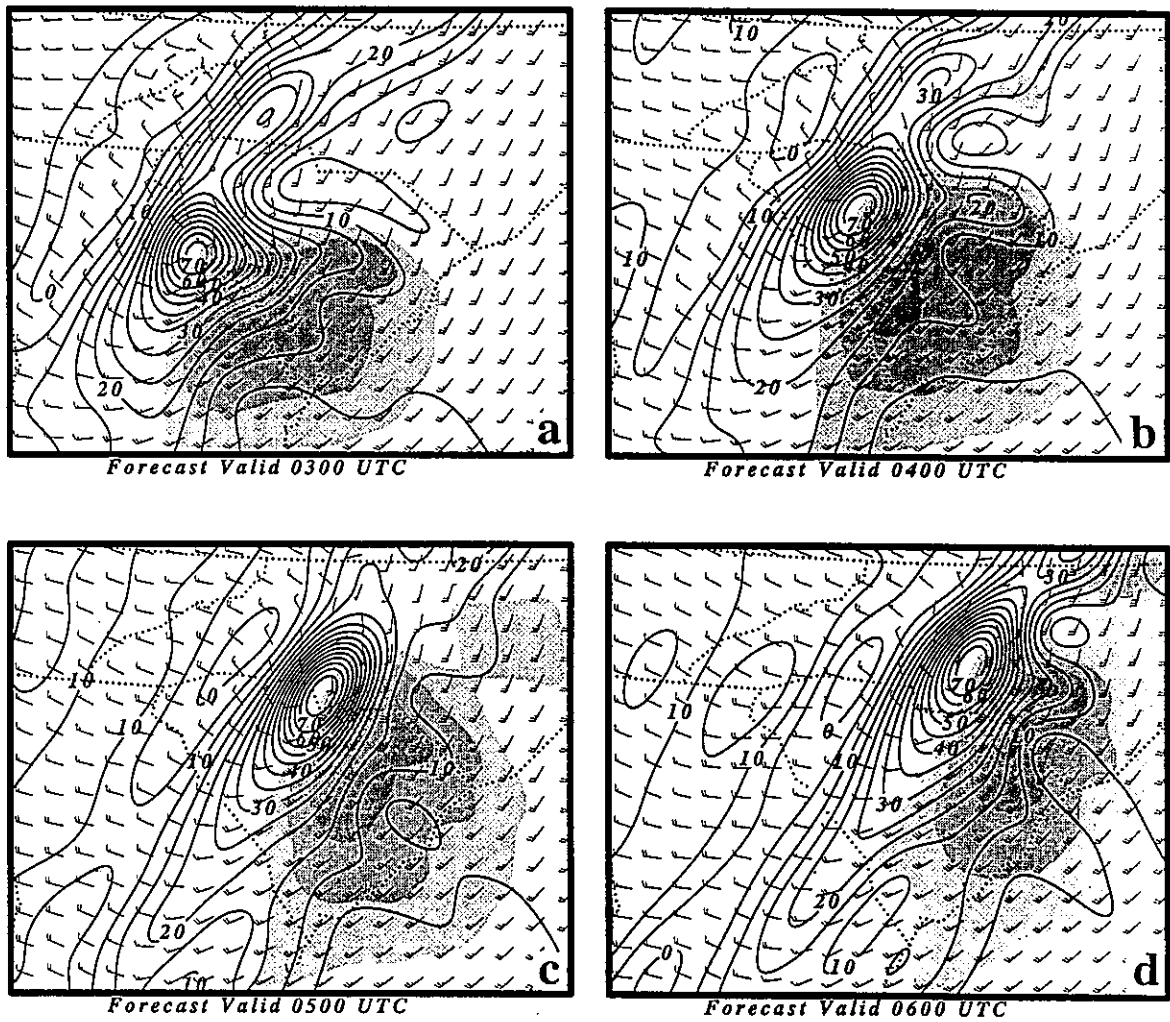


Figure 42. GMASS coarse mesh simulated 850 mb wind vectors (alternate rows and columns), isotachs (shaded every 10ms^{-1} above 20ms^{-1}), and absolute vertical vorticity (solid lines 10^{-5}s^{-1}) valid at (a) 0300, (b) 0400, (c) 0500, (d) 0600, (e) 0700, (f) 0800, and (g) 0900 UTC 28 November 1988.

convective system from upstate South Carolina to near RDU between 0300 UTC and 0600 UTC. The coarse mesh simulation is approximately one hour slow when compared to nature in producing the mesolow and its vorticity maximum over RDU around 0700 UTC.

Figure 44 shows vertical cross sections from Mobile, Alabama (MOB) to RDU valid at 0000 through 0600 UTC. Evident is the vertical structure of W_4 and W_5 as they propagate northeastwards along the Carolina Piedmont front. Note the much stronger ascent with W_5 , consistent

with its lower surface pressure minimum. The location of ascent relative to the deformed isentropes changes in time, however, and there is a general tendency for the upshear tilt of the wave and its amplitude to diminish as the surface cyclone intensifies and as the rear inflow jet momentum maximum descends into the lower troposphere and intensifies.

The importance of this descent of the momentum maximum will be examined during Stage D. As can be seen in Figs. 45 and 46, each wave is accompanied by a midtropospheric cold

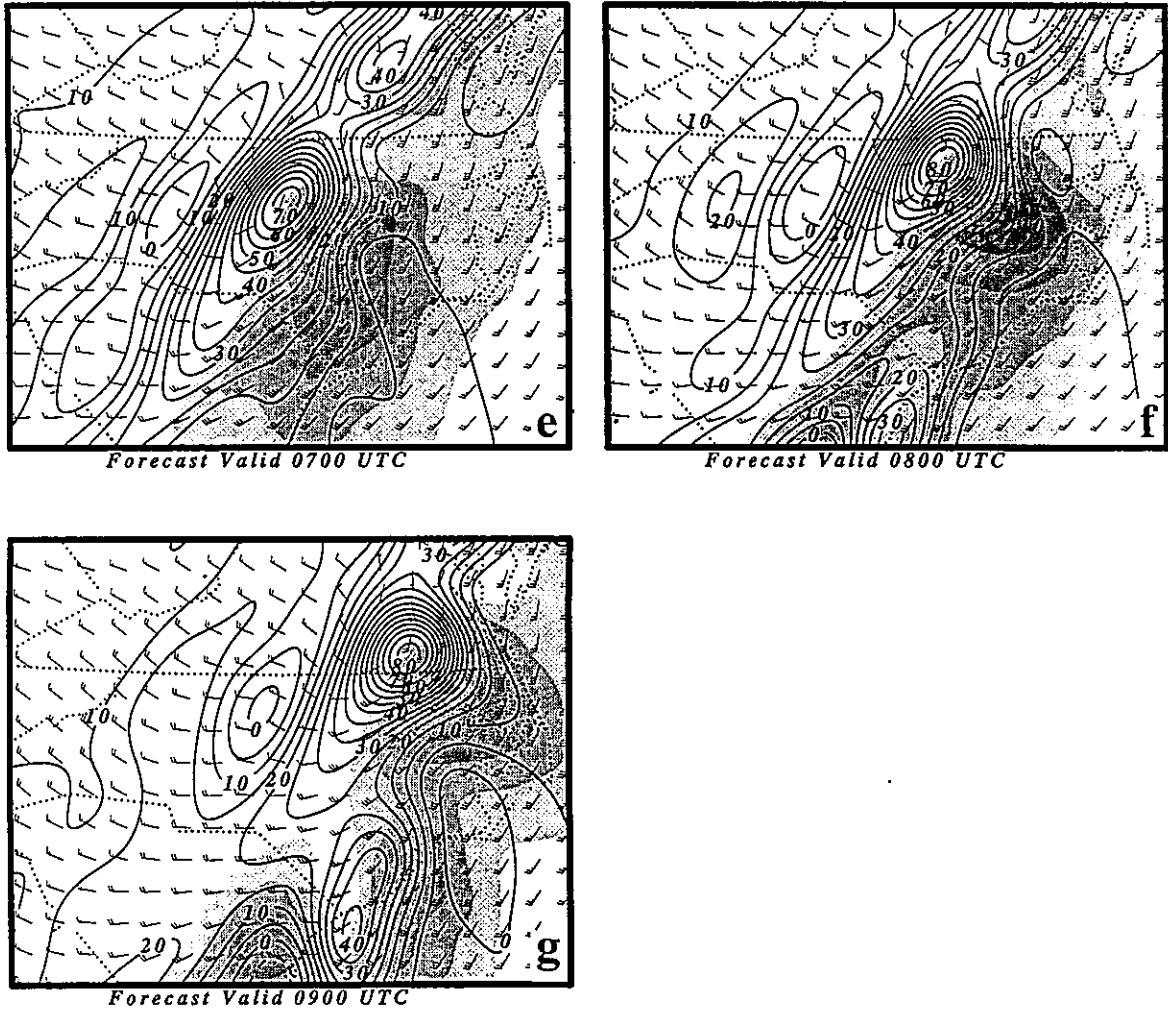


Figure 42. (Continued)

pool within the outflow area ahead of the warm pool within the crest. The convective heating in the crest produces the mass flux divergence, outflow, and ascent within the trough. The surface pressure falls are coupled to the outflow under the trough. Evaporative cooling under the crest maintains the surface pressure rises, thus amplifying convergence in proximity to the surface inflow jet which provides the moisture supply and sustains the convection. Behind the convection, descent at mid levels transports kinetic energy downwards, thus producing the confluent wind flow pattern behind the diffluence ahead of the wave crest. Coincident

with the descent of high momentum, dryer air is transported downward into the mid-levels.

4.9 Summary of Stage C

The key processes which occur during Stage C include:

- 1) The intensification of the Georgia mesocyclone via wave-CISK between Georgia and

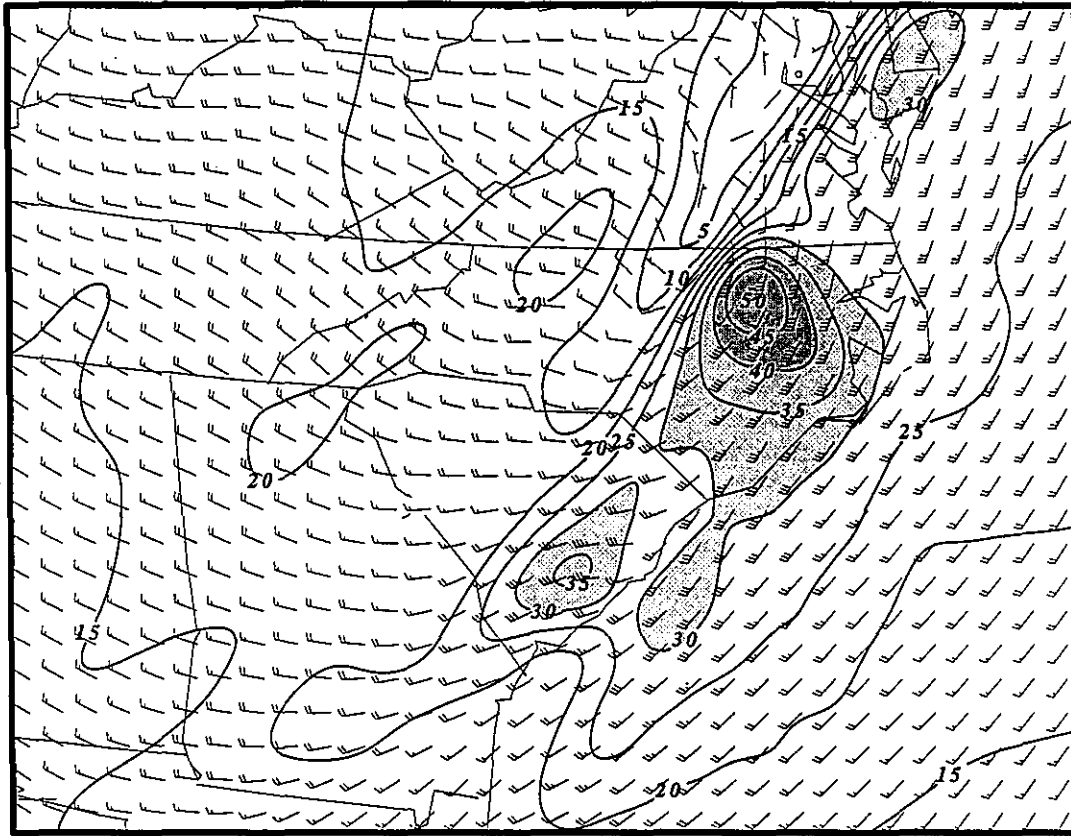


Figure 43. GMASS coarse mesh-simulated 850 mb wind vectors and isotachs (solid lines every 5 ms^{-1} shaded every 10 ms^{-1} above 20 ms^{-1}) valid at 0800 UTC 28 November 1988.

western South Carolina as Atlantic moisture is advected into the system.

2) The diabatic heating accompanying the wave-CISK produces pressure falls, thus increasing the northwestward-directed low-level accelerations over the South Carolina Piedmont.

3) The intensifying pressure gradient force results in a stronger low-level jet and enhanced moisture convergence.

4) The gravity wave accompanying the Georgia mesocyclone/low-level jet propagates 20-30 degrees to the right of the mean tropospheric flow toward the data-sparse region encompassed by AHN, GSP, CAE, CLT, FLO, FAY, GSO, and RDU.

5) The low-level vorticity increases explosively due to vortex tube stretching over the piedmont.

6) A cold pool forms in the mid-troposphere ahead of the wave-CISK enhancing the initiation of

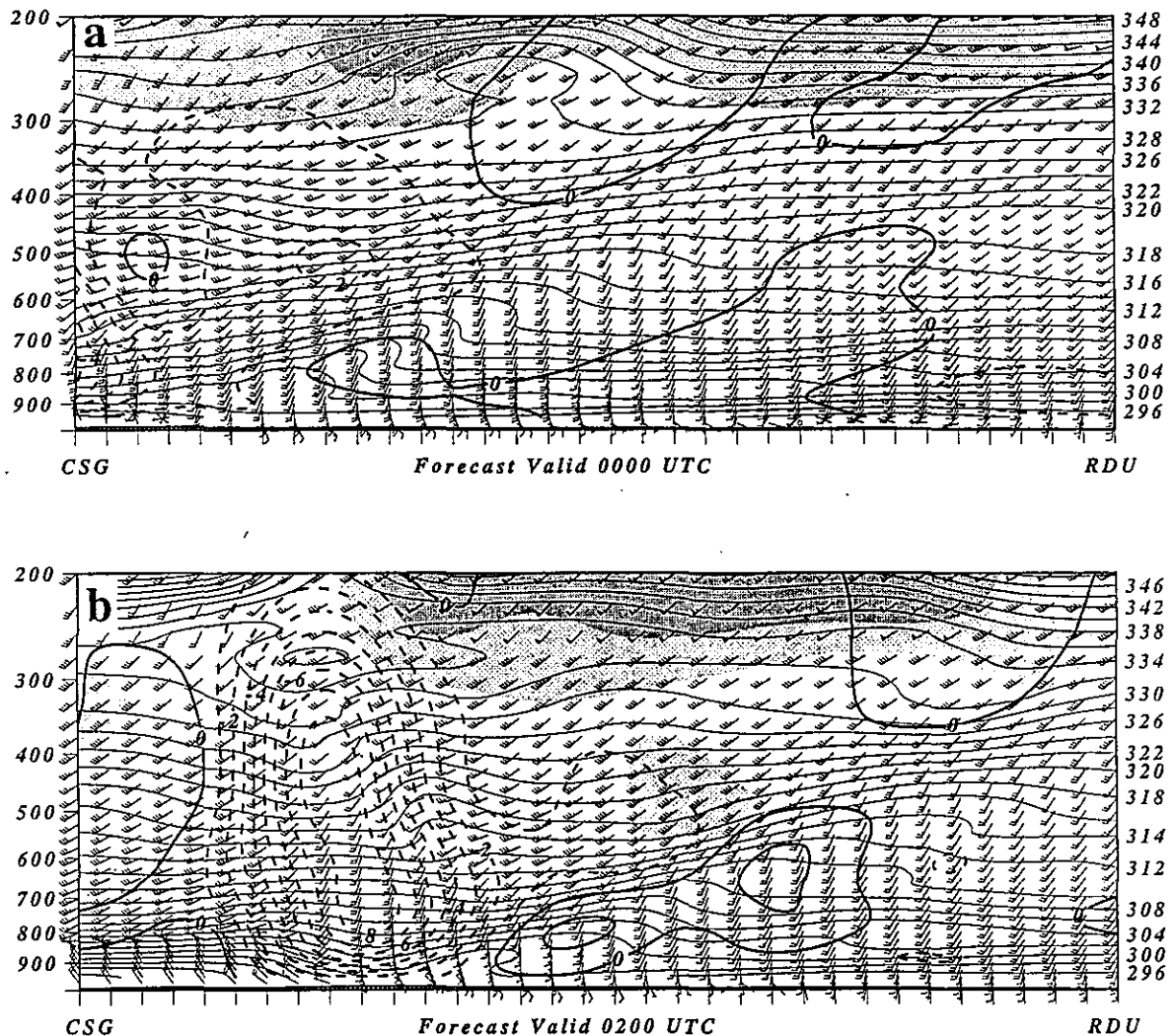


Figure 44. GMASS coarse mesh simulated vertical cross sections from Columbia, South Carolina (CSG) to Raleigh-Durham, North Carolina (RDU) of potential temperature (thin solid lines in K), vertical velocity (thick solid lines are positive values and thick dashed lines are negative values in 10^{-2} mbs^{-1}), isotachs (shaded every 10 ms^{-1} above 40 ms^{-1}), and wind barbs valid at (a) 0000, (b) 0200, (c) 0400, and (d) 0600 UTC 28 November 1988.

convection while sinking behind the wave transports momentum and dry air downward.

7) Secondary mesocyclones/low-level jets form northeast and southeast of the Georgia

mesocyclone as it traverses the South Carolina piedmont.

8) The secondary mesocyclones intensify prior to observed tornadoes in south-central Virginia and coastal North Carolina.

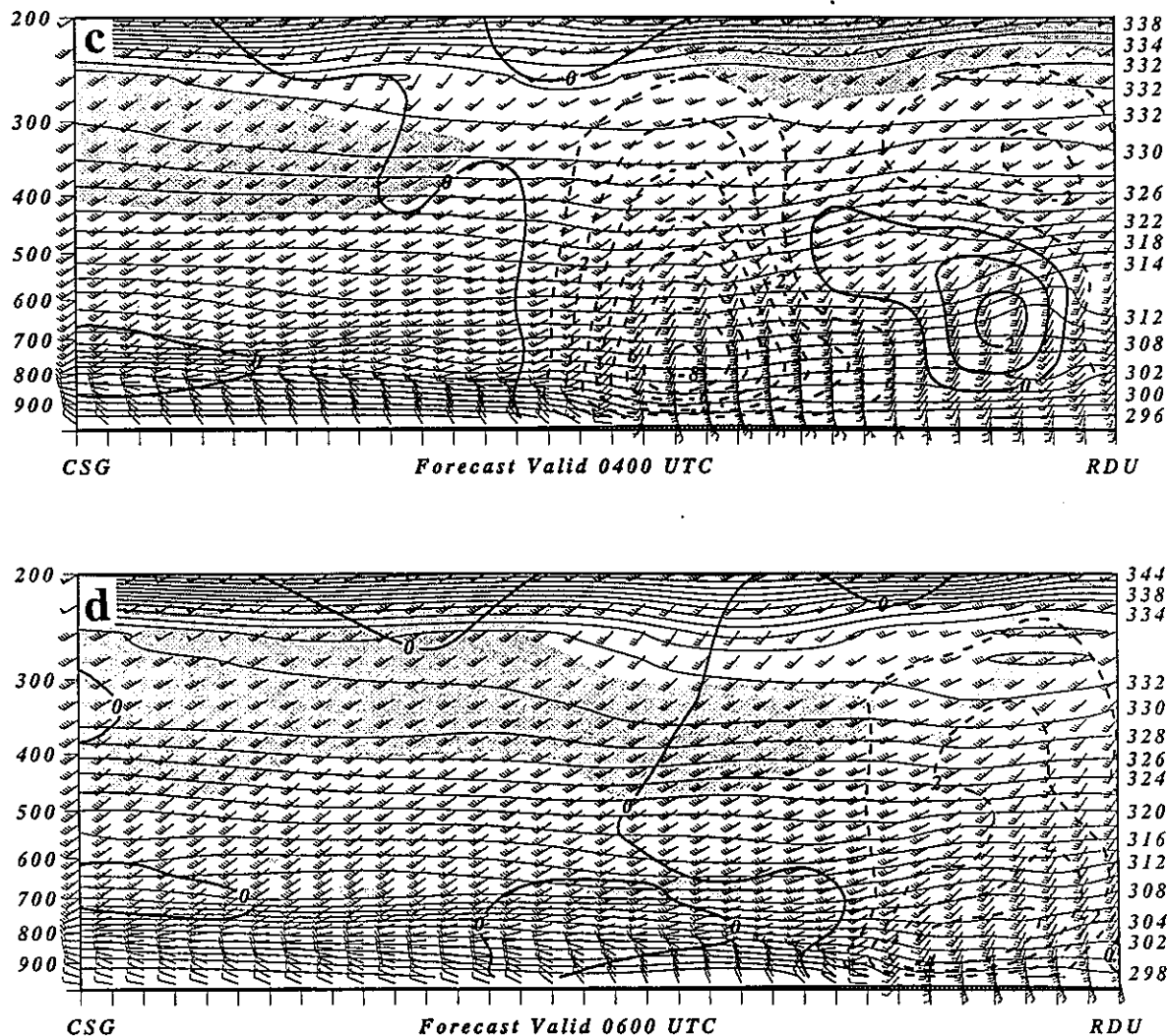


Figure 44. Continued.

4.10 Stage D: Descent of the in-flow Jet, Buoyancy and Rotation Production near RDU - Observations

Figures 37-40 depict the mean sea level pressure, surface wind flow, and cloud distribution around 0600 UTC which is just minutes prior the

time of the RDU tornado. These confirm the presence of a dry slot just southwest of the convective complex over RDU as well as the existence of a mesocyclone and strong low-level southeasterly wind flow. The only other local observational data include pressure and wind data captured by the Carolina Power and Light instruments shortly after 0600 UTC (Fig. 47) as well as fine scale radar data depicted in

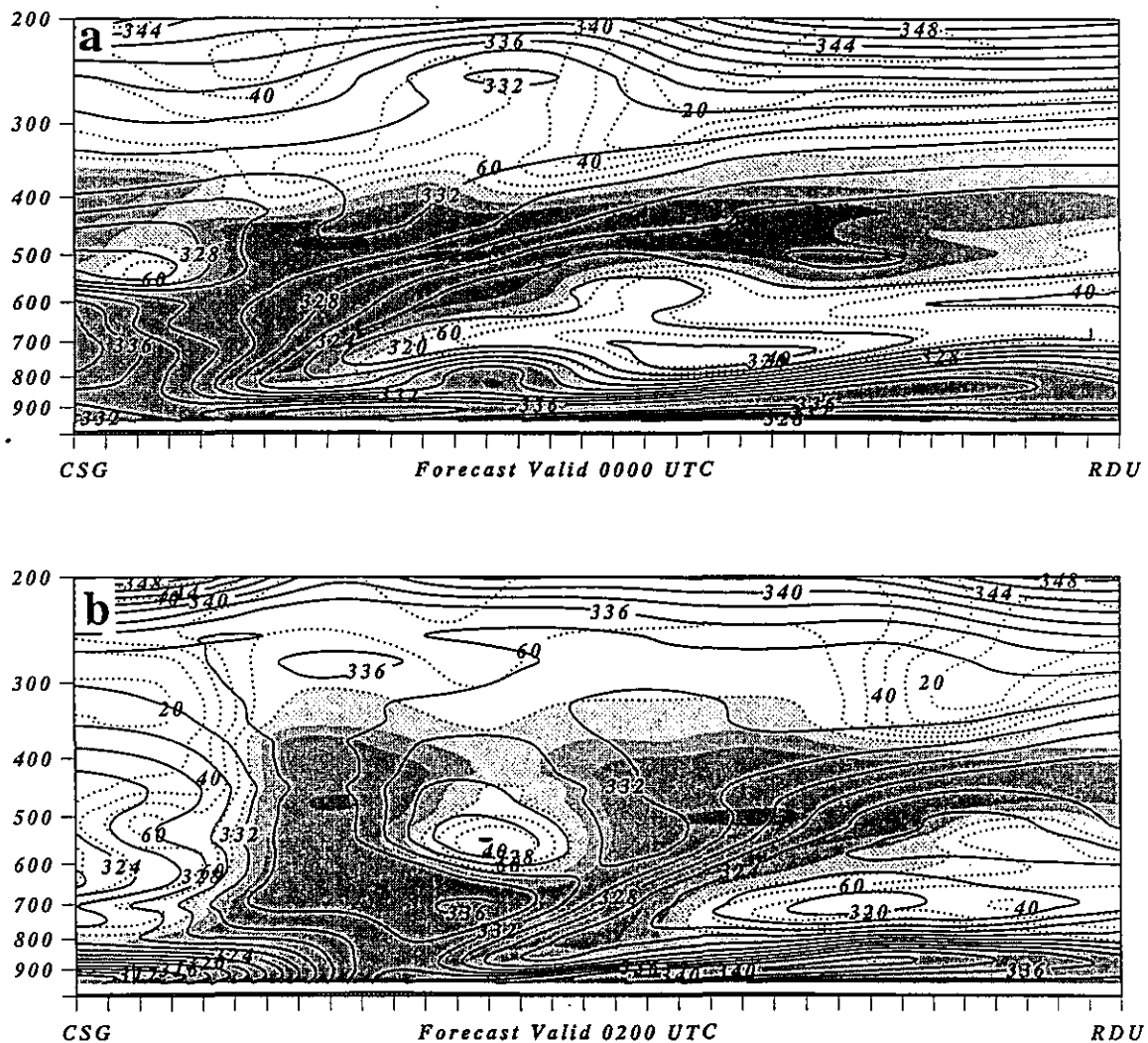


Figure 45. GMASS coarse mesh simulated vertical cross sections from Columbia, South Carolina (CSG) to Raleigh-Durham, North Carolina (RDU) of equivalent potential temperature (thin solid lines in K) and relative humidity (dotted line contoured every 10%, shaded above 70%) valid at (a) 0000, (b) 0200, (c) 0400, and (d) 0600 UTC 28 November 1988.

Przybylinski (1989). These data confirm the existence of a mesocyclone pressure perturbation passing over RDU coupled with gusty south-southeasterly low-level wind flow.

4.11 Stage D - Simulation Results

All simulation results from this section which are depicted in Figs. 48 and 49 are derived from the 12 km nested-grid experiment. At ~0300 UTC the simulation captures a mesocyclone which is located between AHN and CLT. This feature is ~3 mb deeper and ~50 km to the northeast of the

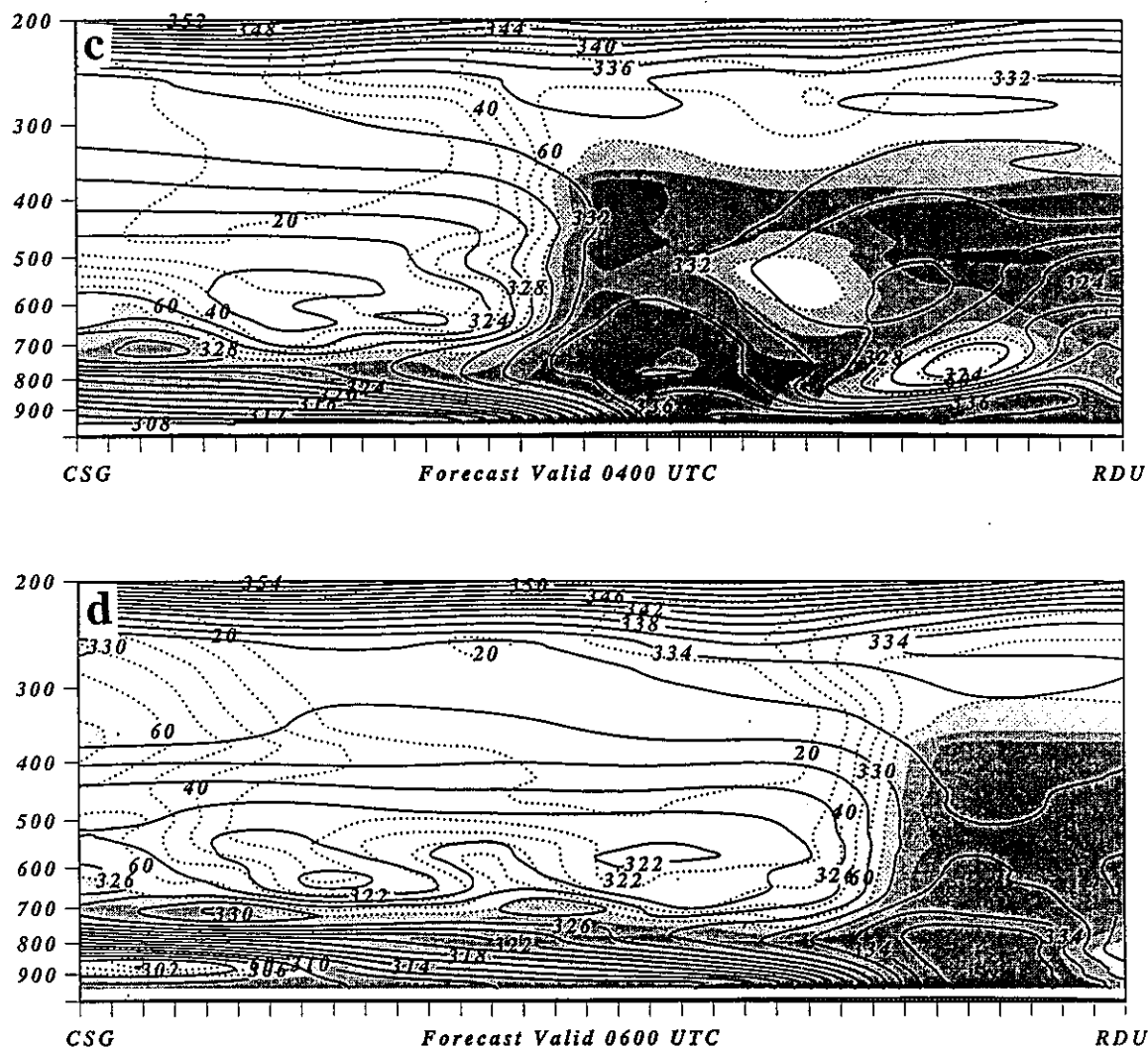


Figure 45. (Continued)

mesocyclone in the coarse mesh simulation. The mesocyclone is flanked by weaker waves of low-pressure to the northeast and southwest along the piedmont frontal boundary separating air with surface temperatures from $\sim 15^{\circ}\text{C}$ to the northwest to $\sim 22^{\circ}\text{C}$ to the southeast.

At 850 mb the axis of multiple confluence maxima is displaced to the west of the piedmont front, however, multiple southerly wind maxima

extend eastward from the region of lowest surface pressure which lies between CAE and GSP. The largest magnitude of absolute vertical vorticity is located just northeast of AHN, which is well southwest of the lowest surface pressure. At 500 mb, diffluent flow is coupled to the mesocyclones ahead of a rear inflow jet which lags each surface pressure perturbation (Fig. 48).

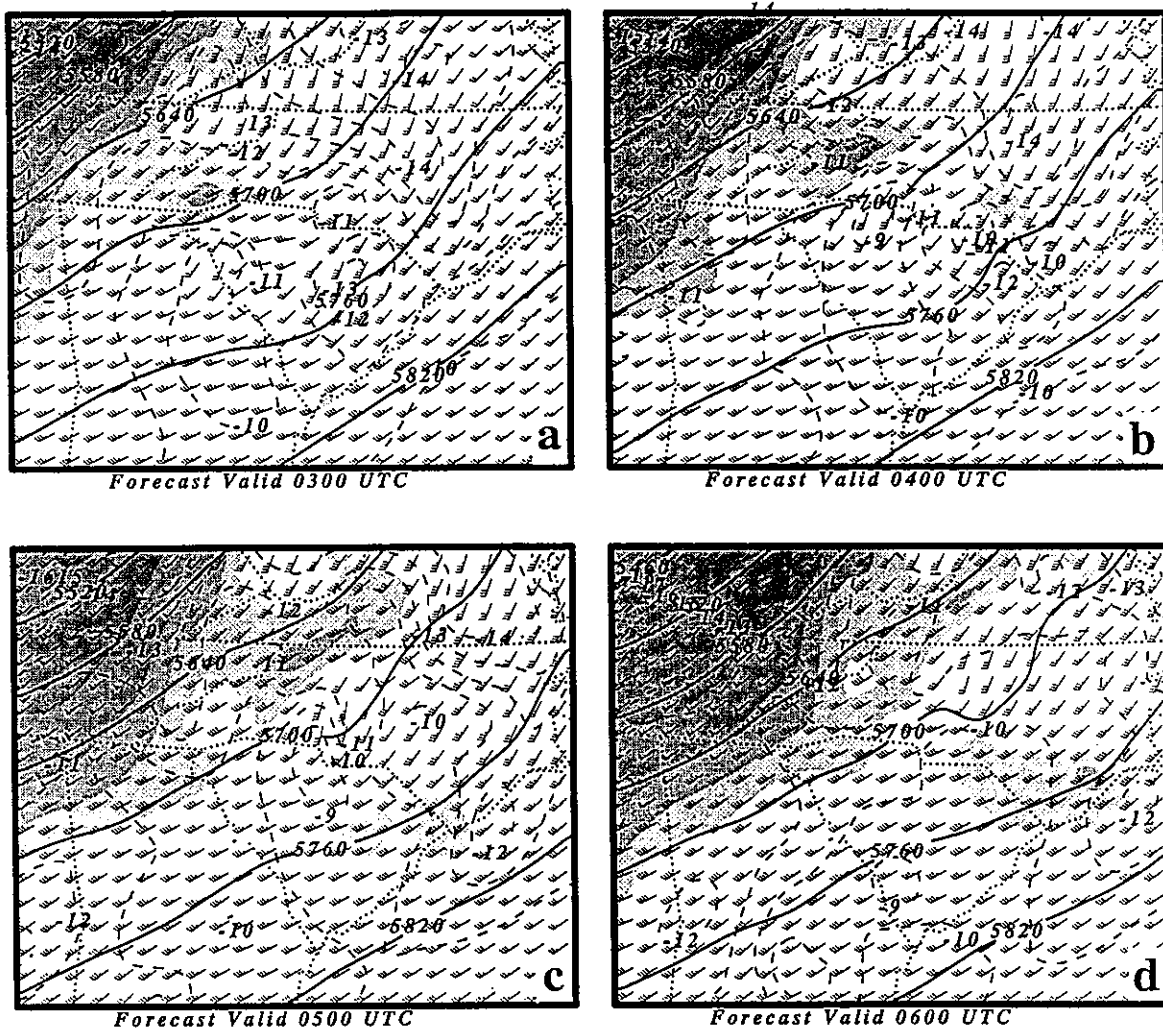


Figure 46. GMASS coarse mesh simulated 500 mb wind vectors (alternate rows and columns) and isotachs (shaded every 10ms^{-1} above 40ms^{-1}), height (solid lines in m), and temperature (dashed lines in $^{\circ}\text{C}$) valid at (a) 0300, (b) 0400, (c) 0500, and (d) 0600 UTC 28 November 1988.

During the time period between ~ 0300 and ~ 0545 UTC the nested-grid analog to the Georgia mesocyclone moves east-northeastward along the piedmont front from upstate South Carolina to just northwest of Pope Air Force Base near FAY. The mean sea level pressure of this low drops at a somewhat greater rate during this period which is considerably greater than the falls accompanying any of the companion mesocyclones. At 850 mb the wind adjusts to the falling pressure resulting in an intensification of vertical vorticity just south-

southeast of the mesocyclone between CLT and FAY by 0545 UTC. This results in a vertical vorticity maximum in excess of 10^{-3}s^{-1} just west of FAY at this time. The low-level jet has increased to values greater than 40ms^{-1} west-southwest of FAY which is larger in magnitude, $\sim 25\text{km}$ southwest, and demonstrably higher in westerly wind flow when compared to its 0600 UTC coarse mesh counterpart. One should note that similar to the coarse mesh simulation, the fine mesh simulation produces a well-defined secondary low-

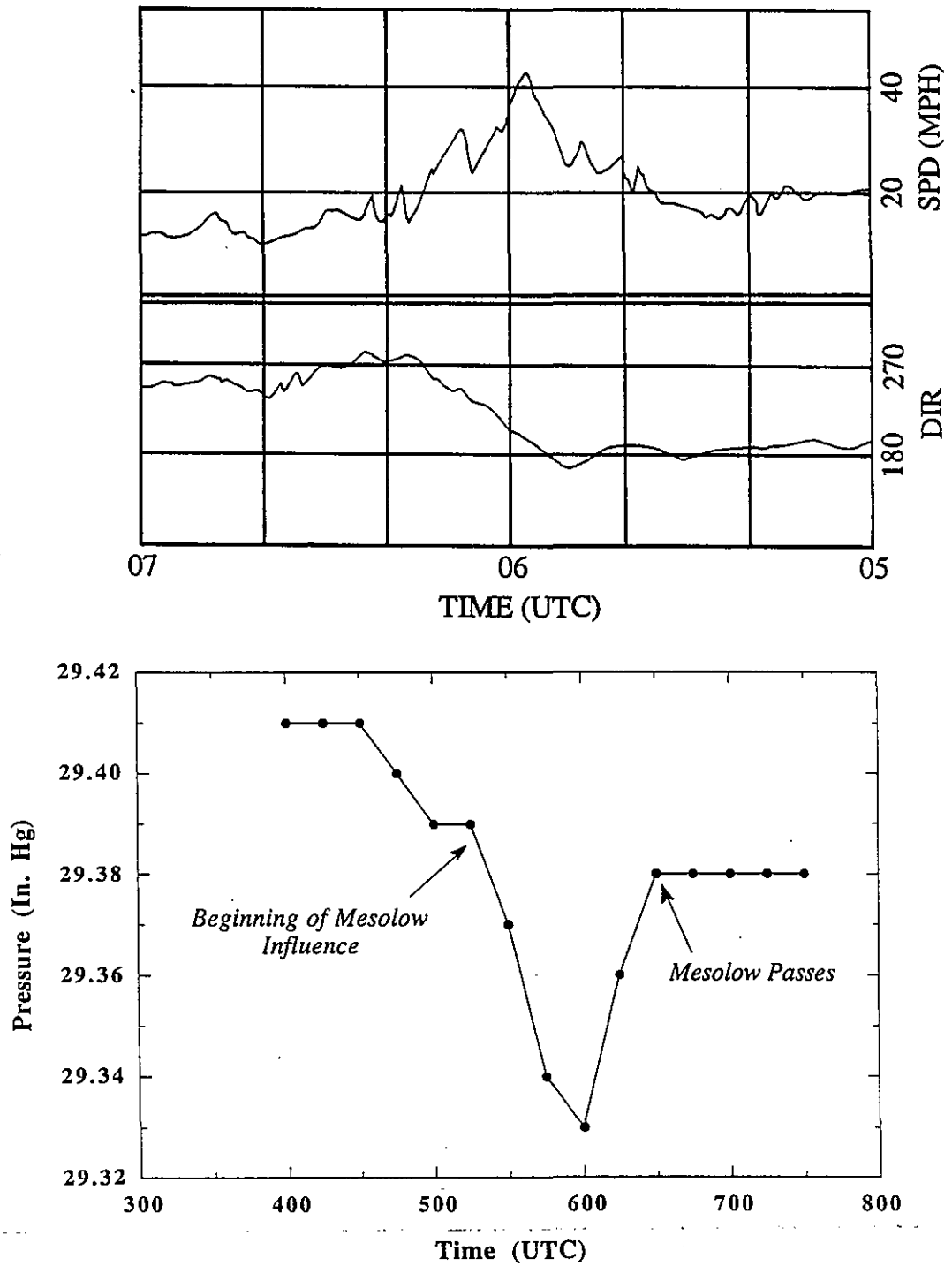


Figure 47. Observed mean sea level pressure (inches of mercury) time section and wind velocity and direction time section (ms^{-1}) derived from a Carolina, Power, and Light plant prior to and during the Raleigh tornado outbreak (after Funk 1991).

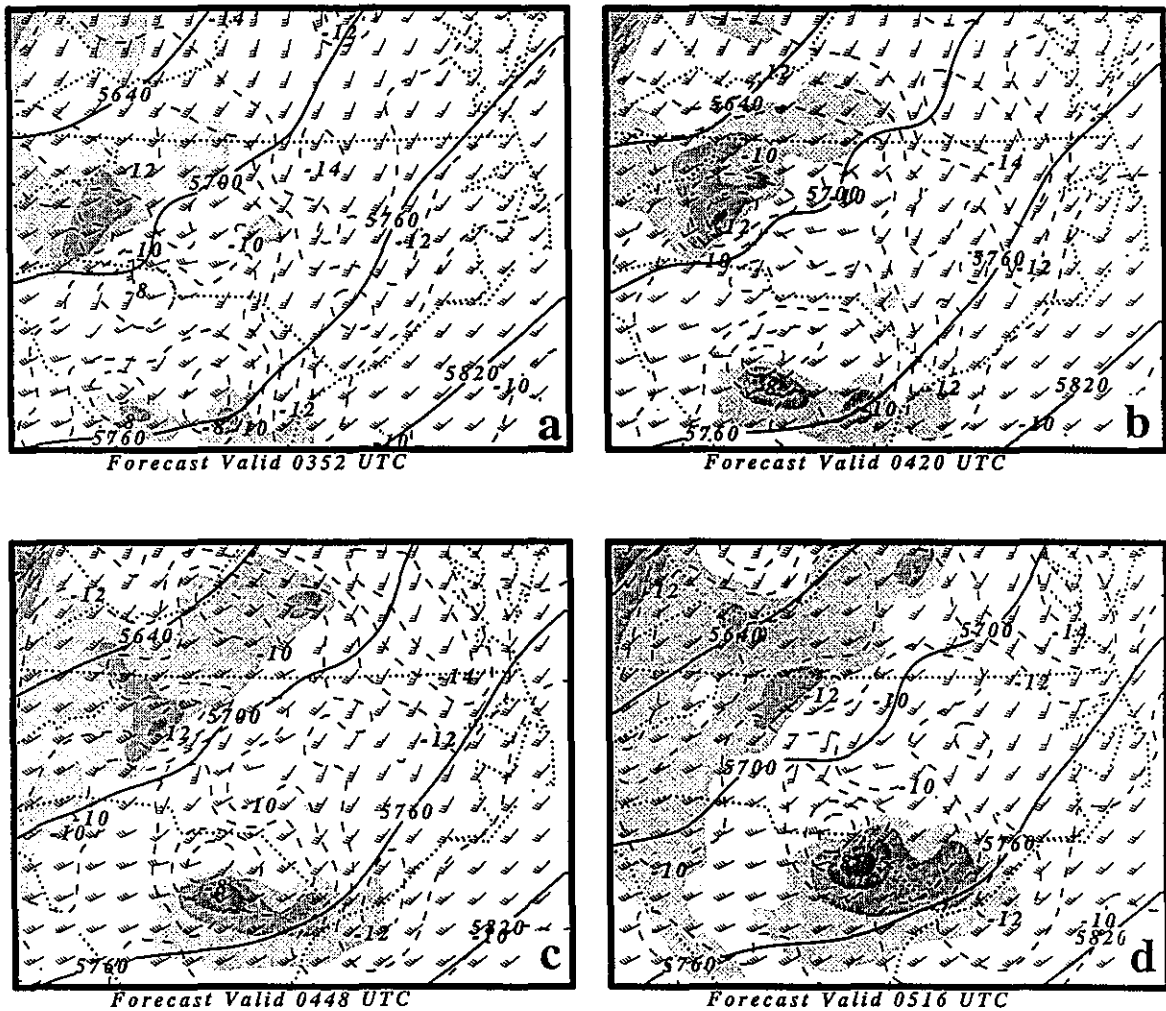


Figure 48. GMASS fine mesh simulated 500 mb height (m), wind vectors and isotachs (shaded every 10 ms⁻¹ above 40 ms⁻¹), and temperature (°C) valid at (a) 0256, (b) 0324, (c) 0352, (d) 0420, (e) 0448, (f) 0516, (g) 0544, (h) 0612, (i) 0638, and (j) 0708 UTC 28 November 1988.

level jet and vertical vorticity maxima after 0600 UTC just north of the North Carolina/Virginia border near Albemarle, Virginia which is the site of the first Virginia tornado. At 500 mb, a west-southwesterly rear inflow jet is propagating over the low-level south-southwesterly jet maximum west of FAY. Just ahead of this rear inflow jet maximum is much weaker highly diffluent southerly flow between FAY, GSO, and RDU resulting in a highly confluent pattern just

southwest of the surface mesocyclone which is northwest of POB.

Figure 49 illustrates the vertical cross sections of equivalent potential temperature and wind velocity from the fine mesh simulation for the region between FLO and Norfolk, Virginia (ORF) at 0640 UTC. These cross sections show the growing vertical gradients of θ_e and wind velocity in proximity to growing horizontal gradients of vertical velocity. At ~0640 UTC the fine mesh analog to W_5 is depicted near the region between

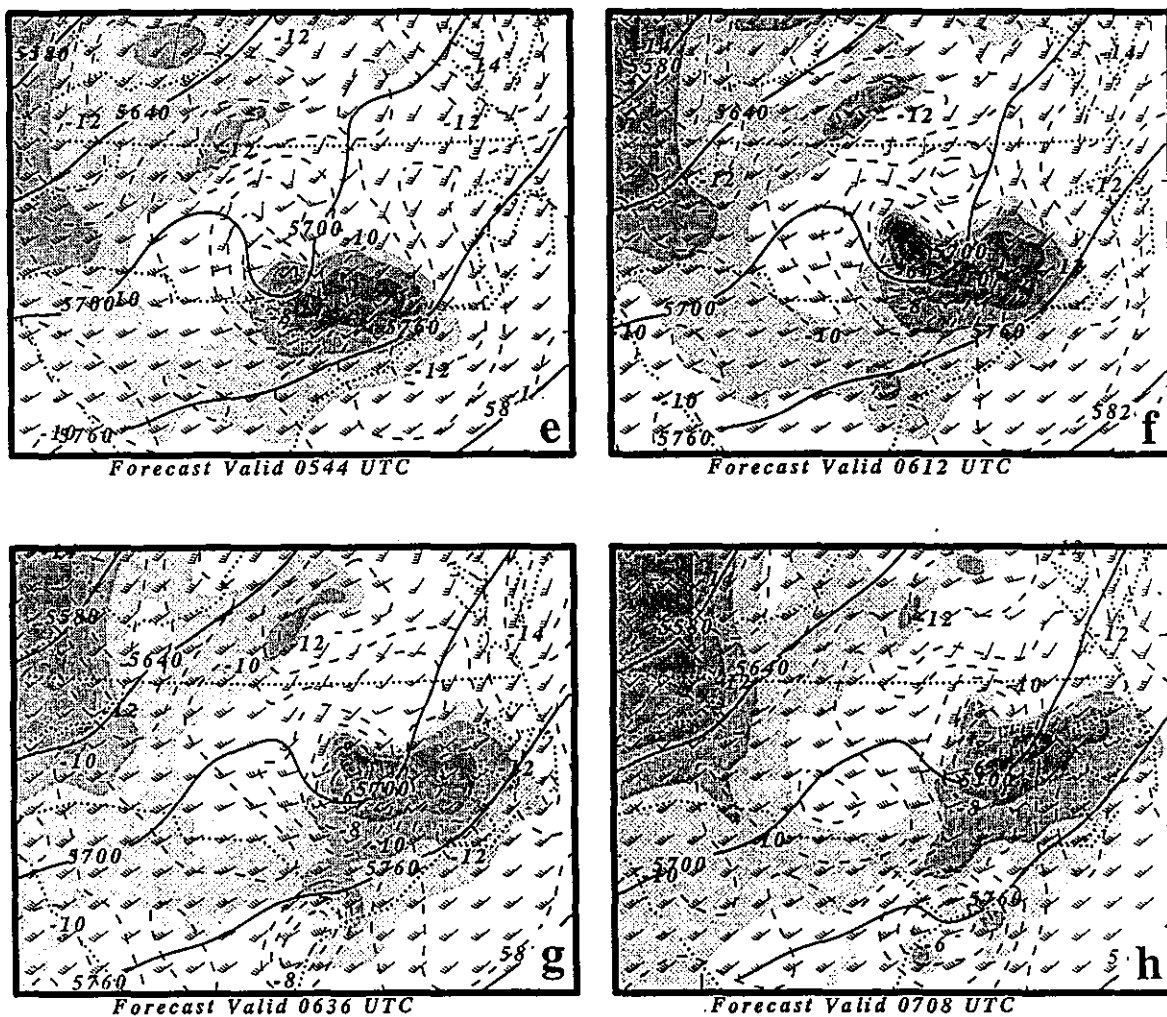


Figure 48. (Continued)

RDU and Rocky Mount, North Carolina (RWI). Note the strong northeast-southwest oriented gradient of vertical velocity and θ_e just northeast of RDU accompanying W_5 . The low θ_e values are the result of enhanced subsidence forced by the descending rear inflow jet accompanying W_5 , wherein confluent flow aloft results in substantial sinking motions behind W_5 . High θ_e values to the northeast of this dry surge are coupled to the moisture convergence accompanying the low-level jet/mesocyclone centered to the east of RDU at this

time. The deep warm moist column indicated by the upper-tropospheric θ_e maximum just south-southwest of the region between RDU and RWI is indicative of latent heat release accompanying the wave-CISK which sustains W_5 . Just south-southwest of RDU the cross section slices through cool dry air indicative of the piedmont front and the descent accompanying the upstream side of W_4 .

By ~0640 UTC, the tilt of W_5 has become progressively more downshear as the west-southwesterly rear inflow jet descends over the

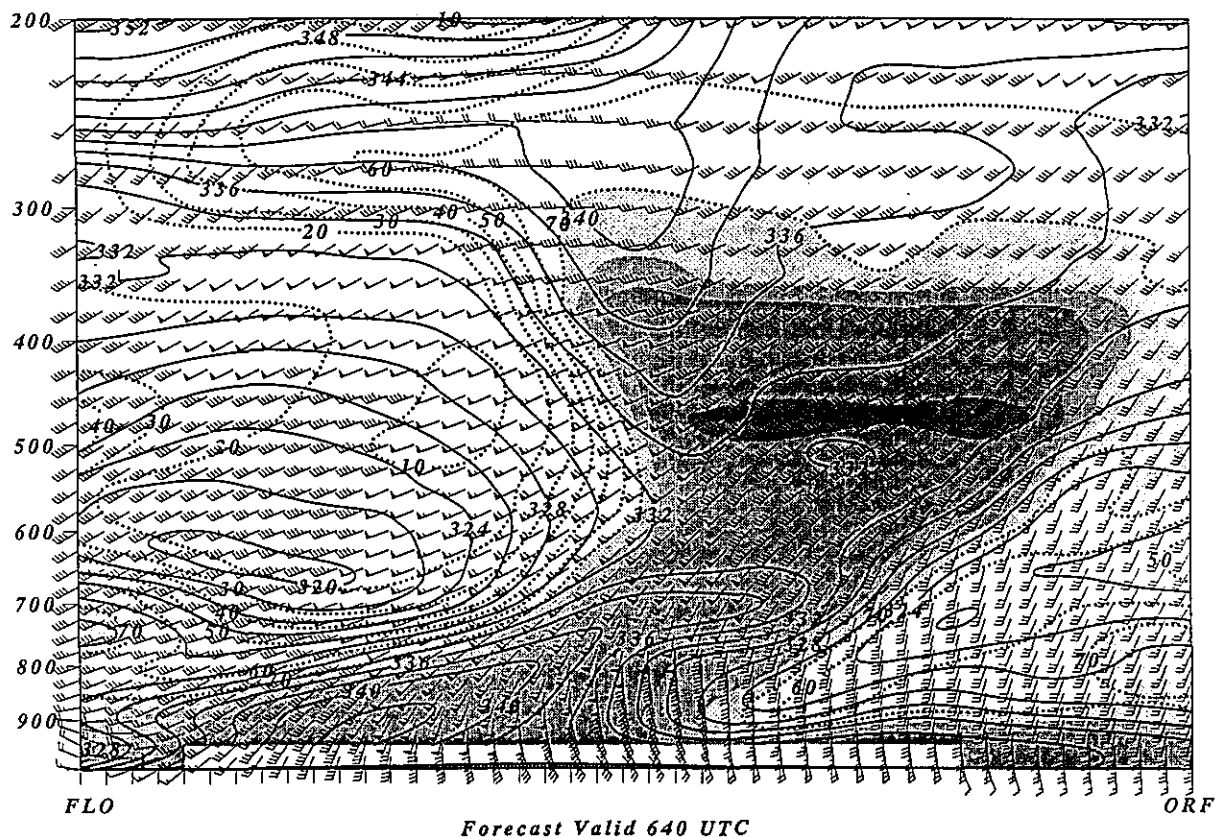


Figure 49. GMASS fine mesh simulated vertical cross section from Florence, South Carolina (FLO) to Norfolk, Virginia (ORF) of equivalent potential temperature (thin solid lines every 2K), relative humidity (shaded every 10% above 60%) isotachs dotted lines every 10 ms^{-1}), and wind vectors valid at 0640 UTC.

southeasterly flow accompanying the low-level jet. This brings θ_e values less than 322K at ~600 mb nearly directly over θ_e values greater than 342K at ~850 mb. This same region where west-southwesterly flow is descending over southeasterly flow, which is increasing the vertical θ_e and momentum gradients, also is coincident with strong northeast-southwest oriented gradients of vertical velocity exceeding $1 \text{ ms}^{-1}/100 \text{ km}$ (not shown). Thus, increasing values of vertical vorticity due to vortex tube stretching are coincident with the tilting of horizontal vorticity into the vertical. The correspondence in space and time between the increase of vertical vorticity and vertical gradients

in θ_e insures very large increases in the equivalent potential vorticity just south-southwest of RDU approximately 40 minutes after the time of the observed tornadic storm.

4.12 Summary of Stage D

The key processes which occur during Stage D include:

- 1) Rear inflow jetlets, i. e., mid-tropospheric momentum surges develop behind the primary

gravity waves where the pressure gradient force is perturbed by diabatic heating.

2) The rear inflow jetlet descends as the downward momentum fluxes change the tilt of the wave accompanying the Georgia mesocyclone from upstream to downstream over the South Carolina Piedmont.

3) Dry air descends from the upper-troposphere with the changing tilt of the gravity wave, thus flowing over warm moist air associated with the low-level jet creating an unstable environment between FLO and RDU.

4) Vortex tube stretching intensifies as the Georgia mesocyclone/low-level jet strengthens and contracts in scale near the South Carolina/North Carolina border.

5) As the rear inflow jetlet descends, tilting increases in the region of strong vertical velocity gradient accompanying the Georgia mesocyclone/low-level jet.

6) Tilting, vortex tube stretching, and diabatic heating all become superimposed over the Georgia mesocyclone between the North Carolina border and RDU.

7) Vertical vorticity increases where the vertical gradient of θ_e is becoming more negative over central North Carolina.

5. Overall Summary of the Meso- β Scale Environment in Which the Raleigh Tornado Outbreak Occurs

The Raleigh tornado outbreak occurred within polar jet right entrance region and the subtropical jet left exit region. Within the thermally-direct ageostrophic circulation of the polar jet, the environment was very moist while values of vertical wind shear and convective instability were quite ordinary. However, the juxtapositioning of the PJ relative to the STJ resulted in a deep mid-lower tropospheric stable layer topped by an extremely cold statically unstable layer which created a region of enhanced ascent as well as a duct for gravity waves. The ageostrophic circulations about the polar and subtropical jet produced cold fronts aloft just downstream of a rich source of low-level moisture over the Gulf of Mexico. Furthermore, the prolonged coupling between the low-level confluence over the Gulf and the upper-level circulations produced a favorable environment for the convergence of vorticity and deep geostrophic adjustment processes over the southeastern U. S..

There are at least four definable stages to the development of the hydrostatic meso- β scale environment which concentrated vertical vorticity and buoyancy over RDU by 0600 UTC on 28 November 1988. The morphology of the atmosphere over the Southeast U.S. was synthesized from synoptic/asynoptic observational data sets and meso- β scale numerical model output. The first of these four stages can be traced back *at least* 18 hours prior to the development of the RDU tornado.

Stage A involves the genesis and initial development of a mesocyclone with strong surface vorticity over southwestern Georgia. This feature was the result of the intersection of four wave-CISK modified mesoscale pressure systems. These mesoscale pressure systems included two cold fronts which were propagating eastward across the

Gulf of Mexico Coastal Plain coincident with convectively-modified mesotroughs, a mesoscale convective outflow boundary which eventually becomes the focal point for additional strong convection and surface pressure falls, and an evaporatively cooled mesohigh which becomes wedged up against the Appalachian Piedmont. Air trajectories from different regions converge over southwestern Georgia under the PJ's entrance region to produce a reservoir of low-level vorticity. The confluence formed by the intersection of these pressure perturbations eventually becomes the organizing process for wave-CISK supported mesoscale convective systems which propagate northeastwards over the Appalachian piedmont.

Stage B involves the development of a secondary mid-upper tropospheric *mesoscale* jet streak over the Tennessee River Valley. This jetlet developed as a result of geostrophic adjustment processes wherein convective heating accompanying the strong eastward moving cold front over northern Mississippi produced a mesoscale height perturbation within the ageostrophic entrance region of the synoptic scale polar jet. The inertial-advective response to the convectively generated mass perturbations propagate east-northeastward at nearly 40 ms⁻¹ passing over southeastern Tennessee, northwestern North Carolina, and southwestern Virginia. The propagation of this mesoscale jetlet occurs in close proximity to a CFA embedded within the STJ just downstream from the PJ's entrance region within a background subgeostrophic flow regime. The secondary gravity waves of depression triggered by this mesoscale "jetogenesis" act to break down the mesoscale surface ridge which had been blocking the low-level flow over the Carolina Piedmont. This allowed the Georgia mesocyclone to move northeastwards, and produced a dry air extrusion as air parcels descended over the Georgia/Carolina Piedmont regions. The longevity of the mesoscale jet streak feature may be, at least in part, the result of baroclinic advective processes accompanying the CFA.

Stage C develops as the mesocyclone and convectively-driven gravity waves propagate northeastward along the Piedmont front and trough.

The CISK which maintained the mesocyclone and primary gravity waves is instrumental in producing additional pressure falls and the amplification of the LLJ. The enhanced moisture convergence over the Carolina Piedmont accompanying the wave-CISK fortified the mesocyclone and increased the low-level vorticity through vortex tube stretching.

During Stage D all of the ingredients necessary for tornadogenesis converge over eastern North Carolina and southeastern Virginia. The propagating wave-CISK modes which maintain the mesocyclones and low-level jet maxima continue to move northeastward along the Carolina Piedmont towards RDU. Aloft, rear inflow jetlets develop behind the primary wave-CISK modes. These mesoscale jetlets are the result of the relaxed pressure gradient force caused by convective heating, and appear to be an integral part of the evolving structure of the CISK modes from up shear to down shear tilting. The confluence aloft accompanying the rear inflow jet results in the downward transport of momentum and dry air behind the low-level region of pressure falls, moisture convergence, and increasing vertical vorticity due to vortex tube stretching. As the dry air descends over the low-level inflow of moisture accompanying the mesocyclone, the vertical gradient of θ_e increases dramatically. The increasing vertical and horizontal gradients of momentum and vertical velocity result in the tilting of horizontal vorticity into the vertical. Thus, vertical vorticity rapidly increases due to the juxtapositioning with vortex tube stretching. The increase in vertical vorticity to values exceeding 10^{-3} s^{-1} is coincident with rapidly increasing vertical gradients of θ_e . Thus, equivalent potential vorticity is explosively developing just south-southwest of RDU by 0545 UTC.

As depicted in Figure 50, the juxtapositioning of the transverse ageostrophic circulations accompanying the subtropical and polar jet streaks produce a moist ascending region fed by a strong low-level branch. Within this environment, convectively-induced circulations effectively evacuate the column mass resulting in convectively-induced wind shear fields, vertical vorticity, and helicity.

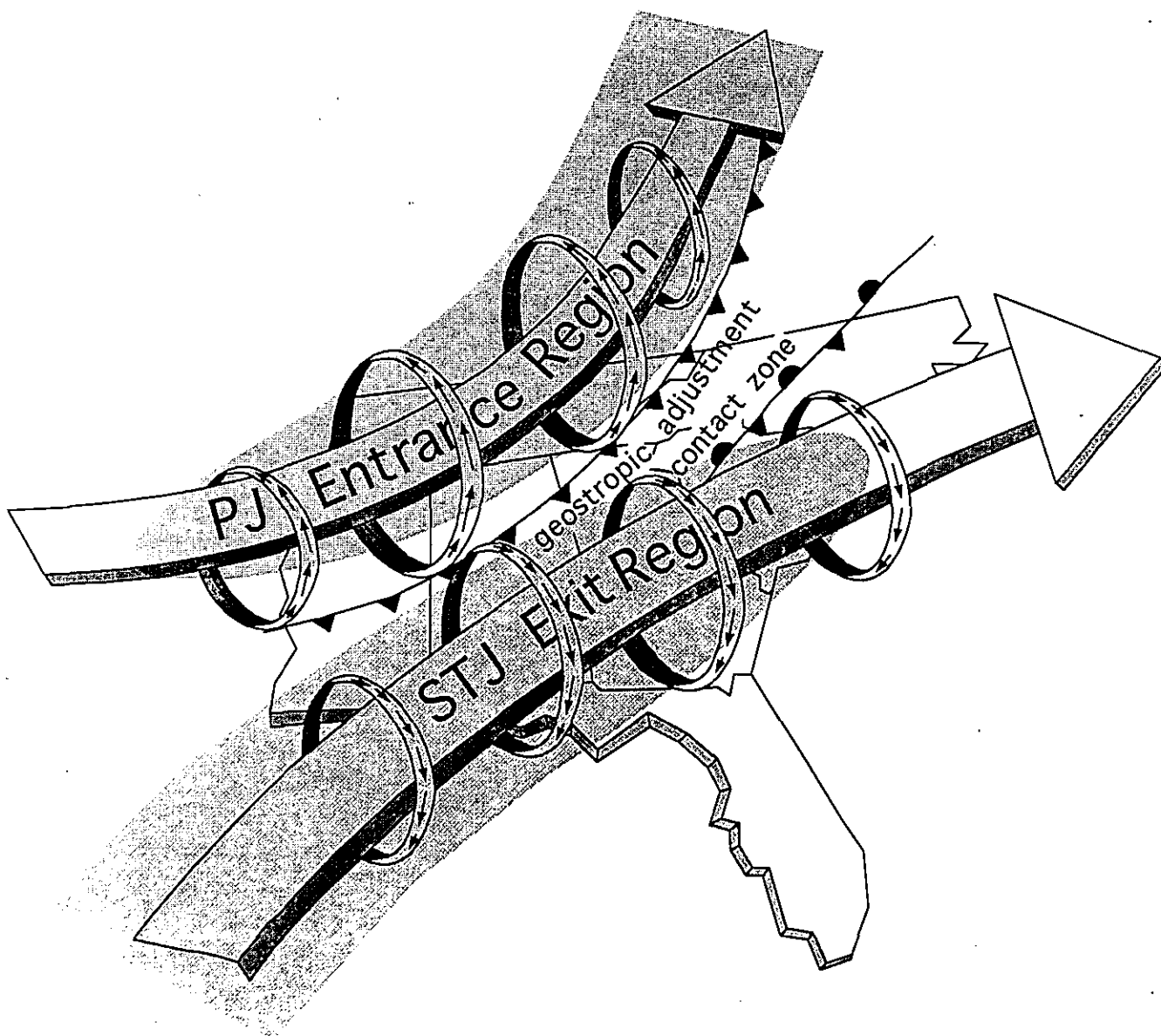


Figure 50. Schematic depicting the coupled polar and subtropical jet streak transverse circulations and their relationship to frontal positions. Thin arrows indicate the thermally indirect circulation within the subtropical jet exit region and the thermally direct circulation about the polar jet entrance region.

6. Jet Streak Exit Versus Jet Streak Entrance Region In Southern Tornado Outbreaks

In an effort to understand the complete spectrum of southeastern tornado outbreaks, we will finish by briefly comparing paradigms for jet streak entrance and exit region outbreaks.

Probably the best known southeastern tornado outbreak is the so called "Carolina" outbreak of 28-29 March 1984 (Kocin *et al.* 1985a; Kaplan *et al.* 1995). In contradistinction to the RDU outbreak, the National Weather Service did an excellent job of forecasting watch boxes over the region of observed tornadogenesis several hours prior to the observed storms. We will first focus on the differences between these two outbreaks followed by the similarities in an effort to synthesize what has been learned from both into scientific

EXIT REGION (Carolina, 1984)	ENTRANCE REGION (RDU, 1988)
1. Forward part of jet streak	Rearward part of jet streak
2. Concurrent cold air advection	Upstream cold air advection
3. 850 mb confluent edgewave, moist vs. dry inflow	850 mb confluent edgewave, moist vs. dry inflow
4. Inertial cross-stream ageostrophic flow directed to the right within the 700-300mb layer	Isobaric cross-stream ageostrophic flow directed toward the left within the 700-300mb layer
5. Strong mid-tropospheric cold air advection resulting in cold mid-troposphere/shear layer	Strong mid-tropospheric warm air advection resulting in warm mid-troposphere/shear layer
6. Southern branch of jet less evident above 300mb	Southern branch of jet very evident above 300mb
7. Warm upper-troposphere above northern jet/shear layer	Cold upper-troposphere within southern jet/shear layer
8. Unstable mid-troposphere, stable upper-troposphere	Stable mid-troposphere, unstable upper-troposphere
9. Shallow moist layer under deep dry layer	Deep moist layer under shallow dry layer
10. Low-level convergence with increasing divergence over deep layer	Low-level convergence with increasing divergence over shallow layer
11. CISK-waves not as crucial for wind shear and destabilization	CISK-waves very crucial for wind shear and destabilization
12. Wave duct near PBL with reflective layer within mid-troposphere	Wave duct within mid-troposphere with reflective layer in upper-troposphere
13. Secondary gravity waves coincident within strong dryline	Secondary gravity waves ahead of weaker dryline

Widespread F2, F3, F4, and F5 storms Isolated F0, F1, and F4 storms

Table 2. A comparison of the important details between the Carolina outbreak of 28-29 March, 1984 and the RDU outbreak of 28 November, 1988.

forecasting paradigms.

Table 2 depicts several differences between the outbreaks. The most notable feature in the Carolina outbreak is the existence of an *easily observable* vertical vorticity maximum accompanying cross-stream ageostrophic flow within the jet streak's exit region. In close proximity is the presence of a low-level jet transporting copious amounts of warm, moist tropical air and is analogous to the conceptual model of Uccellini and Koch (1987). This deep differential advection is fortified by cold air within the mid-troposphere as the low-level jet may be viewed as a response to the mass adjustments directly accompanying the thermal vorticity advection within the exit region. Furthermore, the sinking branch of the thermally-indirect ageostrophic circulation in the exit region is accompanied by dry air, producing a well-defined comma cloud. The existence of gravity waves in exit region outbreaks is very likely initiated by shearing instability or geostrophic adjustment as the exit region encounters a well-developed ridge in the height field. Gravity wave ducting structures are less dependent upon the juxtapositioning of both subtropical and polar jet streaks as the ducting is controlled more by differential advection and the stronger low-level vertical shear.

In contrast, entrance region outbreaks such as the RDU case produce fewer total numbers of devastating storms and are more subtle in their characteristics, as they do not occur with strong synoptic scale differential advection patterns. This means that the strong imbalances occur at smaller scales, thus escaping the synoptic scale observational system. These case studies rely more exclusively on intersecting boundaries, convectively-generated circulations, geostrophic adjustment, and prolonged wave ducting scenarios involving the subtropical jet stream. Low-level vorticity is likely created over longer time periods and upper-level mass perturbations are more likely due to the perturbation of a jet streak entrance region by convectively-generated circulations and by the juxtapositioning of the circulations accompanying the polar jet entrance region and the subtropical jet exit region. Therefore, upscale energetics may dominate and make it very difficult to define the important signals from observed data sources. In this respect, it is not unlike tropical development. Furthermore, since these outbreaks occur in the relatively warm right entrance region of the jet, the lack of cold air aloft often results in lower cloud tops, less and smaller hail, and less frequent lightning. *However, the lack of extreme instability is compensated for by prolonged wave interactions among convectively-generated*

Similarities Between Exit Region (Carolina, 1984) and Entrance Region (Raleigh, 1988) Southeastern Tornado Outbreaks

1. The existence of a jetlet's meso-exit region resulting from geostrophic adjustment caused by the interaction of upstream convection and the polar jet.
2. The existence of a CFA embedded within the subgeostrophic polar jet exit region or entrance region which acts to sustain unbalanced flow within the newly formed jetlet.
3. The existence of a well developed Piedmont thermal-moisture boundary and secondary vorticity maxima which forms near the front as a result of surface convergence zones.
4. The focusing of low-level convergence and a descending rear inflow jet initiated by CISK-related processes.
5. Phasing of the jetlet's meso-entrance region warm air advection and the rear inflow jet descent to produce maximum mesolow pressure falls.

Table 3. Similarities between exit region (Carolina, 1984) and entrance region (Raleigh, 1988) outbreaks

circulations resulting in stronger low-level vorticity and vertical wind shears.

Table 3 depicts similarities among these two types of tornadic outbreaks. While the total number of similarities may be fewer than the differences, they represent powerful ideas for use in forecasting southeastern tornado outbreaks. There is every indication from mesoscale model results that the jet streak exit region in the Carolina outbreak was really a concentrated mesoscale wind maximum perturbed by earlier upstream convection. If this is true, then convectively-

initiated geostrophic adjustment processes may be very ubiquitous as mechanisms for producing highly-imbalance *mesoscale* exit region flows which are detached from the quasi-geostrophic jet streak circulations. Such very strong *mesoscale jetogenesis* results in highly concentrated regions of surface pressure falls due to the significant magnitudes of mass flux divergence aloft. Hence, the processes in both the Carolina and RDU outbreaks may have been rather similar in spite of the fact that the "signal" for exit region imbalance was easier to spot in the Carolina case study due to

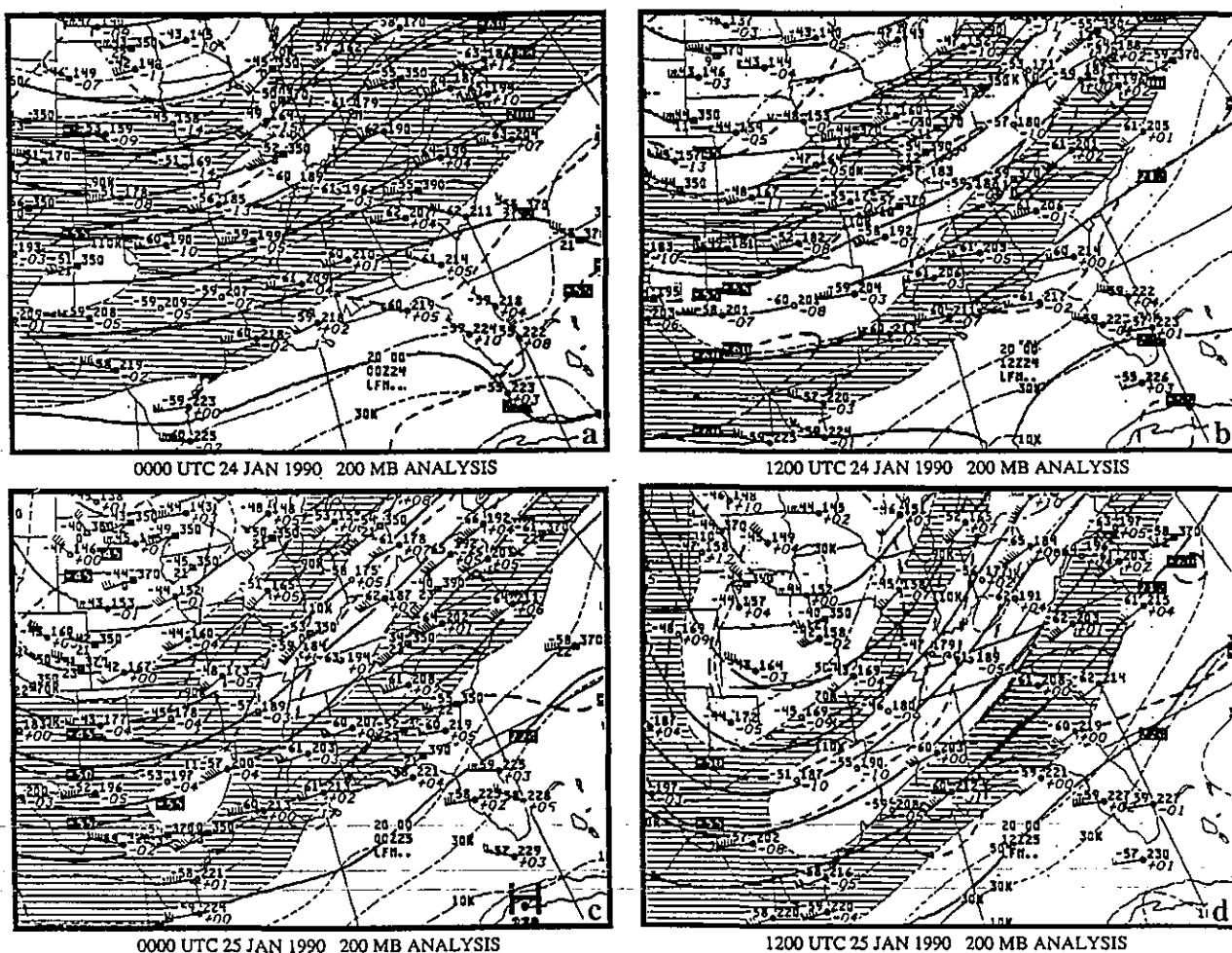


Figure 51. NWS 200 mb analysis charts valid at (a) 0000 UTC 24 January, (b) 1200 UTC 24 January, (c) 0000 UTC 25 January, and (d) 1200 UTC 25 January 1990.

the relatively greater size and intensity of the polar jet exit region. Additionally, in both outbreaks there is an indication that a distinct cold front aloft (CFA) is embedded within the convectively-perturbed exit region. The existence of baroclinic perturbations within the exit region may play a key role in sustaining the longevity of unbalanced accelerating flow within the mesoscale exit region. Baroclinic processes such as mesoscale temperature advection and/or diabatic heating may act to prevent the mass adjustments which would otherwise serve to balance the mesoscale jet streak.

Therefore, CFA adjustments could remain unbalanced and, hence, highly divergent for extended periods of time, thus sustaining low-level pressure falls and compensating accelerations.

In both the Carolina and RDU outbreaks, as is typical of southeastern outbreaks (Businger *et al.* 1991; Vescio *et al.* 1993), the Piedmont front acts as the key surface thermal and moisture boundary along which severe weather occurs. This persistent boundary acts as a convergence focusing mechanism, thus enhancing convective development as well as vortex tube stretching which leads to an

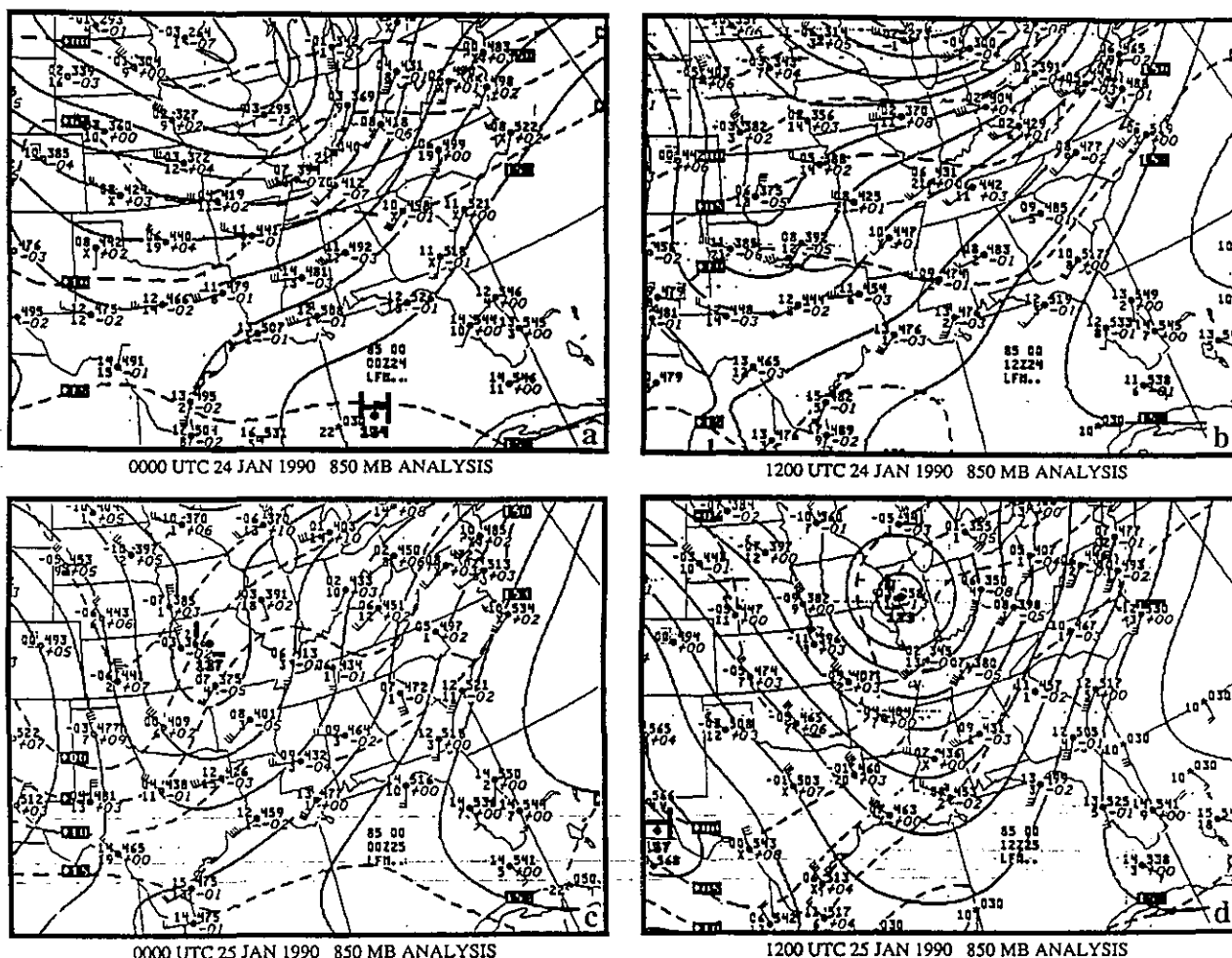


Figure 52. NWS 850 mb analysis charts valid at (a) 0000 UTC 24 January, (b) 1200 UTC 24 January, (c) 0000 UTC 25 January, and (d) 1200 UTC 25 January 1990.

increase in vertical vorticity. Furthermore, any convection which develops along the piedmont frontal boundary produces perturbations in the front which can act as key focusing agents for the growth of vorticity. This is particularly important when wave ducting is well-established since wave-CISK will result in long-lived convergence maxima which develop localized regions of very strong low-level vorticity. In effect, the Piedmont front acts as the lower branch of the polar and/or subtropical jet transverse circulations.

Finally, in order to appreciate the complexity of differentiating tornadic potential in jet entrance region case studies, we will briefly compare the Raleigh case study to the 25 January 1990 case study wherein no severe weather of any type occurred. In this case study, presented in Figures 51 and 52, the evolution of the upper-level jet streaks is different from the RDU case. The polar jet entrance region and subtropical jet exit region are closely aligned in the vertical and unlike the RDU case there are not two easily definable jet streaks during the amplification of the baroclinic wave over the south-central U. S. This lack of separation between the polar and subtropical air streams probably reduces the intensity of the velocity divergence due to geostrophic adjustment as well as the intensity of the ducting structure. As a consequence, the low-level ageostrophic confluence is much weaker as well. One can see that the 850 mb circulation is less ageostrophic and less confluent just prior to the development of weak convection on 25 January, even though the magnitude of upper and lower level jet streaks are quite similar in both cases. Hence, the deep mass fluxes are weaker in the 25 January 1990 case than in the RDU case study. Perhaps, it is the vertical juxtapositioning of divergent ageostrophic circulations that is the key to diagnosing potential severity in *both exit and entrance region case studies*.

7. Operational Aspects and Considerations

Post-mortem studies of the Raleigh Tornado Outbreak have revealed a highly complex environment that presented a challenge for the operational meteorologist to diagnose, especially using only "conventional" means based on the synoptic scale at the time. The rapid advance of technology may help unravel the complexity shown in these studies for an outbreak of strong and violent tornadoes. But placed in the context of complex diagnostic indicators for a multitude of other potential weather hazards on various temporal and spatial scales over a broad geographical area generated by the same dynamical system, the operational dilemma of discriminating between the significant and the non-significant event is likely to continue. *It is critical* that data sets and output from numerical model simulations be rapidly assimilated for real-time decision-making by the forecaster.

The features gleaned from this investigation that are considered to be most important to the successful diagnosis of an environment conducive to the outbreak of strong and violent tornadoes in the Southeast are listed in Table 4. These features are discussed further in the section that follows.

Techniques for readily identifying these important features need to be established by the forecaster community. Artificial Intelligence systems or other computer assisted means for use in real-time may prove very helpful in this process.

Discussion and Analysis of Features:

Jet Stream and Upper Level Considerations.

A. *Are there two definable jet streaks upstream, separate polar and subtropical jets, in an approaching trough?* In Fig. 3, 200 mb isotachs repeatedly showed two branches of maximum velocity winds. The northern

branch polar jet stream could be seen from the southern Plains to the Great Lakes region. The southern branch subtropical jet stream persisted from northern Mexico across the Texas gulf coast to over the Atlantic Ocean off the Carolinas. Water vapor satellite imagery at 1800 UTC, 27 November 1988, (Fig. 53) depicted two sharp gradients in high-level moisture at approximately those same locations. Compare this with the non-event case at similar stages of development (Figs. 3d and 51b and Figs. 53 and 54). There is much less distinction in the isotach pattern and only a singular sharp gradient in high-level moisture between Illinois and Georgia in the latter case than in the former.

A1. *Is there juxtapositioning between the polar jet streak entrance region (usually best seen near 300 mb), and the subtropical jet streak exit region (usually seen higher at 250 or 200 mb)?* In Figs. 3e and f, a broad left front quadrant of the STJ could be seen from the gulf coast of Louisiana to the western Carolinas. Water vapor satellite imagery at 1200 UTC, 27 November 1988, (Fig. 55) showed a wave propagating upstream over the Gulf States and darkening of the image implying subsidence drying aloft off the Texas gulf coast from 1200 to 1800 UTC (Figs. 53 and 55). In Figs. 5a,c and in the satellite imagery, the right rear quadrant of the PJ was drifting from the western Tennessee-Arkansas region to the southern Appalachians. Therefore maximum juxtapositioning was being inferred over northern portions of the Gulf States to northern Georgia at this time.

A2. *Does the exit region of the subtropical jet streak contain rightward-directed cross-stream super-geostrophic flow?* In Figs. 3d and f, winds are being directed toward higher geopotential heights in the southern branch across Georgia and the Carolinas while maintaining speed implying supergeostrophic conditions.

A3. *Does the entrance region of the polar jet streak contain leftward-directed cross-*

TABLE 4

CHECKLIST FOR TORNADIC OUTBREAKS IN THE SOUTHEAST

Jet Stream Level

- A. Distinct polar and subtropical jet streams propagating into the Southeast (south of 40°N and east of 95°W).
 - 1. Juxtapositioning between polar jet entrance region and subtropical jet exit region.
 - 2. Subtropical jet exit region with supergeostrophic flow directed toward higher pressure (cross-stream to the right).
 - 3. Polar jet entrance region with subgeostrophic flow directed toward lower pressure (cross-stream to the left).
- B. Cold front aloft (defined in isentropic cross-sections above 500 mb) in the region encompassed by the polar and subtropical jet stream maxima.

Surface-based

- C. Dual surface fronts including a polar front moving east of the Mississippi River Valley and a quasi-stationary Piedmont front across the central Carolinas.
 - 1. A deep moist layer with RH > 50% between the fronts.
 - 2. Convective precipitation present between the fronts.
 - 3. Evidence of, or potential for gravity waves between the fronts.
 - 4. Mesoscale low pressure perturbations and thermal/moisture gradients between the fronts.

Low Level (850 mb)

- D. Confluent low-level jet (850 mb) directed toward lower pressure (cross-stream to the left).
- E. Pooling of warm (>20° C), dry (>10° C dewpoint depression) air at 850 mb in the region from southern Texas to the gulf coastal states.
- F. Low-level relative vorticity maxima near or along the Piedmont front.

Convective Features

- G. CAPE > 1000 Jkg⁻¹ evaluated to 300 mb south or southeast of the Piedmont front.
- H. Rapid (> 40 kts) and rightward-moving (relative to 0-6 km mean wind) radar echoes.
- I. Drying evident behind individual convective clusters

stream subgeostrophic flow? In Figs. 5a and c, winds are being directed toward lower geopotential heights in the northern branch over northern Mississippi and speeds are reduced relative to surrounding sites under a similar gradient. This implies subgeostrophy. The depiction of objectively analyzed winds and height fields Figs. 6b and d show leftward oriented winds relative to the geostrophic flow over the same area.

- B. *Is there a definable cold front aloft between 500 mb and 200 mb in the region encompassed by the dual jet streaks?* Isentropic cross-sectional analyses in Fig. 8 shows a cold front aloft (CFA) over the Appalachians between HTS and GSO, and between BNA and AHN respectively. This cross-sectional feature is also seen in Fig. 9

Surface-based Considerations

- C. *Are there dual surface cold frontal systems including a propagating polar cold front and a quasi-stationary Piedmont front?* As depicted in Figs. 16b, d, and f, dual cold fronts are present with the cold front propagating east from the Mississippi River Valley and a quasi-stationary Piedmont front evolving over the central Carolinas.

- C1. *Is there a broad, deep moist layer of 1000-500 mb mean relative humidity greater than 50% between the dual surface cold fronts?* Cross-sectional analyses in Figs. 8 and 11 show deep moisture over the Appalachian region, an area between the two surface fronts.
- C2. *Is there ongoing convective precipitation within the region between the dual surface cold fronts?* Radar information in Figs. 17 and 26 illustrated convective elements of precipitation. Satellite imagery also depicted convective cloud structure over the region (Fig. 39).
- C3. *Are there internal gravity wave signatures diagnosed from surface data or*

environmental conditions favorable to the ducting and propagation of gravity waves within the region between the dual surface cold fronts? In Fig. 24, each of the barograph traces showed pressure jumps indicative of gravity waves. The vertical profile of temperature over this region as indicated by the objectively derived soundings from Charlotte and Greensboro, North Carolina (Figs. 12a,b) featured a surface-based inversion layer beneath a deep conditionally unstable layer. This temperature structure is conducive to gravity wave ducting and propagation.

- C4. *Are there surface mesoscale low pressure features and thermal or moisture gradients observed within the region between the dual surface cold fronts?* High resolution surface analyses (Figs. 19, 22, and 37) revealed strong thermal and moisture gradients and low pressure perturbations within the region.

Lower-Tropospheric Considerations

- D. *Is there a highly confluent leftward-directed ageostrophic flow in the form of a low level jet (best seen in this case at 850 mb) on the western side of the subtropical high pressure ridge?* Fig. 4 shows confluent flow directed toward lower heights propagating from Alabama to the southern Appalachians. Lower-tropospheric flow (Fig. 6) and streamline analysis (Figs. 20a,b) also show a confluent pattern directed leftward of the geostrophic flow developing over Alabama-northern Georgia to the southern Appalachians.
- E. *Is there a distinct warm, dry pool at 850 mb within the region encompassed by southern Texas to the Gulf of Mexico coastal states with 850 mb temperatures greater than 20°C and dewpoint depressions greater than 10°C (20°C threshold may be lower in mid-winter)?* In Fig. 4, the warm dry pool reflective of subsidence warming in the left entrance region of the subtropical jet streak

can be seen in southern Texas propagating over the Gulf of Mexico.

- F. *Are there regions in the layer, including the surface and 850 mb levels, of relative vorticity greater than the Coriolis parameter in proximity to the Piedmont front?* A center of maximum low level vorticity could be seen at 0000 UTC, 28 November 1988, over the northeast Alabama-northwest Georgia area. The model simulations clearly depicts low level vorticity at 850 mb emanating from Georgia and moving into North Carolina (Figs. 35 and 42).

Convective Characteristics

- G. *Is there a definable area of convective instability with CAPE values greater than 1000 Jkg^{-1} evaluated to 300 mb, south and/or southeast of the Piedmont front?* The rawinsonde for Greensboro at 0000 UTC, 28 November 1988, modified for Raleigh surface conditions at 06z (Fig. 57) showed that the energy (B+) of a parcel lifted from the surface could have attained values above 1000 Jkg^{-1} .
- H. *Is there rapid movement of existing radar echoes of greater than 40 knots (20 ms^{-1}) in the direction of or to the right of the mean column wind?* Cell movement on radar summary charts (Figs. 26 and 40) was observed at 45 to 60 knots from about 240° . The mean column wind (0-6 km) as derived from the Greensboro sounding that evening was from 218° at 45 knots.
- I. *Is there a distinct dry tongue developing behind the propagating clusters of convection as viewed by satellite?* Areas of middle to high level dryness could be seen on water vapor satellite imagery developing behind propagating cells over eastern Tennessee and Alabama at around 2000 UTC, 27 November 1988 (Fig. 56) continuing into the night (Fig. 39).

1801 27NOV88 093-4ZA 00891 16841 EC3

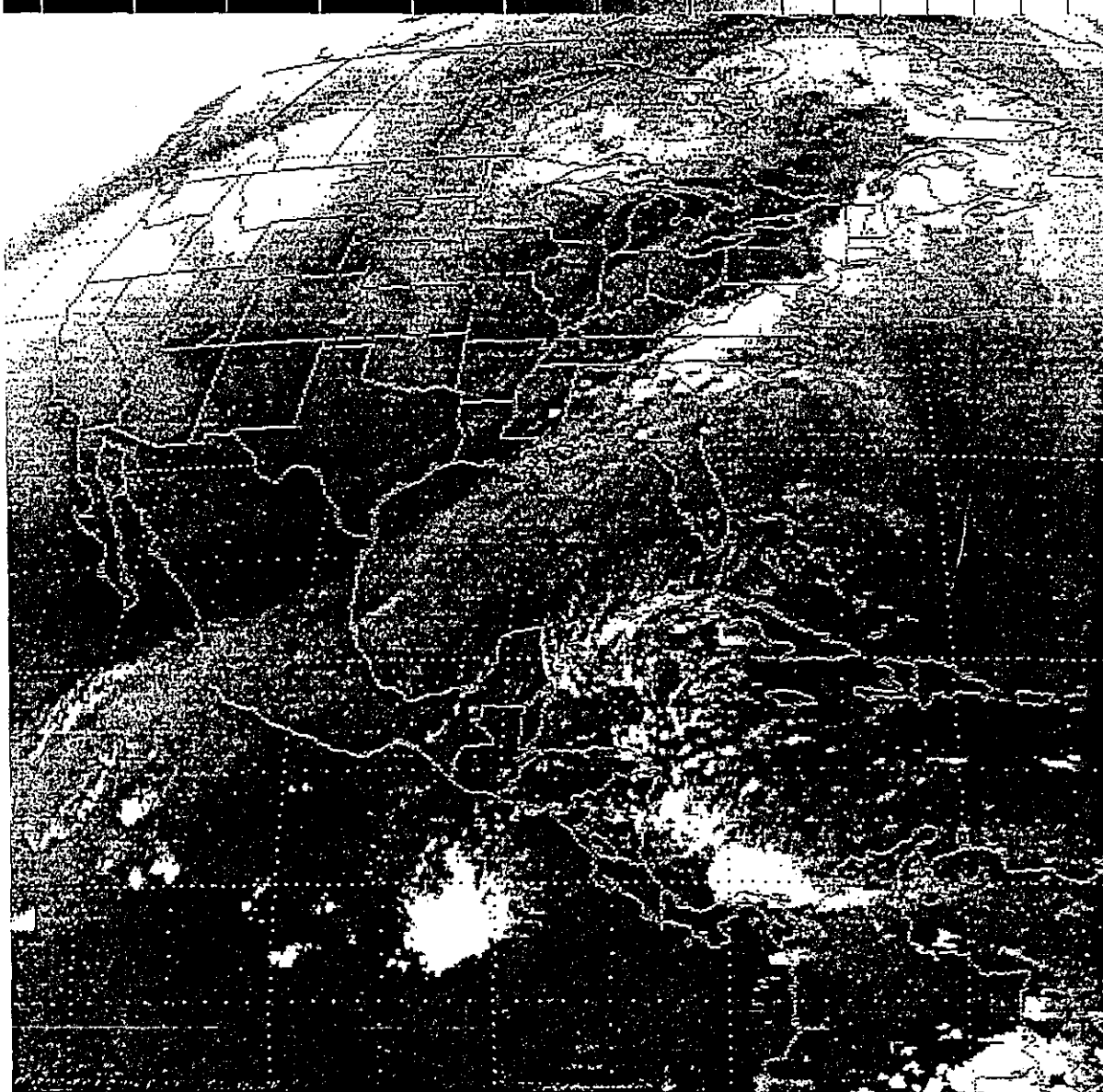


Figure 53. Goes water vapor channel satellite imagery valid at 1800 UTC 27 November 1988.

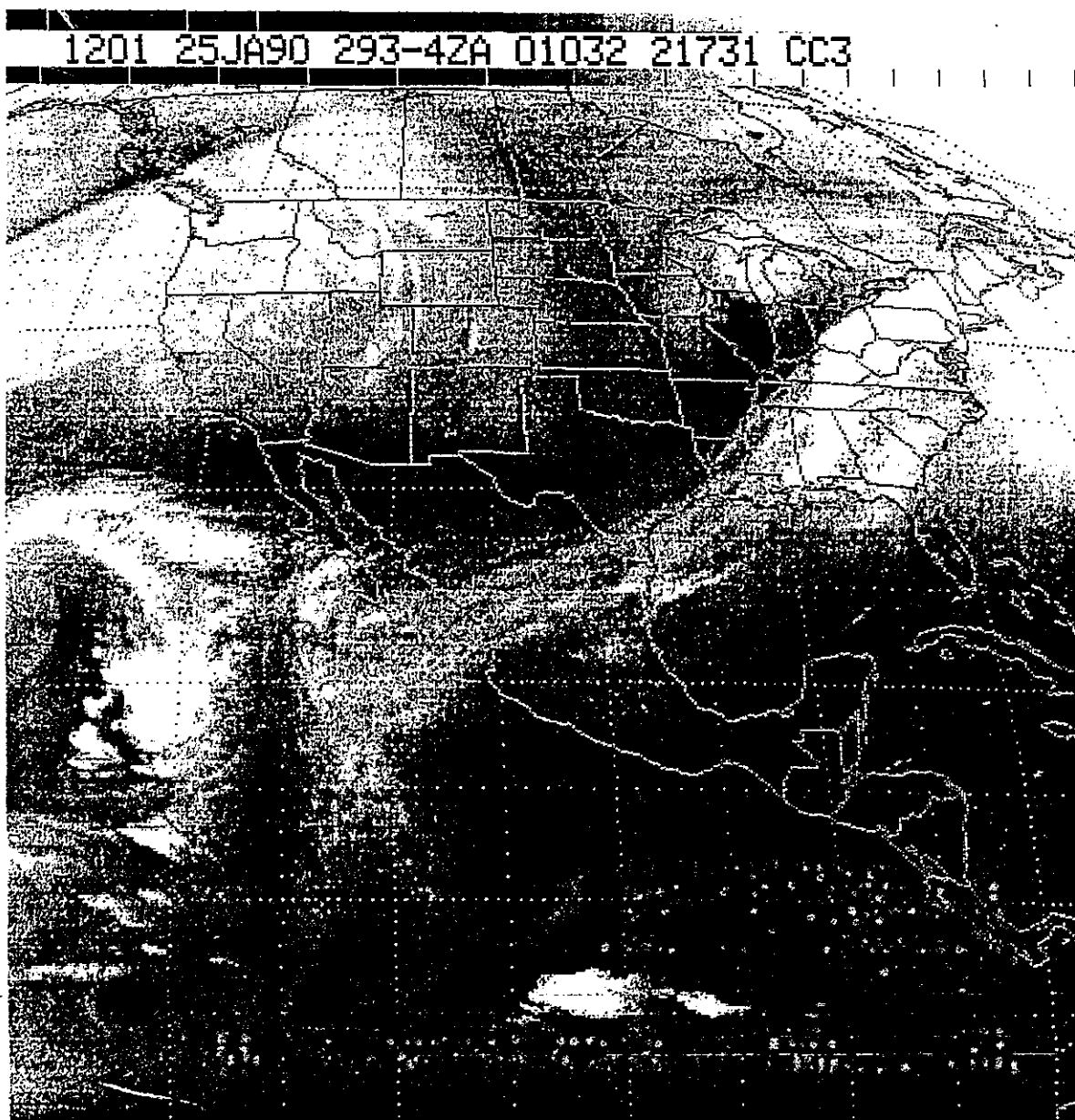


Figure 54. Goes water vapor channel satellite imagery valid at 1200 UTC 25 January 1990.

1201 27NOV88 093-4ZA 00881 16861 EC3

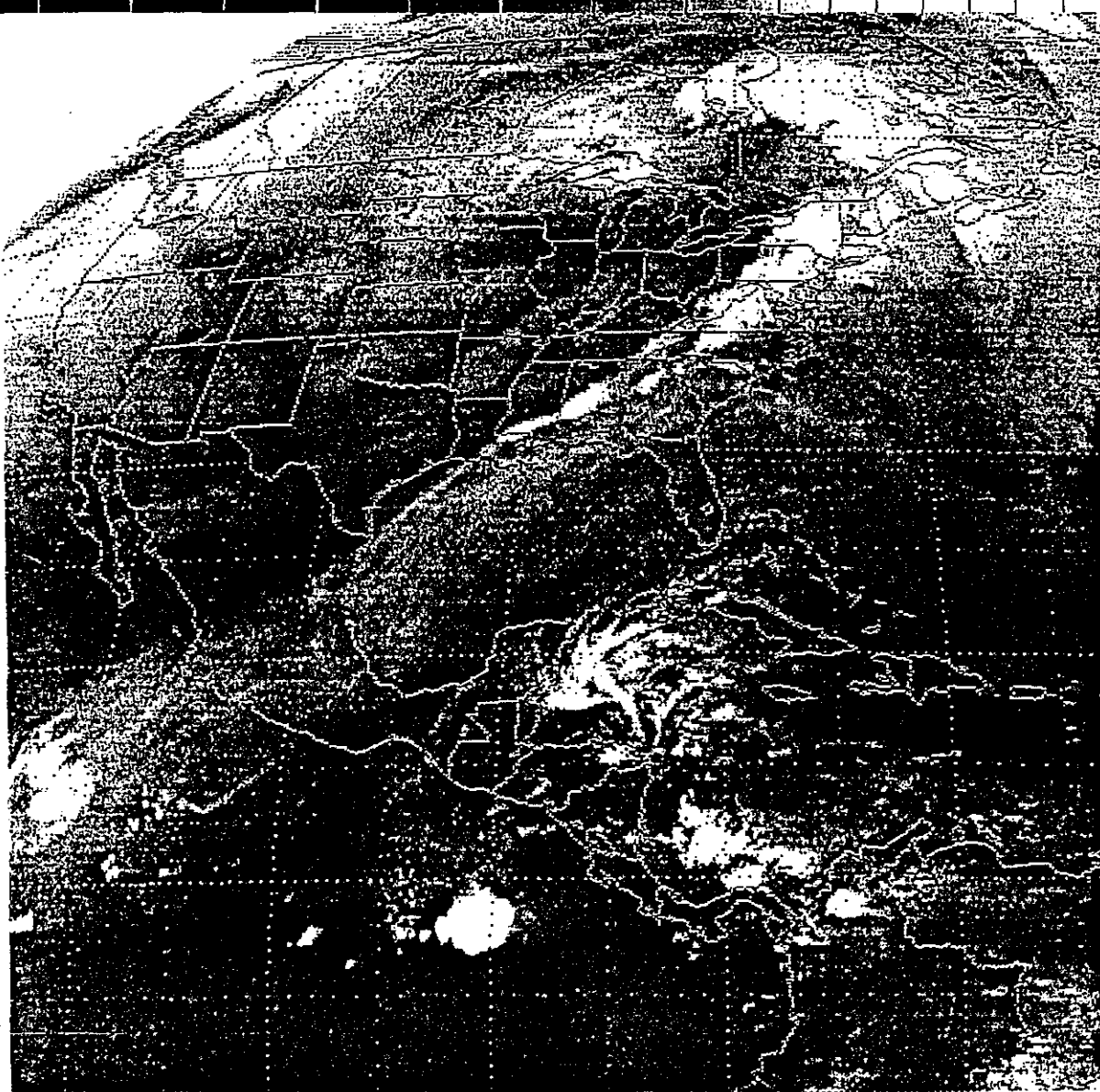


Figure 55. Goes water vapor channel satellite imagery valid at 1200 UTC 27 November 1988.

2001 27ND88 093-4ZA 00901 16841 EC3

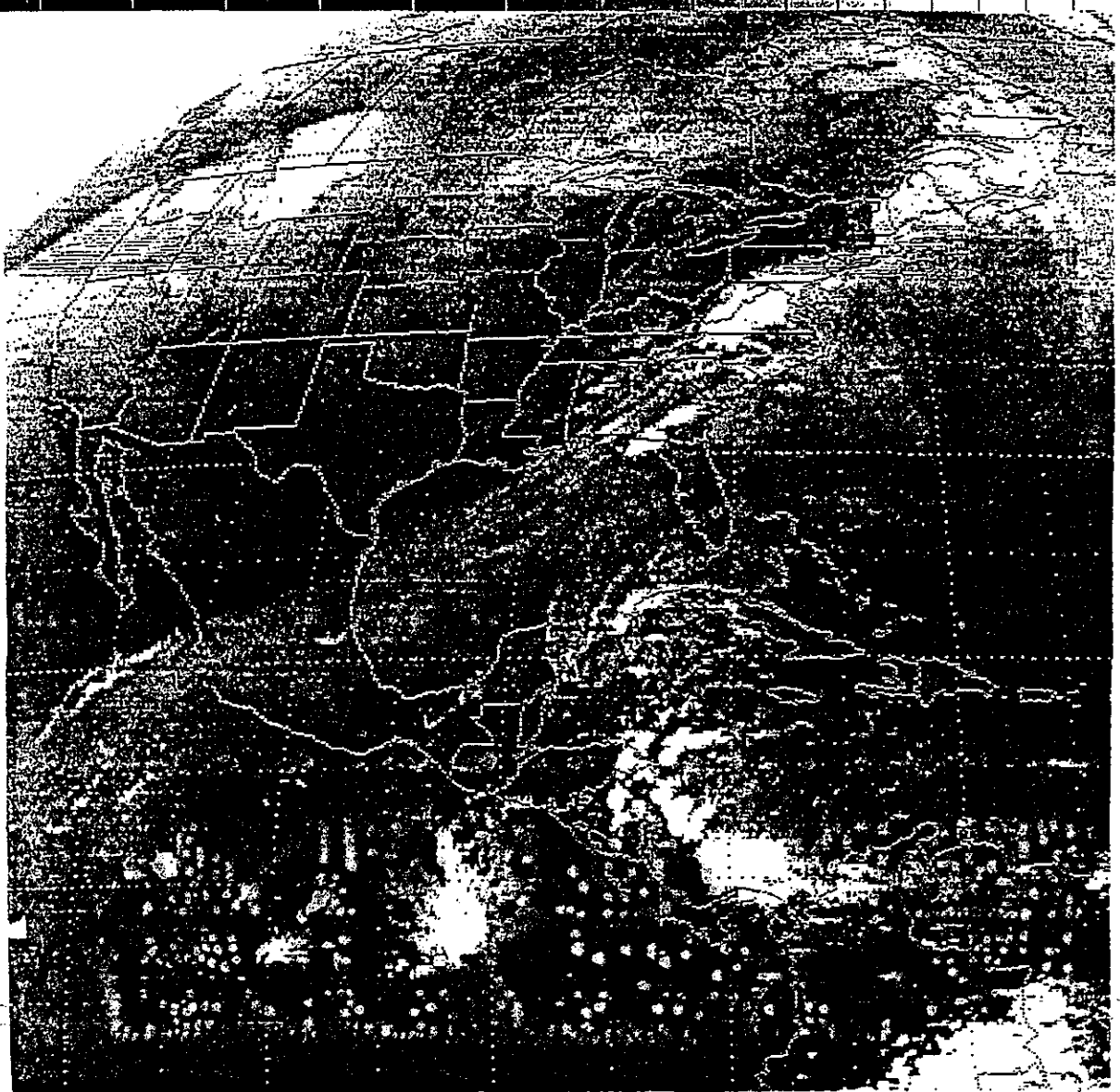


Figure 56. Goes water vapor channel satellite imagery valid at 2000 UTC 27 November 1988.

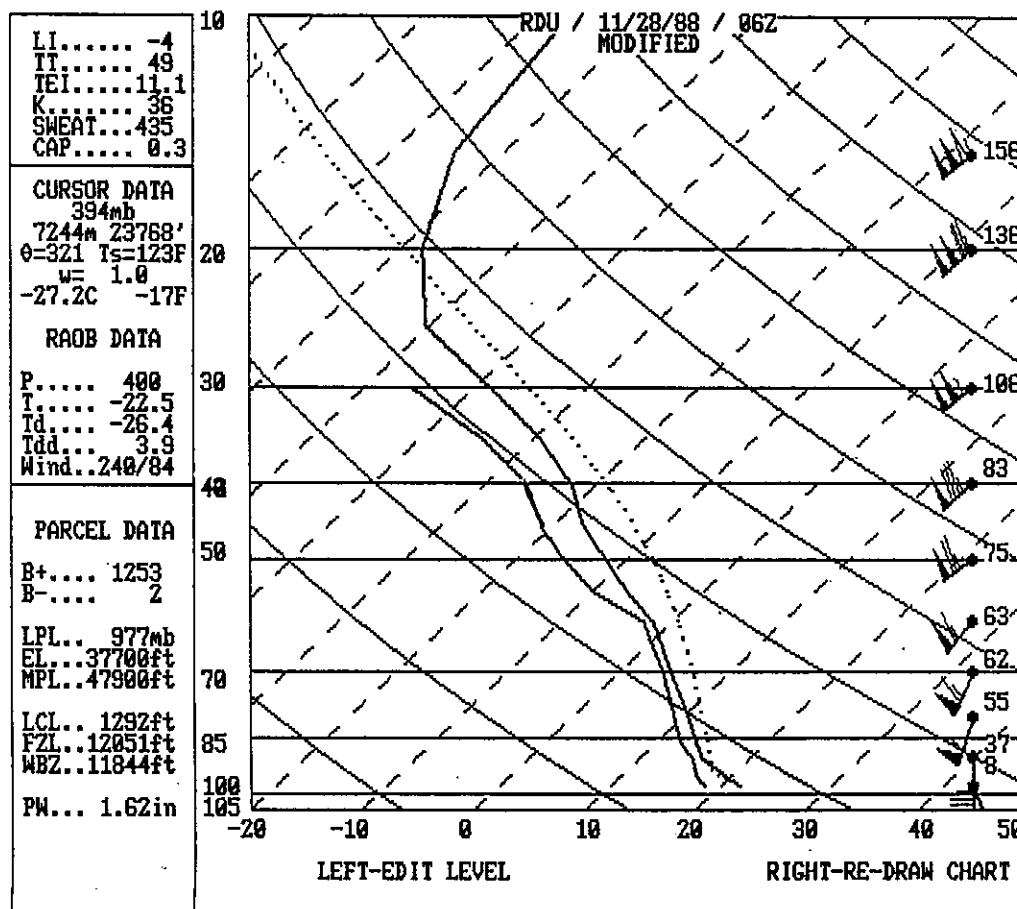


Figure 57. Skew T-log P diagram profile of temperature (right solid line) and dewpoint (left solid line) for RDU from 28 November 1988. Dotted line represents surface parcel lifted adiabatically. Shaded area represents convectively available potential energy (CAPE) of the lifted parcel.

8. Acknowledgments

This research was funded by NOAA under contract #NA27RPO29201 as part of the Southeast Consortium on Severe Thunderstorms and Tornadoes. Computing was performed at the North Carolina Supercomputing Center in Research Triangle Park, North Carolina. The authors would like to acknowledge the assistance of Drs. John Zack and Kenneth Waight of MESO Inc. as well as Drs. Ahmet Akasal and John Manobianco of the NASA Goddard Laboratory for Atmospheres for their aid in understanding various aspects of the GMASS codes. Drs. Zack and Waight also provided assistance which aided in the processing of the NCAR GOI data sets. We Acknowledge Dr. Steven Chiswell at the University of Hawaii for all his computer help and skill. Kevin Schrab of Colorado State University provided key satellite imagery which was employed in the analyses. Mr. Mike Ferguson of MESO Inc. provided radar data which was also invaluable in the observational analyses. Ms. Mary McVicker (NSF ATM-9121126) played a key role in the production of many of the figures used in the paper.

9. References

- Blackadar, A. K., 1979: High resolution models of the planetary boundary layer. *Advances in Environmental Science and Engineering*. Pfafflin and Ziegler, Eds., Gordon and Breach, 50-85.
- Brown, J. M., 1979: Mesoscale unsaturated downdrafts driven by rainfall evaporation: A numerical study. *J. Atmos. Sci.*, **36**, 313-338.
- Browning, P. A., J. E. Hales Jr., and L. F. Wilson, 1989: Factors contributing to the Raleigh tornado of 28 November 1988. Preprint, 12th Conference on Weather Analysis and Forecasting, AMS, Boston, MA, 167-172.
- Clark, T. L., and W. R. Peltier, 1984: Critical level reflection and the nonlinear growth of resonant mountain waves. *J. Atmos. Sci.*, **34**, 1715-1730.
- Cram, J. M., and M. L. Kaplan, 1985: Variational assimilation of VAS data into a mesoscale model; assimilation method and sensitivity experiments. *Mon. Wea. Rev.*, **113**, 467-484.
- _____, 1990: "Numerical Simulation and Analysis of the Propagation of a Pre-Frontal Squall Line". Atmospheric Sciences Paper No. 471, Department of Atmospheric Sciences, Colorado State University. 332 pp.
- _____, M. L. Kaplan, C. A. Mattocks, and J. W. Zack, 1991: The analysis and use of profiler winds to derive mesoscale height and temperature fields; simulation and real data experiments. *Mon. Wea. Rev.*, **119**, 1041-1056.
- Davies, H. C., 1979: Phase-lagged wave-CISK. *Quart. J. Roy. Meteor. Soc.*, **105**, 325-353.
- Funk, S., 1991: An analysis of the tornado-producing Raleigh thunderstorm of November 28, 1988. Masters Thesis. Department of Marine, Earth, and Atmospheric Sciences. North Carolina State University, Raleigh, N. C., 98pp.
- Gonski, R. F., B. P. Woods, and W. D. Korotky, 1989: The Raleigh tornado - 28 November 1988: An operational perspective. Preprint, 12th Conference on Weather Forecasting and Analysis, AMS, Monterey, California, 173-178.
- Hayashi, Y., 1970: A theory of large-scale equatorial waves generated by condensational heating and accelerating the zonal wind. *J. Meteor. Soc. Japan*, **48**, 140-160.
- Johnson, R. H., and P. J. Hamilton, 1988: The relation of surface pressure features to the precipitation and airflow structure of an intense mid-latitude squall line. *Mon. Wea. Rev.*, **116**, 1444-1472.
- Kaplan, M. L., and D. A. Paine, 1977: The observed divergence of the horizontal velocity field and pressure gradient force at the mesoscale: Its implications for the parameterization of three-dimensional momentum transport in synoptic-scale numerical models. *Beitr. Phys. Atmos.*, **50**, 321-330.
- _____, J. W. Zack, V. C. Wong, and J. J. Tuccillo, 1982a: Initial results from a mesoscale atmospheric simulation system and comparisons with the AVE-SESAME I data set. *Mon. Wea. Rev.*, **110**, 1564-1590.
- _____, _____, _____, and _____, 1982b: A sixth-order mesoscale atmospheric simulation system applicable to research and real-time forecasting problems. "Proc. Symp. on Mesoscale Meteorology", Y. Sasaki, Ed., Norman, OK, CIMMS, 38-84.

- _____, _____, _____, and G. D. Coats, 1984: The interactive role of subsynoptic scale jet streak and planetary boundary layer processes in organizing an isolated convective complex. *Mon. Wea. Rev.*, **112**, 2212-2237.
- _____, and V. M. Karyampudi, 1992a: Meso-beta scale numerical simulations of terrain drag-induced along-stream circulations. Part I: Midtropospheric frontogenesis. *Meteorol. Atmos. Phys.*, **49**, 133-156.
- _____, and _____ 1992b: Meso-beta scale numerical simulations of terrain drag-induced along-stream circulations. Part II: Concentration of potential vorticity within dryline bulges. *Meteorol. Atmos. Phys.*, **49**, 157-185.
- _____, R. A. Rozumalski, R. P. Weglarz, and Y.-L. Lin, 1993: Numerical simulation studies of the role of prolonged wave-CISK in contributing to the rotation and buoyancy accompanying the isolated Raleigh tornado outbreak. Preprint Volume, AMS 17th Conference on Severe Local Storms, St. Louis, MO. 633-637.
- _____, _____, _____, and S. Businger, 1995: Numerical simulation studies of the role of convectively-driven polar jet entrance and subtropical jet exit region circulations in contributing to the rotation and buoyancy accompanying the isolated Raleigh tornado outbreak. In preparation, *Mon. Wea. Rev.*.
- _____, _____, _____, and S. E. Koch, 1994b: Numerical simulation studies of the role of convectively-driven ageostrophic jet streak adjustments in creating a favorable environment for the development of an isolated tornado outbreak. Preprint Volume, AMS 6th Conference on Mesoscale Processes, Portland, Oregon, 144-146.
- _____, S. E. Koch, Y.-L. Lin, R. P. Weglarz, and R. A. Rozumalski, 1994c: The numerical simulation of meso-beta scale geostrophic adjustment processes resulting in secondary upper/lower level jet formation and internal gravity waves during CCOPE. Preprint Volume, AMS 6th Conference on Mesoscale Processes, Portland, Oregon, 382-384.
- _____, and S. Businger, 1994: A paradigm linking unbalanced ageostrophic adjustments to the explosive development phase of extratropical cyclones. *The Life Cycles of Extratropical Cyclones*, Bergen, Norway, Vol. 3, 123-128.
- _____, _____, and R. A. Rozumalski, 1995: Observations and simulations of diabatically-induced ageostrophic frontogenesis within the mid-troposphere. Part I: Successive cyclogenesis, severe weather events, and the propagating mid-tropospheric cold front. In preparation, *Mon. Wea. Rev.*.
- Koch, S. E., W. C. Skillman, P. J. Kocin, P. J. Wetzel, K. F. Brill, D. A. Keyser, and M. C. McCumber, 1985: Synoptic scale forecast skill and systematic errors in the MASS 2.0 model. *Mon. Wea. Rev.*, **113**, 1714-1737.
- _____, and P. B. Dorian, 1988: A mesoscale gravity wave observed during CCOPE. Part III: Wave environment and possible source mechanisms. *Mon. Wea. Rev.*, **116**, 2570-2591.
- Kocin, P. J., L. W. Uccellini, J. W. Zack, and M. L. Kaplan, 1985a: "Recent Examples of Mesoscale Numerical Forecasts of Severe Weather Events Along the East Coast". NASA Technical Memorandum 86172, November 1984, NASA Goddard Space Flight Center, Greenbelt, Maryland, 20771, 57 pp.

- _____, _____, _____, and _____, 1985b: A mesoscale numerical forecast of an intense convective snowburst along the East Coast. *Bull. Amer. Meteor. Soc.*, **66**, 1412-1424.
- Korotky, W. D., 1990: The Raleigh tornado of November 28, 1988: The evolution of a tornadic environment. Preprints, 16th Conference on Severe Local Storms, AMS, Boston, MA, 532-537.
- Lindzen, R. S., and K. K. Tung, 1976: Banded convective activity and ducted gravity waves. *Mon. Wea. Rev.*, **104**, 1602-1617.
- Maddox, R. A., 1980: Mesoscale convective complexes. *Bull. Amer. Meteor. Soc.*, **61**, 1374-1387.
- Manobianco, J. L., L. W. Uccellini, K. F. Brill, and Y.-H. Kuo, 1992: The impact of dynamic data assimilation on the numerical simulations of the QE II cyclone and an analysis of the jet streak influencing the precyclogenetic environment. *Mon. Wea. Rev.*, **120**, 1973-1996.
- Mogil, H. M., and G. P. Ellrod, 1989: The Raleigh tornado of November 28, 1988: Interpreting satellite signatures. Preprints, 12th Conference on Weather Forecasting and Analysis, Amer. Meteor. Soc., Monterey, California, 179-185.
- Nehrkorn, T. 1986: Wave-Cisk in a baroclinic base state. *J. Atmos. Sci.*, **43**, 2773-2791.
- NOAA, 1988: STORM DATA, November, **30**, **11**, 72 pp.
- Powers, J. G., and R. J. Reed, 1993: Numerical simulation of the large-amplitude mesoscale gravity-wave event of 15 December 1987 in the central United States. *Mon. Wea. Rev.*, **121**, 2285-2308.
- Przybylinski, R. W., 1989: The Raleigh tornado - 28 November 1988 A radar overview. Preprints, 12th Conference on Weather Analysis and Forecasting, AMS, Boston, MA, 186-191.
- Raymond, D. J., 1975: A model for predicting the movement of continuously propagating convective storms. *J. Atmos. Sci.*, **32**, 1308-1317.
- _____, 1983: Wave-CISK in mass flux form. *J. Atmos. Sci.*, **40**, 2561-2572.
- _____, 1984: A wave-CISK model of squall-lines. *J. Atmos. Sci.*, **41**, 1946-1958.
- _____, 1986: Prescribed heating of a stratified atmosphere as a model for moist convection. *J. Atmos. Sci.*, **43**, 1101-1111.
- _____, 1987: A forced gravity wave model of self-organizing convection. *J. Atmos. Sci.*, **44**, 3528-3543.
- _____, and R. J. Rotunno, 1989: Response of a stably stratified flow to cooling. *J. Atmos. Sci.*, **46**, 2830-2837.
- _____, and H. Jiang, 1990: A theory for long-lived mesoscale convective systems. *J. Atmos. Sci.*, **47**, 3067-3077.
- Schneider, R. S., 1990: Large-amplitude mesoscale wave disturbances within the intense midwestern extratropical cyclone of 15 December 1987. *Wea. Forecasting*, **5**, 533-558.
- Uccellini, L. W., and D. R. Johnson, 1979: The coupling of upper- and lower-tropospheric jet streaks and implications for the development of severe convective storms. *Mon. Wea. Rev.*, **107**, 662-673.
- _____, and P. J. Kocin, 1987: The interaction of jet streak circulations during heavy snow events along the East Coast of the United States. *Weather and Forecasting*, **2**, 289-308.
- _____, and S. E. Koch, 1987: The synoptic setting and possible energy sources for mesoscale wave disturbances. *Mon. Wea. Rev.*, **115**, 721-729.

- Vescio, M. D., Keeter, K. K., Dial, G., Badgett, P., and A. J. Riordan, 1993: A low-top weak-reflectivity, severe weather episode along a thermal/moisture boundary in eastern North Carolina. AMS 17th Conference on Severe Local Storms, St. Louis, MO., 628-632.
- Whitaker, J. S., L. W. Uccellini, and K. F. Brill, 1988: A model-based diagnostic study of the explosive development phase of the Presidents' Day cyclone. *Mon. Wea. Rev.*, **116**, 2337-2365.
- Xu, Q., and J. H. E. Clark, 1984: Wave-CISK and mesoscale convective systems. *J. Atmos. Sci.*, **41**, 2089-2107.
- Zack, J. W., and M. L. Kaplan, 1987: Numerical simulations of the subsynoptic features associated with the AVE-SESAME I case. Part I: The preconvective environment. *Mon. Wea. Rev.*, **115**, 2367-2394.
- _____, P. E. Price, K. R. Waight III, and M. D. Bousquet, 1993: "Numerical Simulation and Analysis of Cold Season Severe Weather Events". SBIR Phase I Feasibility Study, NOAA Contract No. 50-DKNA-2-00120, MESO Inc., 131 pp.
- Zhang, D.-L., and K. Gao, 1989: Numerical simulations of an intense squall line during 10-11 June 1985 PRE-STORM. Part II: Review of surface pressure perturbations and stratiform precipitation. *Mon. Wea. Rev.*, **117**, 2067-2094.

- NWS ER 46 An Objective Method of Forecasting Summertime Thunderstorms. John F. Townsend and Russell J. Younkin. May 1972. (COM-72-10765).
- NWS ER 47 An Objective Method of Preparing Cloud Cover Forecasts. James R. Sims. August 1972. (COM-72-11382).
- NWS ER 48 Accuracy of Automated Temperature Forecasts for Philadelphia as Related to Sky Condition and Wind Direction. Robert B. Wassall. September 1972. (COM-72-11473).
- NWS ER 49 A Procedure for Improving National Meteorological Center Objective Precipitation Forecasts. Joseph A. Ronco, Jr. November 1972. (COM-73-10132).
- NWS ER 50 PEATMOS Probability of Precipitation Forecasts as an Aid in Predicting Precipitation Amounts. Stanley E. Wasserman. December 1972. (COM-73-10243).
- NWS ER 51 Frequency and Intensity of Freezing Rain/Drizzle in Ohio. Marvin E. Miller. February 1973. (COM-73-10570).
- NWS ER 52 Forecast and Warning Utilization of Radar Remote Facsimile Data. Robert E. Hamilton. July 1973. (COM-73-11275).
- NWS ER 53 Summary of 1969 and 1970 Public Severe Thunderstorm and Tornado Watches Within the National Weather Service, Eastern Region. Marvin E. Miller and Lewis H. Ramey. October 1973. (COM-74-10160).
- NWS ER 54 A Procedure for Improving National Meteorological Center Objective Precipitation Forecasts - Winter Season. Joseph A. Ronco, Jr. November 1973. (COM-74-10200).
- NWS ER 55 Cause and Prediction of Beach Erosion. Stanley E. Wasserman and David B. Gilhousen. December 1973. (COM-74-10036).
- NWS ER 56 Biometeorological Factors Affecting the Development and Spread of Plant Diseases. V.J. Valli. July 1974. (COM-74-11625/AS).
- NWS ER 57 Heavy Fall and Winter Rain In The Carolina Mountains. David B. Gilhousen. October 1974. (COM-74-11761/AS).
- NWS ER 58 An Analysis of Forecasters' Propensities In Maximum/Minimum Temperature Forecasts. I. Randy Racer. November 1974. (COM-75-10063/AS).
- NWS ER 59 Digital Radar Data and its Application in Flash Flood Potential. David D. Sisk. March 1975. (COM-75-10582/AS).
- NWS ER 60 Use of Radar Information in Determining Flash Flood Potential. Stanley E. Wasserman. December 1975. (PB250071/AS).
- NWS ER 61 Improving Short-Range Precipitation Guidance During the Summer Months. David B. Gilhousen. March 1976. (PB256427).
- NWS ER 62 Locally Heavy Snow Downwind from Cooling Towers. Reese E. Ott. December 1976. (PB263390/AS).
- NWS ER 63 Snow in West Virginia. Marvin E. Miller. January 1977. (PB265419/AS).
- NWS ER 64 Wind Forecasting for the Monongahela National Forest. Donald E. Risher. August 1977. (PB272138/AS).
- NWS ER 65 A Procedure for Spraying Spruce Budworms in Maine during Stable Wind Conditions. Monte Glovinsky. May 1980. (PB80-203243).
- NWS ER 66 Contributing Factors to the 1980-81 Water Supply Drought, Northeast U.S. Solomon G. Summer. June 1981. (PB82-172974).
- NWS ER 67 A Computer Calculation and Display System for SLOSH Hurricane Surge Model Data. John F. Townsend. May 1984. (PB84-198753).
- NWS ER 68 A Comparison Among Various Thermodynamic Parameters for the Prediction of Convective Activity. Hugh M. Stone. April 1985. (PB85-206217/AS).
- NWS ER 69 A Comparison Among Various Thermodynamic Parameters for the Prediction of Convective Activity, Part II. Hugh M. Stone. December 1985. (PB86-142353/AS).
- NWS ER 70 Hurricane Gloria's Potential Storm Surge. Anthony G. Gigi and David A. Wert. July 1986. (PB86-226644/AS).
- NWS ER 71 Washington Metropolitan Wind Study 1981-1986. Clarence Burke, Jr. and Carl C. Ewald. February 1987. (PB87-151908/AS).
- NWS ER 72 Mesoscale Forecasting Topics. Hugh M. Stone. March 1987. (PB87-180246/AS).
- NWS ER 73 A Procedure for Improving First Period Model Output Statistics Precipitation Forecasts. Antonio J. Lacroix and Joseph A. Ronco, Jr. April 1987. (PB87-180238/AS).
- NWS ER 74 The Climatology of Lake Erie's South Shoreline. John Kwiatkowski. June 1987. (PB87-205514/AS).
- NWS ER 75 Wind Shear as a Predictor of Severe Weather for the Eastern United States. Hugh M. Stone. January 1988. (PB88-157144).
- NWS ER 76 Is There A Temperature Relationship Between Autumn and the Following Winter? Anthony Gigi. February 1988. (PB88-173224).
- NWS ER 77 River Stage Data for South Carolina. Clara Cillettine. April 1988. (PB88-201991/AS).
- NWS ER 78 National Weather Service Philadelphia Forecast Office 1987 NOAA Weather Radio Survey & Questionnaire. Robert P. Wanton. October 1988. (PB89-111785/AS).
- NWS ER 79 An Examination of NGM Low Level Temperature. Joseph A. Ronco, Jr. November 1988. (PB89-122543/AS).
- NWS ER 80 Relationship of Wind Shear, Buoyancy, and Radar Tops to Severe Weather 1988. Hugh M. Stone. November 1988. (PB89-1222419/AS).
- NWS ER 81 Relation of Wind Field and Buoyancy to Rainfall Inferred from Radar. Hugh M. Stone. April 1989. (PB89-208326/AS).
- NWS ER 82 Second National Winter Weather Workshop, 26-30 Sept. 1988: Postprints. Laurence G. Lee. June 1989. (PB90-147414/AS).
- NWS ER 83 A Historical Account of Tropical Cyclones that Have Impacted North Carolina Since 1586. James D. Stevenson. July 1990. (PB90-259201).
- NWS ER 84 A Seasonal Analysis of the Performance of the Probability of Precipitation Type Guidance System. George J. Maglaras and Barry S. Goldsmith. September 1990. (PB93-160802).
- NWS ER 85 The Use of ADAP to Examine Warm and Quasi-Stationary Frontal Events in the Northeastern United States. David R. Vallee. July 1991. (PB91-225037).
- NWS ER 86 Rhode Island Hurricanes and Tropical Storms A Fifty-Six Year Summary 1936-0991. David R. Vallee. March 1993. (PB93-162006).
- NWS ER 87 Post-print Volume, Third National Heavy Precipitation Workshop, 16-20 Nov. 1992. April 1993. (PB93-186625).
- NWS ER 88 A Synoptic and Mesoscale Examination of the Northern New England Winter Storm of 29-30 January 1990. Robert A. Marine and Steven J. Capriola. July 1994. (PB94-209426).
- NWS ER 89 An Initial Comparison of Manual and Automated Surface Observing System Observations at the Atlantic City, New Jersey International Airport. James C. Hayes. January 1995.

NOAA SCIENTIFIC AND TECHNICAL PUBLICATIONS

The National Oceanic and Atmospheric Administration was established as part of the Department of Commerce on October 3, 1970. The mission responsibilities of NOAA are to assess the socioeconomic impact of natural and technological changes in the environment and to monitor and predict the state of the solid Earth, the oceans and their living resources, the atmosphere, and the space environment of the Earth.

The major components of NOAA regularly produce various types of scientific and technical information in the following kinds of publications:

PROFESSIONAL PAPERS--Important definitive research results, major techniques, and special investigations.

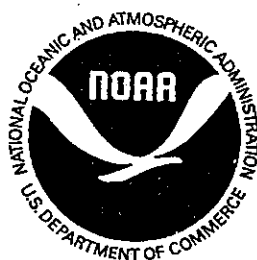
CONTRACT AND GRANT REPORTS--Reports prepared by contractors or grantees under NOAA sponsorship.

ATLAS--Presentation of analyzed data generally in the form of maps showing distribution of rainfall, chemical and physical conditions of oceans and atmosphere, distribution of fishes and marine mammals, ionospheric conditions, etc.

TECHNICAL SERVICE PUBLICATIONS--Reports containing data, observations, instructions, etc. A partial listing includes data serials; prediction and outlook periodicals; technical manuals, training papers, planning reports, and information serials; and miscellaneous technical publications.

TECHNICAL REPORTS--Journal quality with extensive details, mathematical developments, or data listings.

TECHNICAL MEMORANDUMS--Reports of preliminary, partial, or negative research or technology results, interim instructions, and the like.



Information on availability of NOAA publications can be obtained from:

NATIONAL TECHNICAL INFORMATION SERVICE
U.S. DEPARTMENT OF COMMERCE
5285 PORT ROYAL ROAD
SPRINGFIELD, VA 22161